

**STUDIES OF SOME LAMELLAR INORGANIC HOST
COMPOUNDS AND THEIR ORGANIC
INTERCALATES**

THESIS

Submitted for the degree of

Doctor of Philosophy

By

IVONNE MARCELA DIAZ MESA

At

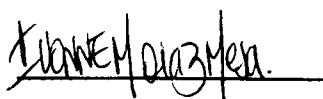
KINGSTON UNIVERSITY LONDON

Faculty of Science, Engineering and Computing
Penrhyn Road, Kingston upon Thames
Surrey, KT1 2EE

May 2014

DECLARATION

This thesis entitled "**Studies of some lamellar inorganic host compounds and their organic intercalates**" is based upon work conducted by the author in the School of Pharmacy and Chemistry at Kingston University London between October 2009 and April 2014. All of the work described herein is original unless otherwise acknowledged in the text or by references. None of the work has been submitted for another degree in this or any other university.

A handwritten signature in black ink, reading "Ivonne Marcela Diaz Mesa", written over a horizontal line.

Ivonne Marcela Diaz Mesa

**“TO MY FAMILY FOR THEIR UNCONDITIONAL
SUPPORT “**

Acknowledgements

First of all I would like to express my deepest gratitude to my supervisors, Professor Peter Foot and Dr Roman Kresinski for their valuable guidance, support and encouragement throughout my research.

I am also thankful to Dr Trish Hill for helping me during different stages of this project.

Special thanks to all the technical staff at the faculty of SEC for their advice and training.

Thanks also to my friends and colleagues in the Materials research office at Kingston University, particularly to Bruno Morais for his unconditional help and support during this research, his encouragement kept me going during difficult times.

Sincere thanks to my brother Leo and the rest of my family in Colombia for everything they provided me with to be where I am now, for their love, patience, constant support and inspiration that kept me going.

And finally, big thanks to all my friends for their patience and support during the completion of this work.

Abstract

For many years organic conducting polymers have been used for electronic and photonic applications. Although there are many advantages of using these sorts of polymers, their poor environmental stability is still an issue that needs further investigation. Intercalation of organic polymer into the interlayer space of inorganic host materials is an effective way of producing well organised nanocomposites with properties that can be used for various industrial applications, including the production of electronic devices which are environmentally more stable.

The preparation of a number of luminescent semiconducting nanocomposites of manganese phosphorus trisulphide (MnPS_3), cadmium phosphorus trisulphide (CdPS_3) and vanadyl phosphate (VOPO_4) containing the organic polymer poly(phenylene vinylene) (PPV) by intercalation is herein described along with the characterisation by thermogravimetric analysis (TGA), infrared (IR) and raman spectroscopy, and X ray diffraction (XRD). In addition to this we used scanning electron microscopy (SEM) to monitor the physical changes in crystallinity of the host materials.

An average increase of 5.05 Å in the interlayer distance was observed through XRD, a strong indicator of intercalation of the polymer. It was also found that the environmental stability of the composites was enhanced in comparison with PPV alone by doing fluorescence analysis. Moreover, electrical conductivity studies showed that the composites presented higher conductivity relative to the constituent inorganic hosts.

List of Abbreviations

P-xylylene-bis(tetrahydrothiophenium chloride)	Monomer 1
Poly (p-xylylene-bis(tetrahydrothiophenium chloride))	Precursor Polymer
Poly(p-phenylene vinylene)	PPV
Manganese phosphorus trisulfide	MnPS₃
Potassium intercalated MnPS ₃	K_MnPS₃
Precursor polymer intercalated MnPS ₃	PP_MnPS₃
PPV intercalated MnPS ₃ (Cation exchanged)	PPV_MnPS₃
PPV intercalated MnPS ₃ (<i>In-situ</i> polymerisation)	PPV2_MnPS₃
Cadmium phosphorus trisulfide	CdPS₃
Potassium intercalated CdPS ₃	K_CdPS₃
PPV precursor polymer intercalated CdPS ₃	PP_CdPS₃
PPV intercalated CdPS ₃	PPV_CdPS₃
Sodium hexathiohypophosphate	Na₄P₂S₆·6H₂O
Sodium thioorthophosphates	Na₃PS₄
Manganese phosphorus trisulfide (solution approach)	MnPS₃_Sln
Potassium intercalated MnPS ₃ _Sln	K_MnPS₃_Sln
PPV intercalated MnPS ₃ _Sln	PPV_MnPS₃_Sln
Vanadium phosphate dihydrate	VOPO₄·2H₂O
Lithium intercalated VOPO ₄ ·2H ₂ O	Li_VOPO₄
Potassium intercalated VOPO ₄ ·2H ₂ O	K_VOPO₄
Precursor polymer intercalated VOPO ₄ ·2H ₂ O	PPV_VOPO₄
Palladium thiophosphate	Pd₃P₂S₈
Poly(3,4-ethylenedioxythiophene) poly(styrenesulfonate)	PEDOT:PS

Table of Contents

CHAPTER 1:	10
INTRODUCTION	10
CHAPTER 2:	13
LITERATURE REVIEW	13
2.1 INTRODUCTION TO COMPOSITES AND NANOCOMPOSITES	13
2.2 COMPOSITE PREPARATIONS	14
2.2.1 <i>Intercalation Chemistry</i>	14
2.3 INORGANIC HOST STRUCTURES	18
2.3.1 <i>Layered inorganic hosts</i>	19
2.4 ORGANIC GUEST MOLECULES	23
2.4.1 <i>Conducting Polymers: A Brief Introduction</i>	24
2.4.2 <i>Luminescent Polymers</i>	28
CHAPTER 3:	34
SYNTHESIS AND CHARACTERISATION OF POLY(P-PHENYLENE VINYLENE) (PPV) .34	
3.1 REAGENTS AND INSTRUMENTS USED	35
3.1.1 <i>Infrared spectroscopy</i>	35
3.1.2 <i>Absorption Spectrometry</i>	36
3.1.3 <i>Photoluminescence Studies</i>	36
3.1.4 <i>Nuclear Magnetic Resonance (NMR)</i>	36
3.1.5 <i>Polymer Molecular weight</i>	36
3.2 SYNTHETIC ROUTE.....	37
3.3 RESULTS AND DISCUSSION.....	39
3.3.1 <i>Reaction mechanism</i>	39
3.3.2 <i>Nuclear Magnetic Resonance (NMR)</i>	41
3.3.3 <i>Infrared Spectroscopy</i>	42
3.3.4 <i>UV-vis Absorption spectroscopy</i>	44
3.3.5 <i>Fluorescence Spectroscopy</i>	47
3.3.6 <i>Estimation of the polymer molecular weight by viscometry</i>	49
CHAPTER 4:	53
SYNTHESIS, CHARACTERISATION AND INTERCALATION OF CRYSTALLINE METAL PHOSPHORUS TRISULFIDES	53
4.1 REAGENTS AND INSTRUMENTS USED	54
4.1.1 <i>X-ray Diffraction</i>	54
4.1.2 <i>Scanning Electron Microscopy</i>	55
4.1.3 <i>Infrared Spectroscopy</i>	55
4.1.4 <i>Raman Spectroscopy</i>	55
4.1.5 <i>UV-vis Spectroscopy</i>	55
4.1.6 <i>Photoluminescence Studies</i>	55
4.1.7 <i>Elemental Analysis</i>	56
4.2 SYNTHESIS OF METAL PHOSPHORUS TRISULPHIDES (CRYSTAL GROWTH).....	56
4.2.1 <i>MnPS₃</i>	56
4.2.2 <i>CdPS₃</i>	57
4.3 SYNTHESIS OF COMPOSITES BY INTERCALATION	57
4.3.1 <i>MnPS₃</i>	58
4.3.2 <i>CdPS₃</i>	59

4.4 RESULTS AND DISCUSSION.....	60
4.4.1 <i>MnPS₃ and MnPS₃ intercalates</i>	60
4.4.2 <i>CdPS₃</i>	77
CHAPTER 5:	85
SYNTHESIS, CHARACTERISATION AND INTERCALATION OF AMORPHOUS THIOHYPOPHOSPHATES AND THIOORTHOPHOSPHATES	85
THIOHYPOPHOSPHATES ($M^{II}PS_3$ OR $M^{II}_2P_2S_6$)	85
THIOORTHOPHOSPHATES [$M_3^{II}(PS_4)_2$]	86
5.1 REAGENTS AND INSTRUMENTS USED	87
5.2 SYNTHESIS OF AMORPHOUS MPS_3	88
5.2.1 <i>Synthesis of sodium hexathiohypophosphate $Na_4P_2S_6 \cdot 6H_2O$</i>	88
5.2.2 <i>Synthesis of $Na_3PS_4 \cdot 8H_2O$</i>	89
5.2.3 <i>Synthesis of amorphous $MnPS_3$ SLN</i>	89
5.3 SYNTHESIS OF INTERCALATED $MNPS_3$ _SLN	90
5.3.1 <i>Intercalation of Potassium ions (K^+)</i>	90
5.3.2 <i>Intercalation of precursor polymer</i>	90
5.4 RESULTS AND DISCUSSION	91
5.4.1 <i>Elemental Analysis</i>	91
5.4.2 <i>X-ray Diffractometry</i>	91
5.4.3 <i>Infrared and Raman Spectroscopy</i>	97
CHAPTER 6:	103
SYNTHESIS, CHARACTERISATION AND INTERCALATION OF LAMELLAR OXOVANADIUM PHOSPHATES	103
6.1 REAGENTS AND INSTRUMENTS USED	104
6.2 SYNTHESIS OF $VOPO_4 \cdot 2H_2O$	104
6.3 $VOPO_4 \cdot 2H_2O$ INTERCALATION	105
6.3.1 <i>Intercalation of Lithium ions (Li^+) (Li_VOPO_4)</i>	105
6.3.2 <i>Intercalation of Potassium ions (K^+) (K_VOPO_4)</i>	105
6.3.3 <i>Intercalation of precursor polymer</i>	105
6.4 RESULTS AND DISCUSSION	106
6.4.1 <i>Elemental Analysis</i>	106
6.4.2 <i>Powder x-ray diffraction</i>	106
6.4.3 <i>Scanning Electron Microscopy (SEM)</i>	109
6.4.4 <i>Infrared Spectroscopy and Raman Spectroscopy</i>	111
CHAPTER 7:	116
OPTICAL AND ELECTRONIC PROPERTIES OF INTERCALATED COMPOSITES.....	116
7.1 UV-VIS ABSORPTION	116
7.1.1 <i>PPV intercalated $MnPS_3$ and $CdPS_3$</i>	116
7.1.2 <i>PPV intercalated $VOPO_4$</i>	119
7.2 PHOTOLUMINESCENCE STUDIES	121
7.2.1 <i>PPV-intercalated $MnPS_3$</i>	121
7.3 PHOTODEGRADATION STUDIES	124
7.3.1 <i>PPV Photodegradation</i>	125
7.3.2 <i>PPV intercalated $MnPS_3$ photodegradation</i>	128
7.3.3 <i>PPV intercalated $MnPS_3$ SLN</i>	129
7.4 ELECTRICAL CHARACTERISTICS	131
7.4.1 <i>Ambient temperature conductivity measurements</i>	131
7.4.2 <i>Diode Preparation</i>	135

CHAPTER 8:	149
EXPLORATORY WORK ON PALLADIUM THIOPHOSPHATE	149
8.1 PALLADIUM THIOPHOSPHATE	150
8.2 SYNTHESIS OF Pd ₃ P ₂ S ₈ AND INTERCALATES	151
8.2.1 Pd ₃ P ₂ S ₈	151
8.2.2 Intercalation of Na ⁺ ions into Pd ₃ P ₂ S ₈	151
8.2.3 Intercalation of 2,2'-bipyridine into Pd ₃ P ₂ S ₈	151
8.3 RESULTS AND DISCUSSION	152
8.3.1 Elemental analysis.....	152
8.3.2 X-Ray Diffraction.....	152
8.3.3 Infrared and Raman Spectral Data	154
8.3.4 Conductivity and Photoconductivity Measurements.....	156
CHAPTER 9:	157
FINAL CONCLUSIONS AND FUTURE WORK	157
APPENDIX	161
REFERENCES	164

Table of Figures

Chapter 2

Figure 2 1: Schematic representation of intercalation.....	14
Figure 2 2: Preparation of nanocomposites by exfoliation-adsorption	16
Figure 2 3: <i>In-situ</i> polymerization of acrylonitrile inside the channels of a zeolite host	17
Figure 2 4: MnPS ₃ Crystal Structure.....	21
Figure 2 5: Simplified version of the energy level scheme adopted to describe the electronic band structure of MnPS ₃	22
Figure 2 6: VOPO ₄ ·2H ₂ O Crystal Structure.....	23
Figure 2 7 Oxidative polymerization of aniline carried out in acidic conditions	24
Figure 2 8: Some conducting polymers.....	25
Figure 2 9: Conjugated polyacetylene.....	25
Figure 2 10: Variation of the band structure upon doping conjugated polymers.	27
Figure 2 11: Energy levels of molecular orbital in formaldehyde	31
Figure 2 12: A Jablonski diagram showing the energy transitions that take place during fluorescence.	32

Chapter 3

Figure 3 1: α,α' -Dichloro-p-xylene and p-xylene-bis(tetrahydrothiophenium chloride) (monomer 1) IR spectra	43
Figure 3 2: P-xylene-bis(tetrahydrothiophenium chloride) and Poly (p-xylene tetrahydrothiophenium chloride) IR spectra	43
Figure 3 3: Sulfonium precursor polymer (left) and PPV (right) UV-visible.....	46
Figure 3 4: Fluorescence under a long range UV lamp of precursor polymer and PPV	47
Figure 3 5: Emission spectrum of precursor polymer.....	48
Figure 3 6: Configurational coordinate diagram for transitions between different states of PPV.....	48
Figure 3 7: Plot of viscosity number (n_{rel}) against concentration (C)..	52

Chapter 4

Figure 4 1: X-ray diffractogram of polycrystalline MnPS ₃	61
Figure 4 2: Powder X-ray diffractogram of (a) dried K ⁺ intercalated MnPS ₃ and (b) K ⁺ and H ₂ O intercalated MnPS ₃	63
Figure 4 3: X-ray diffractogram showing intercalation of PPV precursor in MnPS ₃	64
Figure 4 4: X-ray diffractogram of intercalated PPV precursor prepared by <i>in situ</i> polymerisation.	65
Figure 4 5: TGA curve of precursor polymer intercalated MnPS ₃	67
Figure 4 6: TGA curve of PPV intercalated MnPS ₃	68
Figure 4 7: SEM images of MnPS ₃	69
Figure 4 8: SEM images of K ₊ MnPS ₃	69
Figure 4 9: SEM images of PP ₊ MnPS ₃	69
Figure 4 10: Single crystal of MnPS ₃ IR Spectrum.....	71
Figure 4 11: MnPS ₃ Raman Spectrum.	71
Figure 4 12: K ₊ MnPS ₃ IR spectrum.	73

Figure 4 13: K ₂ MnPS ₃ and MnPS ₃ Raman spectra.....	73
Figure 4 14: PPV intercalated MnPS ₃ IR spectra.....	75
Figure 4 15: PPV-intercalated MnPS ₃ Raman spectrum	76
Figure 4 16: UV-visible spectrum of a MnPS ₃ single crystal (left) and a graphical representation of the energy levels of MnPS ₃ with the appropriate energy values (right)	77
Figure 4 17: X-ray diffractogram of Polycrystalline CdPS ₃	78
Figure 4 18: X-ray diffractogram of K ⁺ Intercalated CdPS ₃	80
Figure 4 19: X-ray diffractogram of precursor polymer-intercalated CdPS ₃	81
Figure 4 20: TGA diagram of precursor polymer intercalated CdPS ₃	82
Figure 4 21: TGA diagram of PPV-intercalated CdPS ₃	83
Figure 4 22: a.SEM image of lamellar CdPS ₃ and b.SEM image of K ⁺ intercalated CdPS ₃	84
Figure 4 23: SEM image of precursor polymer-intercalated CdPS ₃	84

Chapter 5

Figure 5 1: X-ray diffractogram of Na ₄ P ₂ S ₆ .6H ₂ O.	92
Figure 5 2: XRD pattern of amorphous MnPS ₃ _SIn before annealing.	93
Figure 5 3: XRD pattern of amorphous MnPS ₃ _SIn after annealing.	93
Figure 5 4: X-ray diffractogram of K ⁺ intercalated MnPS ₃ _SIn.....	95
Figure 5 5: X-ray diffractogram of PPV-intercalated MnPS ₃ _SIn.....	96
Figure 5 6: Infrared Spectra of crude (black) and recrystallised (red) Na ₄ P ₂ S ₆ .6H ₂ O.....	98
Figure 5 7: Na ₄ P ₂ S ₆ .6H ₂ O Raman spectrum.....	98
Figure 5 8: MnPS ₃ _SIn IR (left) and Raman (right) spectra.	99
Figure 5 9: MnPS ₃ _SIn and K ⁺ -intercalated MnPS ₃ _SIn IR spectra.....	100
Figure 5 10: PPV-intercalated MnPS ₃ _SIn IR spectra.	101
Figure 5 11: Raman spectrum of PPV-intercalated MnPS ₃ _SIn.	102

Chapter 6

Figure 6 1: X-ray diffractogram of VOPO ₄ .2H ₂ O	107
Figure 6 2: X-ray diffractogram of K ⁺ -intercalated VOPO ₄ .2H ₂ O.....	108
Figure 6 3: X-ray diffractogram of Precursor polymer intercalated VOPO ₄	109
Figure 6 4: VOPO ₄ .2H ₂ O SEM image.	110
Figure 6 5: K ⁺ intercalated VOPO ₄	110
Figure 6 6: PPV intercalated VOPO ₄	110
Figure 6 7: VOPO ₄ .2H ₂ O IR spectrum.	112
Figure 6 8: VOPO ₄ .2H ₂ O Raman spectrum.	112
Figure 6 9: K ⁺ intercalated VOPO ₄ (black) and VOPO ₄ .2H ₂ O (Red) IR spectra.	113
Figure 6 10: K ⁺ intercalated VOPO ₄ Raman spectrum.....	114
Figure 6 11: K ⁺ intercalated (red) and partially converted sulfonium polymer intercalated (black) VOPO ₄ IR spectra.	115
Figure 6 12: Sulfonium precursor polymer intercalated VOPO ₄ Raman spectrum.....	115

Chapter 7

Figure 7 1: UV-visible spectra of precursor polymer-intercalated MnPS ₃ (left) and PPV-intercalated MnPS ₃ (right).....	118
---	-----

Figure 7 2: UV-visible spectra of precursor polymer-intercalated CdPS ₃ (left) and PPV-intercalated CdPS ₃ (right).....	118
Figure 7 3 UV-visible spectra of PPV (left) and pristine MnPS ₃ (right)	118
Figure 7 4: UV-visible spectra of VOPO ₄ ·2H ₂ O in ethanol (left) and precursor polymer-intercalated VOPO ₄ in ethanol (right).....	120
Figure 7 5: UV-visible spectrum of PPV intercalated VOPO ₄	120
Figure 7 6: Emission Spectra of a. PPV and b. PPV intercalated in MnPS ₃	121
Figure 7 7: Left: PPV (above) and PPV intercalated (below).....	123
Figure 7 8: Emission spectra caused by 400 nm excitation of PPV films before and after irradiation during several periods of time.	125
Figure 7 9: Photodegradation mechanism proposed by Chambon <i>et al</i> (2001)	127
Figure 7 10: IR spectrum of PPV prior and after 2 h of irradiation	127
Figure 7 11: Emission Spectra of PPV-intercalated MnPS ₃ at various irradiation times.....	128
Figure 7 12: IR spectra PPV-intercalated MnPS ₃ before and after 2 hours of irradiation	129
Figure 7 13: PPV intercalated MnPS ₃ _Sn emission spectrum.....	130
Figure 7 14: Emission Spectra of PPV intercalated MnPS ₃ _Sn after irradiation.....	130
Figure 7 15: I-V curve of a single crystal of MnPS ₃	132
Figure 7 16: I-V curve of PPV intercalated MnPS ₃	133
Figure 7 17: Schematic diagram of a Schottky diode.....	136
Figure 7 18: Schematic representation of the p-type Schottky barrier formation.....	137
Figure 7 19: I-V curve of ITO/PEDOT:PSS/PPV/ Al.....	138
Figure 7 20: Plot of Ln (I) against voltage of ITO/PEDOT:PSS/PPV/ Al	139
Figure 7 21: Proposed energy level alignment for ITO/PEDOT:PSS/PPV/Al	140
Figure 7 22: I-V curve of ITO/PEDOT:PSS/PPV_MnPS ₃ / Al	141
Figure 7 23: Plot of Ln(I) against V for ITO/PEDOT:PSS/PPV_MnPS ₃ /Al	142
Figure 7 24: Proposed energy level alignment for ITO/PEDOT:PSS/PPV_MnPS ₃ /Al	142
Figure 7 25: Plot of I against V for ITO/PEDOT:PSS/PPV_MnPS ₃ _Sn /Al	143
Figure 7 26: Plot of Ln(I) against V for ITO/PEDOT:PSS/PPV_MnPS ₃ _Sn /Al	144
Figure 7 27: Proposed energy level alignment for ITO/PEDOT:PSS/PPV_MnPS ₃ _Sn/Al..	145
Figure 7 28: Plot of I against V for ITO/PEDOT:PSS/PPV_VOPO ₄ /Al	146
Figure 7 29: Plot of Ln (I) against V for ITO/PEDOT:PSS/PPV_VOPO ₄ /Al.....	146

Chapter 8

Figure 8 1: Pd ₃ (PS ₄) ₂ Crystal Structure.	150
Figure 8 2: X-ray diffractogram of polycrystalline Pd ₃ P ₂ S ₈	153
Figure 8 3: Pd ₃ P ₂ S ₈ IR Spectrum (left) and Pd ₃ P ₂ S ₈ _Bipy IR Spectrum (right)	155
Figure 8 4: Pd ₃ P ₂ S (left) and Pd ₃ P ₂ S ₈ _ Bipy (right) Raman Spectra.	155
Figure 8 5: Variation of dark current and photocurrent with applied voltage at 690 nm.	156

Chapter 1:

INTRODUCTION

The use of conducting polymers as electroluminescent materials in large-area luminous displays has increased since the electroluminescence of poly (p-phenylene vinylene) (PPV) was first demonstrated in 1990. Since then, considerable research has taken place in an urge to overcome the main drawbacks that limit the uses of this conjugated polymer for technological applications, such as poor stability towards oxygen that can be trapped in the device. This results in the generation of excited singlet oxygen which has the capability to cause chain scission of the linear polymer or to cross-link between polymer strands, leading to loss of delocalisation. Both of these actions result in decreased conduction of the polymer, and dictate that polymer production must take place in the absence of oxygen, thus inflating production costs.

A possible solution to such problems is to synthesise composites containing the emissive polymer inside a lamellar-structured inorganic host that can accommodate molecules between its layers. The geometrical restrictions imposed by the inorganic host could result not only in an improved environmental stability but also in the formation of a more organised polymer chain that facilitates charge injection and charge transfer between conducting units.

This thesis reports the synthesis and characterisation of composites of this type.

The following chapter begins with a brief introduction to composites and their synthesis with the main emphasis on intercalation chemistry. This is followed by a description of the physical properties of the lamellar inorganic hosts and ends with an overview of conjugated polymers and their luminescent properties.

Chapter 3 describes the preparation and characterisation of luminescent poly (p-phenylene vinylene) (PPV). The technical specifications and instruments used for the spectral analysis are all described.

Chapter 4 focuses on the solid state synthesis of lamellar MPS_3 and their structural analysis mainly by x-ray diffraction. Other techniques used include SEM, IR and Raman spectroscopy. This chapter also includes the formation of intercalated composites and the respective spectroscopic analysis.

A modified method of preparing MnPS_3 at low temperature (solution approach) instead of the solid state synthesis is described in chapter 5.

Chapter 6 illustrates the synthesis and characterisation of $\text{VOPO}_4 \cdot 2\text{H}_2\text{O}$ as an alternative inorganic host. The intercalation reaction and the spectroscopic analysis of the resulting composites are all described there.

Chapter 7 assesses the optical and electrical properties of the final composites including optical absorption, emission spectroscopy, photodegradation studies, and two probe conductivity measurements. This chapter also describes the construction of Schottky type diodes and the performance under applied voltage.

Chapter 8 includes some exploratory work carried out on $\text{Pd}_3\text{P}_2\text{S}_8$. This material was of particular interest due to the photoconductive properties that were important for this work. Although intercalation was not achieved,

the results of structural characterisation and some photoconduction studies are shown in this chapter.

Lastly, chapter 9 outlines the conclusions and possibilities and proposals for future research stemming from this work.

Chapter 2:

LITERATURE REVIEW

2.1 Introduction to Composites and Nanocomposites

Composites are formed by combining two or more material phases that possess different physical or chemical properties. Since each individual component of the composite material retains its own characteristics, the final amalgamated product can acquire an array of attributes; hence composites can be lighter, stronger and more stable than their constituent parts.¹ This ability to tailor a material's property has made composites of great importance to engineering and materials science. It has been discovered that the useful electrical, optical and mechanical properties of materials of this kind can often be improved when they are prepared on the nanoscale (1-100 nm) giving rise to nanocomposites. Nanocomposite materials, just like normal composites, can be synthesised from metals, ceramics or organic materials.²⁻⁴ They can be formed as multilayer structures or in some cases, as organic-inorganic hybrids which have distinctive structures based on layered inorganic hosts which can easily accommodate organic guests by ion exchange in a process called intercalation.⁵⁻⁶ The use and preparation of nanomaterials has become a highly active area of research, applicable to a wide array of scientific enquiry such as energy conversion, water treatment, catalysis and regenerative medicine.

2.2 Composite Preparations

Intercalation of molecules into an inorganic host has been an efficient route to prepare nanocomposites. Small molecules can usually be directly intercalated into layered or porous lattices with minor effects on the host's structure; however, when it comes to incorporating polymers, a few synthetic challenges have arisen. Due to the greater size of polymers relative to small molecules, their rate of diffusion into the confined galleries of the hosts is much reduced. To overcome this problem a number of different methods to prepare intercalated polymer nanocomposites have been developed over the years.^{1,5-6}

2.2.1 Intercalation Chemistry

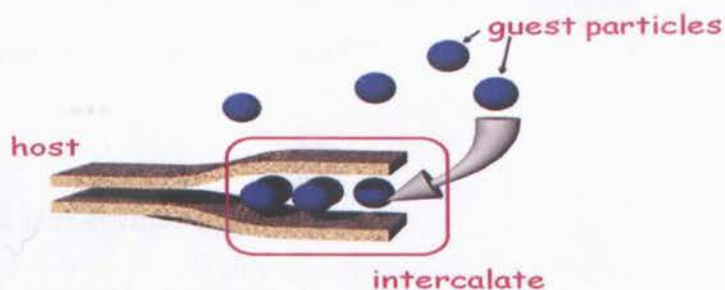


Figure 2 1: Schematic representation of intercalation.⁷

Intercalation is a reversible chemical process in which a guest species of an appropriate size occupies vacant space within a solid lattice formed by the host compound. A host material is required to have either a two-dimensional layered structure or a three-dimensional tunnelled structure with van der Waals gaps in between the structural units, where guest molecules can be accommodated. This type of reaction usually does not involve any bond rupture, but it requires a host lattice with strong covalent

network of atoms which remains unchanged on reaction, and vacant sites in the structure to permit diffusion of the guest species into the solid.⁵⁻⁶

The general reaction can be written as:



where \square represents a vacant lattice site.

In an intercalation process different types of interfaces can occur depending on the states of matter of the constituent parts, although the most common at room temperature is a solid – solid interface. It may happen that an increase in temperature results in a solid – liquid interface where the intercalate melts while the host remains rigid. Solid-gas interfaces have also been observed.⁵⁻⁶

2.2.1.1 Direct Intercalation

As mentioned before, direct intercalation usually occurs with small guest ions or molecules; however, there have been few cases where direct insertion of polymers such as poly(ethylene oxide) (PEO) into inorganic hosts such as montmorillonite has been possible by heating mixtures containing both starting compounds above the polymer's melting or glass-transition temperatures.^{1,8} This method is ideal in cases where the polymer is insoluble or the use of solvents is to be avoided. The actual mechanism is not very well understood; however, studies have shown that as the polymer is incorporated, the delamination of the host occurs which leads to an alternative method for the formation of nanocomposites by *exfoliation* of layered hosts.¹

2.2.1.2 Exfoliation-adsorption

This method has been widely used to intercalate water-soluble polymers into clay. The layered host is exfoliated and dispersed using solvents (usually water) forming colloidal suspensions containing individual host sheets. When the polymer solution is introduced, the polymer interacts with the host surfaces (adsorption). This interaction is maintained when the solvent is evaporated, giving rise to an organised multilayered structure. In cases where the polymer is not soluble, a similar approach can be used, by having the polymer dispersed in a solvent.¹

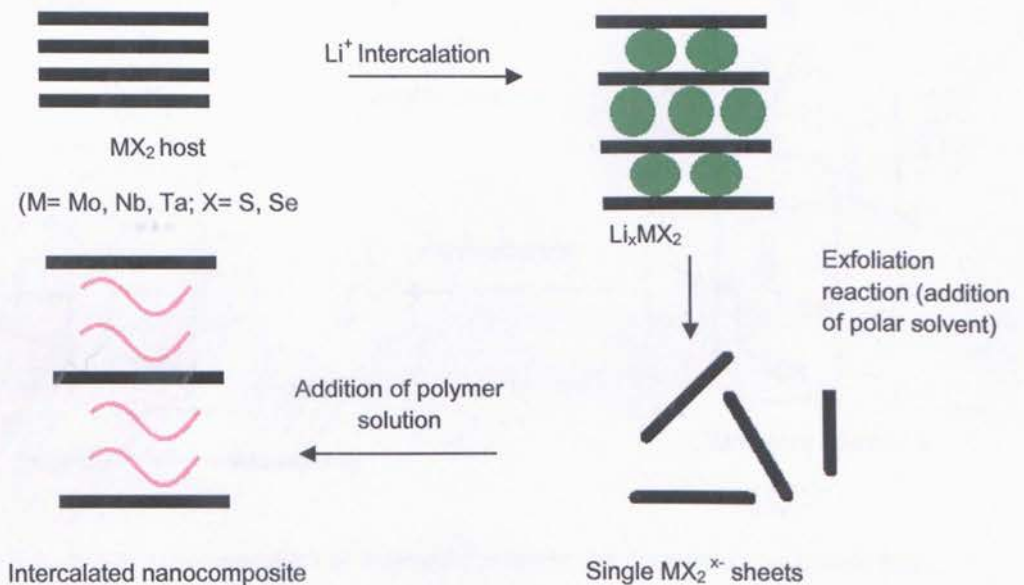


Figure 2 2: Preparation of nanocomposites by exfoliation-adsorption.¹

2.2.1.3 In-situ polymerisation

This method is particularly useful in cases where the monomers are soluble, but the final polymer is not. A precursor monomer is incorporated into the cavities of a layered host, followed by the *in-situ* polymerisation

within the host itself. In some cases polymerisation is achieved by using initiating agents in solution; in some others it can be done by ultraviolet irradiation, or alternatively the host itself can act as the polymerising agent. Although this method is ideal for the insertion of polymers and the formation of organised nanocomposites it is difficult to control their chain length and therefore the properties that it conveys such as electrical conductivity in the case of conjugated polymers.¹

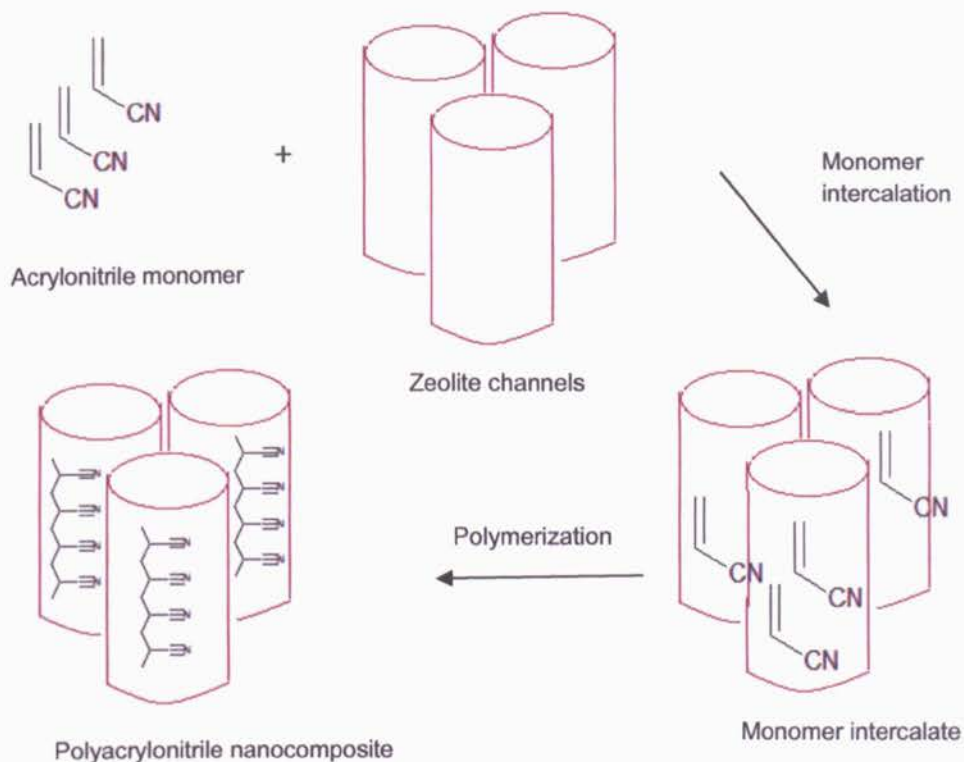


Figure 2 3: *In-situ* polymerization of acrylonitrile inside the channels of a zeolite host.¹

2.2.1.4 Thermal or chemical conversion

This method involves the incorporation of a precursor polymer or derivative of the desired polymer either by direct intercalation or exfoliation, followed by chemical or thermal conversion into the final polymer. An example of this method is the formation of nanocomposites

containing poly(phenylene vinylene) which is formed when films of its precursor polymer are heated above 230 °C.¹

2.3 Inorganic Host Structures

Ideal intercalation hosts normally possess lamellar lattice-type structures able to accommodate guest ions or molecules between their inter-layer sites. They also require strong in-plane bonding combined with weak interplanar bonding to allow the expansion of the interlayer gap. Graphite was the first material that was found to have a layered structure and, since then, a search for other potential host species has ensued.

Metallic oxides, for example, have been extensively used due to their fast redox kinetics as well as their low cost. MoO₃, WO₃, V₂O₅, MPS₃ compounds, clays, etc are among the extended list of inorganic host materials.⁴⁻⁶

Hosts can also be three dimensional tunnelled structures such as zeolites, which can incorporate small ions or polymers with linear backbone structures; however the polymer orientation and organisation is restricted by the pore size of the zeolites or tunnelled structures in general.^{1,5-6}

2.3.1 Layered inorganic hosts

Neutral Layers	
<i>Graphite</i>	
<i>Ni(CN)₂</i>	
<i>MX₂</i>	(M=Ti, Zr, Hf, V, Nb, Ta, Mo, W; X= S, Se, Te)
<i>MPX₃</i>	(M= Mg, V, Mn, Fe, Co, Ni, Zn, Cd, In; X= Se, S)
<i>MoO₃, V₂O₅</i>	
<i>MOXO₄</i>	(M=V, Nb, Ta, Mo; X= P, As)
<i>MOX</i>	(M= Ti, V, Cr, Fe; X= Cl, Br)
Negatively Charged layers	
<i>CaSi₂</i>	
	(A= group IA; M= Ti, V, Cr, Mn, Fe, Co, Ni; X= O, S)
<i>AMX₂</i>	
<i>Clays and layered silicates</i>	
<i>Titanates</i>	<i>K₂Ti₄O₉</i>
<i>Niobates</i>	
<i>M(HPO₄)₂</i>	(M= Ti, Zr, Hf, Ce, Sn)
Positively Charged layers	
<i>Hydrotalcites</i>	<i>LiAl₂(OH)₆OH.2H₂O, Zn₂Cr(OH)₆Cl₂.2H₂O</i>

Table 2.1: Layered structures for intercalation.⁶

The main advantage of layered hosts is their ability to accommodate large molecules interstitially by adjustment of their interlayer separation. Their layers can be neutral, negatively or positively charged; in cases where the layers are neutral, van der Waals forces hold the layers together. However if the layers are charged, the lattice is held together by electrostatic forces with the interlayer spaces filled or partially filled by counter ions.^{6,9} Depending on the host, different types of reactions can occur. In the case of clays for instance, ion exchange may take place where the charge of the layers remains unaltered, but compounds containing transition metals can undergo redox reactions, where the host is either oxidised or reduced

and the overall charge balance is maintained by intercalation or deintercalation of ions or molecules.^{6,10} Some examples of the main layered hosts are given in Table 2.1.

2.3.1.1 Metal Phosphorus Trisulphides (MPS₃)

Layered compounds of formula MPS₃ where M = Mn, Fe, Zn, Ni and Cd have been widely used for intercalation purposes; they can be prepared by direct combination of the pure elements at temperatures above 600°C.⁵ Their crystal structure is made up of M²⁺ ions with P₂S₆²⁻ bridging ligands in a hexagonal arrangement where the P-S bond distance is constant (2.032 Å) but the P-P bond distance varies depending on the size of the M²⁺ cation (see Figure 2.4). MPS₃ compounds exhibit a variety of properties depending on the transition metal present. They can be insulators or semiconductors depending on their band gap and some of them possess magnetic properties due to the high spin octahedral cations.¹¹

2.3.1.1.1 MnPS₃ and CdPS₃

These materials have attracted much attention due to the variety of properties they possess. They are mechanically and thermally stable, optically transparent and can undergo reversible intercalation reactions based on cation exchange between host and guest where M²⁺ (Mn, Cd) ions are lost to maintain the electrical charge balance of the lattice.^{5-6,8-9} The structure also allows the intercalation of small ions such as alkali metal cations with a minimum interlayer space variation, making them a good option for the preparation of low-cost, high energy density batteries. Furthermore, the guest species can be ion-exchanged for other cationic

guest species, thus making it possible to obtain a variety of intercalation compounds.^{8-9,11-13} The electrical properties of these materials have been extensively studied, with work by Grasso *et al* (1989)¹⁴ suggesting that the 3d orbitals have little to do with the overall arrangement of the electronic levels and that the valence and conduction bands originate from the $P_2S_6^{4-}$ cluster orbitals. $MnPS_3$ is catalogued as a wide band gap semiconductor (3.0 eV) whereas $CdPS_3$ is an insulator (3.5 eV).

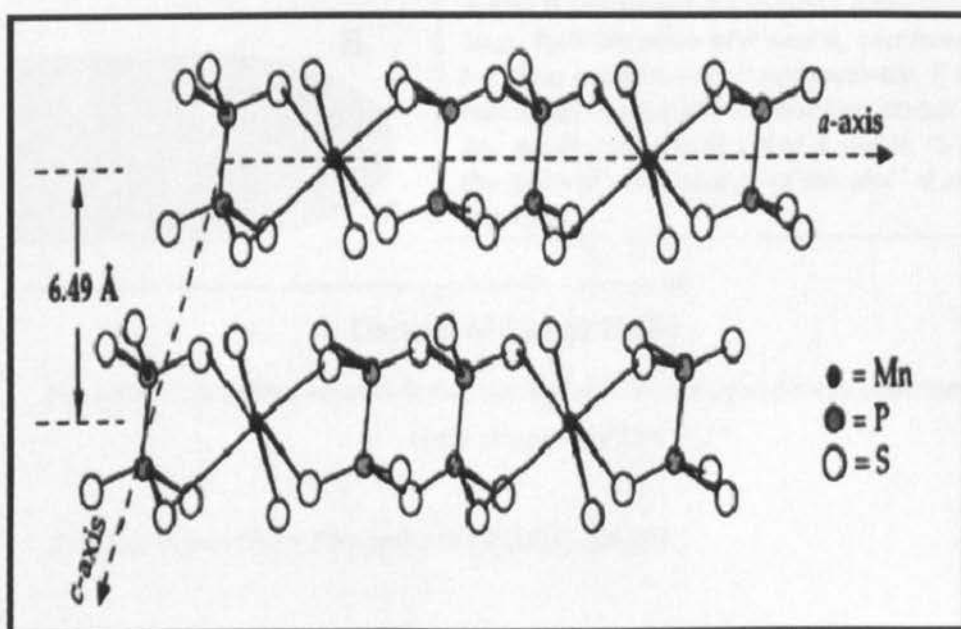


Figure 2 4: $MnPS_3$ Crystal Structure.⁵

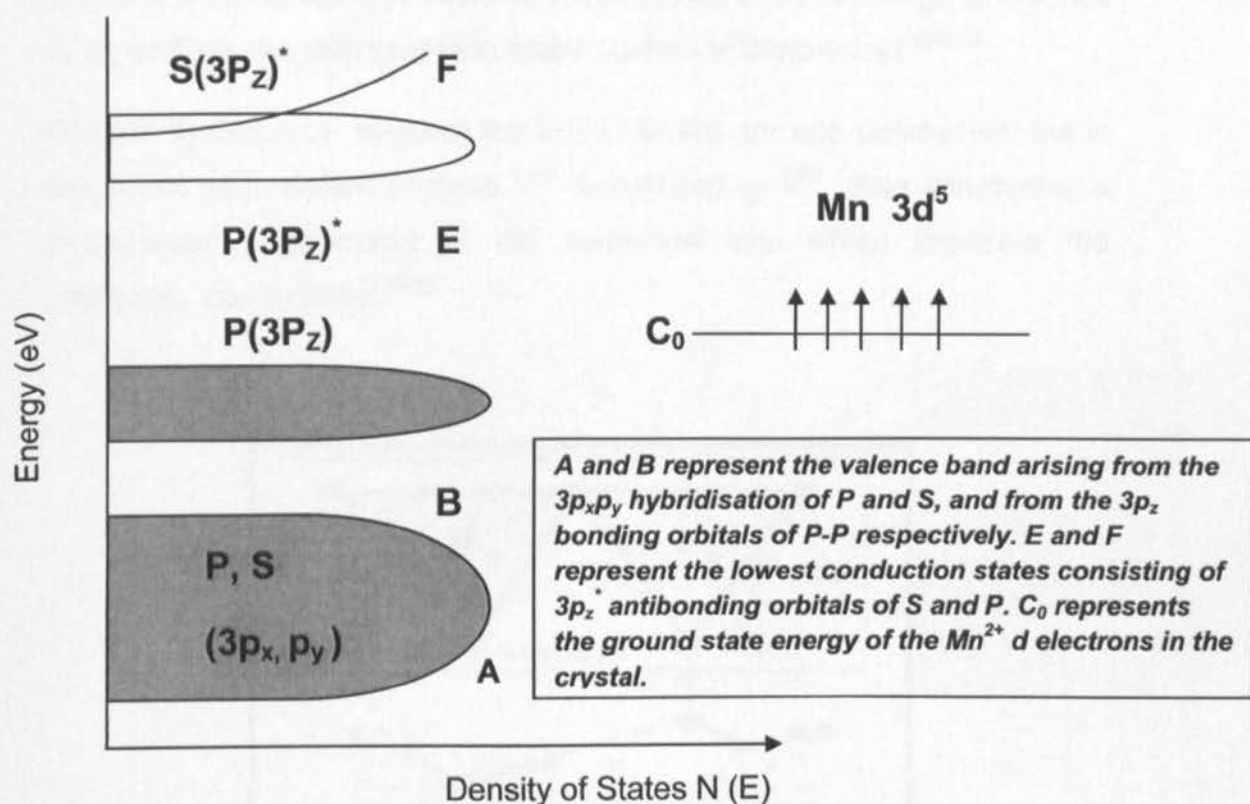


Figure 2.5: Simplified version of the energy level scheme adopted to describe the electronic band structure of MnPS_3 .¹⁴

2.3.1.2 Vanadium Phosphate ($\text{VOPO}_4 \cdot 2\text{H}_2\text{O}$)

The layered structure of this compound consists of distorted chains of VO_6 octahedra and PO_4 tetrahedra linked by corner sharing oxygen atoms; see Figure 2.6. The most stable phase under ambient conditions is $\text{VOPO}_4 \cdot 2\text{H}_2\text{O}$ where one water molecule is coordinated to the vanadium atom and the other one is held within the interstitial space. This material can intercalate molecules by a redox mechanism in which V^{5+} is reduced and a charge-compensating cation is introduced into the interlayer space. The redox intercalation process occurs according to the reaction:



where x is the amount of intercalated cation M , z is the charge or valence of M , and y is the change of the water content in the product.^{6,10,15}

Studies by Sukanta suggest the V-P-O layers are non conductive, but in the redox intercalation process V^{5+} is reduced to V^{4+} , thus introducing a mixed-valence behaviour of the vanadium ions which improves the electronic conductivity.¹⁴⁻¹⁶

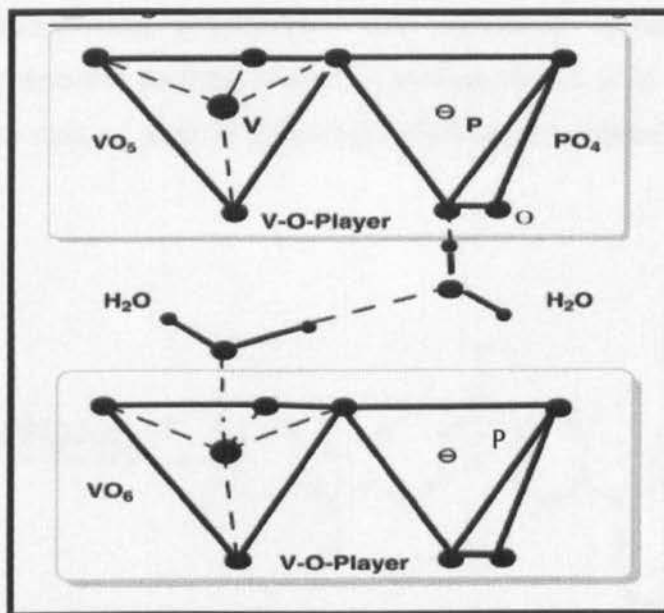


Figure 2 6: $VOPO_4 \cdot 2H_2O$ Crystal Structure.¹⁶

2.4 Organic Guest Molecules

Many different organic molecules can be inserted in the interstitial spacing of inorganic host matrices. However, the main focus of this investigation was the incorporation of conducting polymers, particularly the insertion of poly(p-phenylene vinylene) (PPV).

2.4.1 Conducting Polymers: A Brief Introduction

2.4.1.1 History

The study of conducting polymers dates back to the 19th century when the oxidative polymerization of aniline by nitric acid was first reported. During this time aniline was important in the synthesis of many dyes associated with the Victorian era. Despite the concept of linear polymerisation not being fully understood, polyaniline was somehow synthesised in the 1860s; it was reported as the product of aniline oxidation in acidic medium and hence the role of acid in effecting its electrical conductivity was first discovered.¹⁷

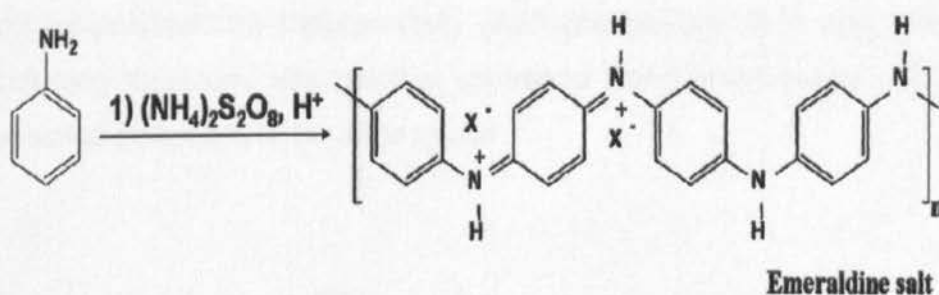


Figure 2 7 Oxidative polymerization of aniline carried out in acidic conditions¹⁷

Since then, the synthesis of oligomers and polymers of pyrrole, thiophene and other heterocycles has been reported. Despite the poor characterization of these materials it became commonplace to measure their electrical conductivity.

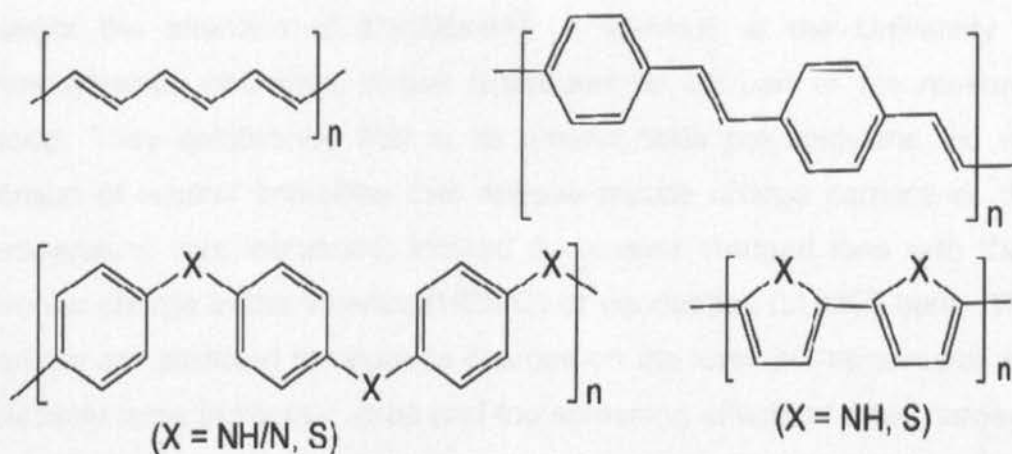


Figure 2 8: Some conducting polymers.¹⁷

In the late 1960s, Wegner showed that single crystals of diacetylenes could be polymerized topotactically (their original structure was retained) introducing structural studies that permitted bond lengths and angles in conducting polymers to be determined.¹⁷

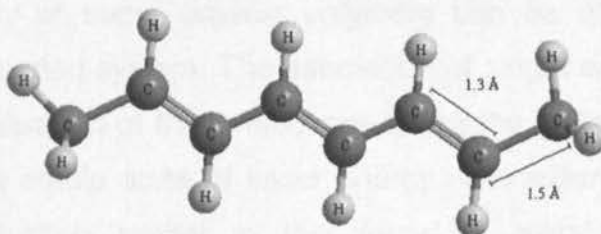


Figure 2 9: Conjugated polyacetylene.¹⁷

Later on in the 1970s, while studying the Ziegler-Natta polymerisation of acetylene Shirakawa found that with high concentrations of about 1 mol.dm^{-3} of a particular organometallic catalyst, when acetylene gas was bubbled through the solution a silvery conducting film of polyacetylene was deposited on the walls of the reaction vessel.¹⁷⁻¹⁸ This discovery

caught the attention of MacDiarmid, a scientist at the University of Pennsylvania, who then invited Shirakawa to be part of his research group. They established that in its ground state polyacetylene did not consist of neutral impurities that release mobile charge carriers as the temperature was increased; instead it contains charged ions with their counter charge in the valence (HOMO) or conduction (LUMO) band. The carriers are attracted to opposite charges on the ions, but because of the relatively large molecular sizes and the screening effects of other carriers, the binding energy is relatively low and at room temperature the carriers are quite mobile. This theory provided the foundations of the development of conducting polymers and since their publication in 1977 an increase in the research and development of new and better materials has been observed. Heeger, MacDiarmid and Shirakawa were awarded the Nobel Prize for Chemistry in 2000 for their contribution to the development of conducting polymers.¹⁷⁻¹⁸

2.4.1.2 How do conductive polymers work?

The conductivity of some organic polymers can be attributed to their conjugated π -bonded system. The alternation of single and double bonds provides delocalisation of the π -electrons along the molecule, and brings them to a more stable state of lower energy. The extended conjugation produces a situation similar to that found in metals and inorganic semiconductors, while in inorganic materials the atomic orbitals combine to form continuous bands;¹⁹ in conjugated polymers it is the π and π^* orbitals of the conjugated bonds that combine.²⁰ As the degree of conjugation increases, the number of π orbitals that combine becomes so large that the energy between the new molecular orbitals becomes negligible, resulting in the formation of broad energy bands and a band gap just like those in inorganic semiconductors. The highest energy

occupied band is the valence band and the lowest unoccupied band is the conduction band.²¹

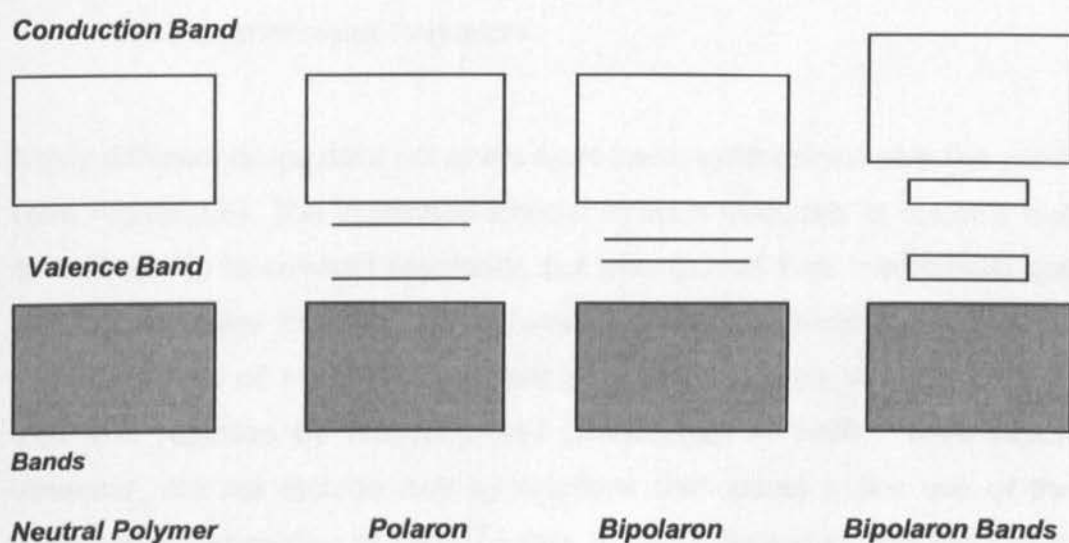


Figure 2 10: Variation of the band structure upon doping conjugated polymers.²⁰

The addition (or removal) of electrons to or from the delocalised π -system makes the polymer an ionic unit rather than neutral; this process is called doping and can be achieved through oxidation or reduction. It is known that when an inorganic semiconductor is doped with impurities, the formation of acceptor levels above the valence band or donor levels below the conduction band takes place.²¹ However this model cannot be applied when it comes to conductive polymers. When electrons are added or removed, a radical ion is formed in some part of the polymer chain and since this new charged species is now localised, an unfavourable lattice distortion is generated where the local geometry is of higher energy.^{18,20} These new species are called polarons, and they can either be cationic or anionic radicals. Upon further doping, the addition or removal of a second electron gives rise to bipolarons.^{18,20-21} Those species form localised levels between the valence band and the conduction band and when the polymer is highly doped, there are bipolaron levels formed close to the

conduction and valence bands, forming partially-filled bands which are similar to the ones in metals.^{18,20}

2.4.2 Luminescent Polymers

Many different conjugated polymers have been synthesised over the years (see Figure 2.8). The increased interest in such materials is not only due to their ability to conduct electricity, but also due to their mechanical and optical properties including electroluminescence and photoluminescence. The synthesis of electroluminescent poly (p-phenylene vinylene) (PPV) was first reported by Wessling and Zimmerman in 1968. Their report however, did not include any applications that would make use of the luminescent properties of PPV.²² Later, in 1983, Partridge was the first to outline the synthesis and characterisation of some electroluminescent polymers and the possible advantages they could have over their inorganic counterparts²³. Then, in 1990 a research group led by R. Friend in Cambridge discovered the luminescent properties of poly(phenylene vinylene). This discovery led to the development of device structures such as polymer light-emitting diodes (PLEDs) using PPV as the emissive layer.²⁴ Since then, interest in such technologies has rapidly increased due to the advantages they present over more traditional inorganic alternatives. These advantages include the easier and therefore less expensive manufacturing process, the possibility of producing thin films that can be coated on flexible surfaces for use in panel displays and lighting, as well as the lower operational energy consumption.²⁵

2.4.2.1 The principles of Luminescence

Luminescence is the emission of photons from electronically excited species. The term luminescence was first introduced to describe "the phenomena of light which are not only conditioned by the rise of

temperature”, as opposed to incandescence. Luminescence is *cold* light whereas incandescence is *hot* light.²¹ The different types of luminescence are classified according to the mode of excitation (see Table 2.2), for example, in fluorescence and phosphorescence the mode of excitation is by absorption of a photon, which brings the absorbing species into an electronic excited state, in the case of electroluminescence, electrons are excited when an electric field is applied,²⁶ however, this work is only concerned with *fluorescence*.

Type of Luminescence	Mode of excitation
Photoluminescence (Fluorescence, phosphorescence)	Absorption of light (photons)
Radioluminescence	Ionizing radiation (X-ray, α , β , γ)
Cathodoluminescence	Cathode rays (electron beams)
Electroluminescence	Electric field
Thermoluminescence	Heating after storage of energy (e.g
Chemiluminescence	radioactive irradiation)
Bioluminescence	Biochemical process
Sonoluminescence	Ultrasounds

Table 2.2 Types of Luminescence, taken from Molecular fluorescence principles and applications.²⁶

Fluorescence

As previously mentioned, fluorescence is the emission of light by a substance that has been excited by absorption of a photon of light.

Absorption of light

When a molecule is irradiated with light of a suitable wavelength, the absorption of a photon will promote an electron from its ground state energy level to an unoccupied orbital. The molecule is then said to be in an excited state.^{21,26} In the case of molecules containing C=C units (formed by a σ and a π bond), the absorption of a photon of appropriate energy can promote one of the π electrons to an antibonding orbital denoted π^* . This is called a π - π^* transition. The promotion of a σ electron to a σ^* requires a lot more energy, and therefore this transition is only seen in the far UV. Transitions involving non-bonding electrons can occur in the case of molecules containing atoms such as oxygen or nitrogen, as in the case of formaldehyde. The diagram below (Figure 2.11) illustrates the energy levels and possible transitions of formaldehyde as an example.

In molecules such as formaldehyde containing bonding and non bonding orbitals, the electrons are localised between pairs of atoms. Localisation of electrons also occurs in σ orbitals of single bonds and in π orbitals of isolated double bonds.

In the case of conjugated molecules, the overlap of π orbitals permits the delocalisation of electrons over the whole molecule, lowering the overall energy of the molecule, and decreasing the energy required for a π - π^* transition, this results in the absorption of longer wavelength light.²¹⁻²⁶

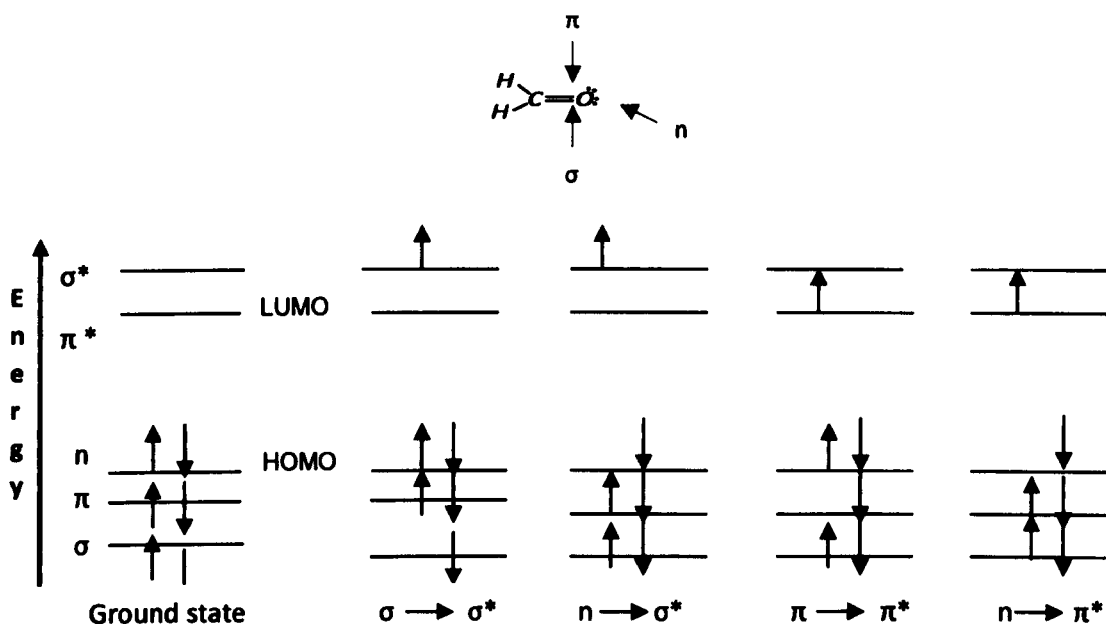
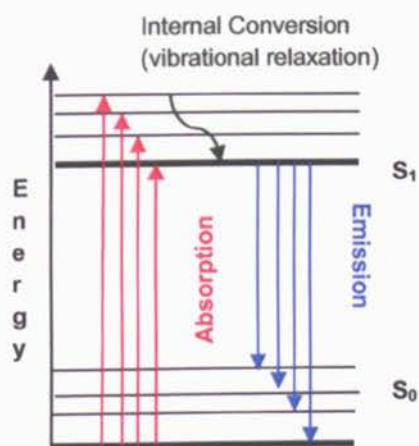


Figure 2 11: Energy levels of molecular orbital in formaldehyde (HOMO: Highest Occupied Molecular Orbital; LUMO: Lowest Occupied Molecular Orbital and possible electronic transitions.²⁶

Emission of Light

After the absorption of light, a molecule is in an excited state of higher energy. This excited state is short-lived and will quickly decay back to the ground state by emission of a photon. Absorption of a photon can bring electrons to an energy level higher than the lowest vibrational level of the first electronic state. Before emission can take place, electrons are relaxed to the lowest vibrational level via non-radiative process, resulting in the emission wavelength being longer than the absorption wavelength.²⁶

A Jablonski diagram (Figure 2.12) is used to illustrate the process and transitions that occur during fluorescence.



The first transition takes place upon light absorption and is from the ground singlet state (S_0) to the first excited singlet state (S_1). This is followed by vibrational relaxation in which some of the excitation energy is converted to vibrational energy and lost as heat. Once the lowest vibrational energy level associated with the excited state is reached, electrons return to the ground electronic state (S_0) by emitting a photon.

Figure 2.12: A Jablonski diagram showing the energy transitions that take place during fluorescence.²¹

2.4.2.2 Common Luminescent polymers

Polymers including polythiophenes, polyfluorenes and poly(phenylene vinylene) are amongst the group of polymers that have been highly investigated due to their luminescent properties. Moreover, modifications made to the backbone can lead to improvements on the chain ordering and therefore on their electronic properties such as charge mobility. Addition of electron donating groups, such as alkoxy group, results in a reduction of the energy band gap leading to a red shift of the emitting light. On the other hand, addition of electron withdrawing groups will lead to an increase in the energy gap and therefore will shift the emission wavelength towards the blue region.²⁷ Additionally, electron withdrawing groups are also known to increase the ease of electron injection into the polymer and

the mobility of electrons in the devices containing the substituted polymer.²⁷⁻²⁹

Poly (p-phenylene vinylene) (PPV)

PPV is one of the most studied electroluminescent conductive polymers. It exhibits bright yellow-green fluorescence with an emission maximum at 551 nm (2.25 eV) which makes it a promising candidate for light-emitting diodes. Its conductivity is enhanced upon oxidation, which creates radical cations making it a p-type semiconducting polymer. Many synthetic pathways have been developed in order to improve the properties of PPV. However, there are still several problems limiting the applications of this luminescent polymer. It is insoluble and thus intractable: furthermore polymer light-emitting devices become more unstable with time as they are susceptible to oxygen and moisture which often results in the formation of cross links between polymer strands, leading to loss of delocalisation, hence decreasing the conductivity of the polymer.^{17,20,23}

Chapter 3:

SYNTHESIS AND CHARACTERISATION OF POLY(P-PHENYLENE VINYLENE) (PPV)

PPV can be synthesised by a variety of direct routes that can achieve high molecular weight polymers with good optical and electronic properties. The main disadvantage of the polymers produced by those routes is that in most cases they are insoluble and therefore unusable for practical applications. This has led to the development of alternative routes that involved the formation of intermediate processable polymers that could be later converted into PPV.³⁰

3.1 Reagents and instruments used

The materials used for the synthesis of poly (p-phenylene vinylene), their grades and suppliers are all given in Table 3.1. All chemicals were used without further purification.

Material name	Grade	Supplier
α,α' -Dichloro-p-xylene	97 %	Sigma-Aldrich
Tetrahydrothiophene	99 %	Sigma-Aldrich
Methanol	Analar grade	VWR International
Acetone	99.5 %	VWR International
Sodium hydroxide pellets	99.0 %	VWR International
Conc. hydrochloric acid	37 %	Fisher Scientific
Dialysis tubing cellulose membrane (12400 Da)	-	Sigma-Aldrich

Table 3.1 Details of materials used for the synthesis of poly(p-phenylene vinylene).

3.1.1 Infrared spectroscopy

Attenuated total reflection infrared (ATR-IR) spectroscopy was carried out on powder samples in the case of the monomer and on coated quartz slides in the case of the polymers using a Thermo Scientific Nicolet IS5 iD5 ATR, 16 scans, over the range 650-4000 cm^{-1}

3.1.2 Absorption Spectrometry

UV-visible spectroscopy of the solid polymer films was carried out on coated quartz slides, using a Cary 100 Bio, UV-visible spectrophotometer over the range 300-650 nm.

3.1.3 Photoluminescence Studies

Fluorescence spectroscopy was carried out on films coated on quartz slides positioned at an incident angle of about 60 degrees to limit direct reflection from the quartz slides, using a Varian Cary Eclipse Spectrophotometer over the range 300-800 nm.

3.1.4 Nuclear Magnetic Resonance (NMR)

NMR spectra were recorded on a Jeol Eclipse 400 NMR spectrometer (400 MHz for ^1H and 100 MHz for ^{13}C) with Jeol Delta version 4.3.6. control and processing software. Chemical shifts were reported in parts per million and referenced to residual solvent proton resonances calibrated against external TMS.

3.1.5 Polymer Molecular weight

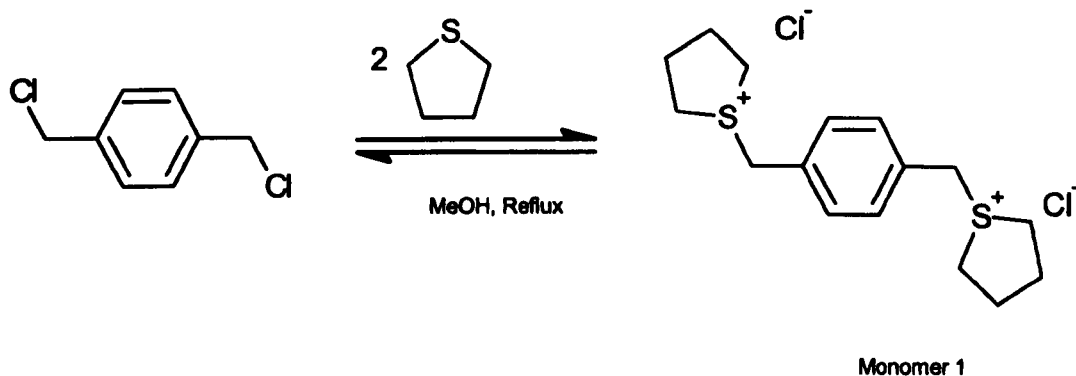
The average polymer molecular weight was estimated using viscometry analysis using an aqueous solution of poly (vinyl alcohol) (PVA) as the standard.

3.2 Synthetic Route

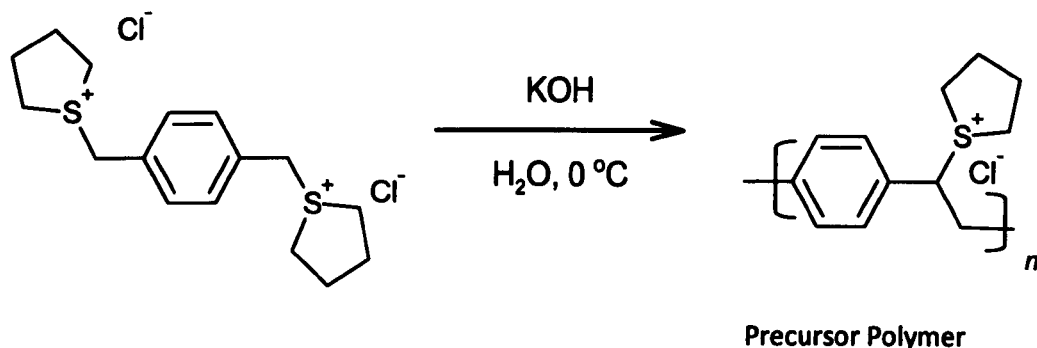
The best known and perhaps the most used precursor route to PPV is the thermoconversion route proposed by Wessling and Zimmerman²² which involves a three-step reaction mechanism and was the one used on this project as follows:

Step 1: Synthesis of p-xylene-bis(tetrahydrothiophenium chloride) monomer (monomer 1)

α,α -dichloro-p-xylene (6.60 g, 0.04 mol) was dissolved in methanol (50 ml). Then tetrahydrothiophene (9.0 ml) was added to it and the solution was refluxed for 18 hours, after which the monomer was precipitated with cold acetone (300 ml, 0 °C). The white precipitate was then filtered off, washed with cold acetone and dried in air for 24 hours. Finally it was dried in the vacuum oven at 60 °C for 24 hours. The product was white and crystalline and highly hygroscopic; yield after drying 6.24 g (47%)



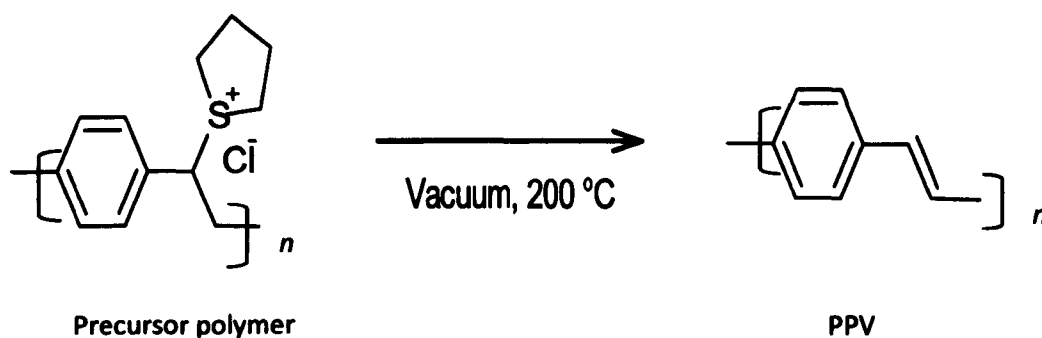
Step 2: Synthesis of poly (p-xylylene-bis(tetrahydrothiophenium chloride) (precursor polymer)



The success of this reaction depends on the existence of an oxygen-free environment throughout the whole reaction; therefore all the chemicals were thoroughly degassed prior to use. In the case of solvents (H_2O or CH_3OH) a freeze-thaw method was used.

The precursor polymer was prepared by addition of aqueous KOH (25 ml, 0.2M) into an aqueous solution of monomer 1 (25 ml, 0.2M). Both solutions were cooled down to $0\text{ }^\circ\text{C}$ before mixing. The reaction was carried out at $0\text{ }^\circ\text{C}$ for 1 hour and was terminated by addition of sufficient cold aqueous HCl (1M) to neutralise the reaction mixture. A viscous cloudy solution was obtained. This solution was dialysed against H_2O (3 x 2L) for three days (making sure that the solution was protected from light) to remove ionic or low molar mass organic impurities. The final solution was colourless and viscous and presented blue fluorescence under a UV lamp (long wavelength range). This solution was stored at $-24\text{ }^\circ\text{C}$.

Step 3: Thermal elimination to form PPV

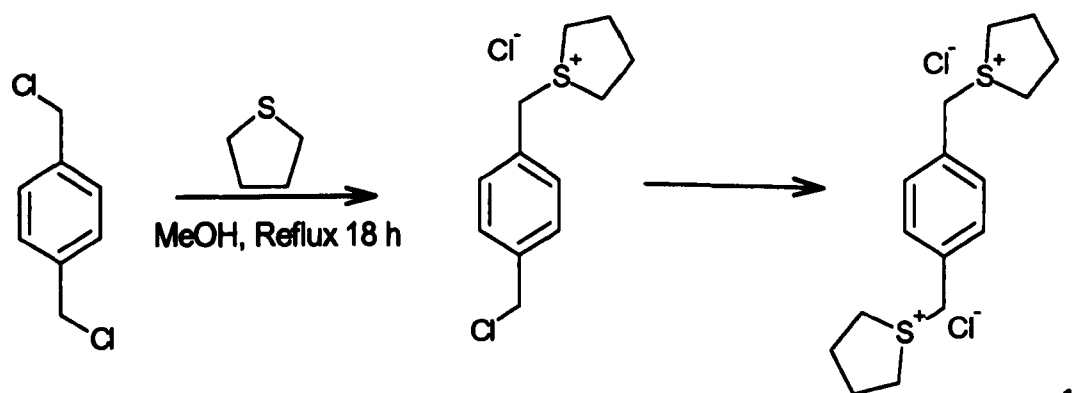


Quartz slides were coated with PPV precursor polymer solution. The slides were dried in air (protected from light) and then heated under vacuum at 200 °C for 6 hours. The final PPV films were yellowish-green and presented green fluorescence under a long wavelength range UV lamp.

3.3 Results and Discussion

3.3.1 Reaction mechanism

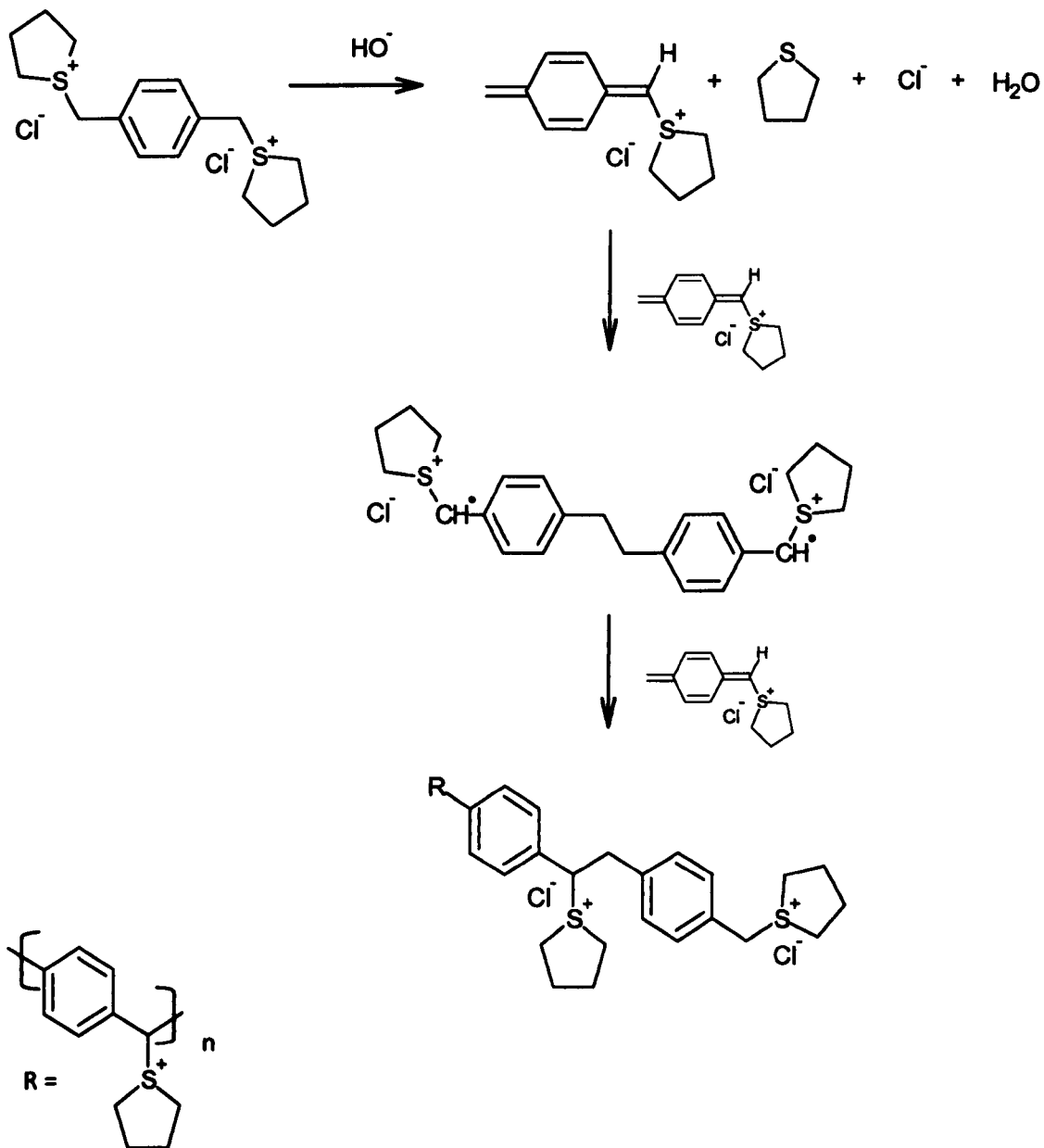
Step 1: Synthesis of p-xylylene-bis(tetrahydrothiophenium chloride) monomer (monomer 1) by a S_N2 mechanism:



1

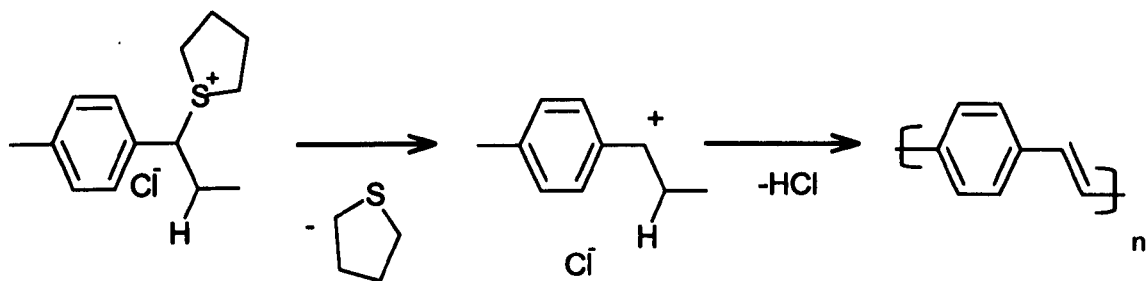
Step 2: Polymerisation reaction

The polymerisation reaction took place via a radical mechanism which involved the formation of a quinoidal intermediate, followed by radical initiation and propagation leading to polymerisation^{22, 31-32}

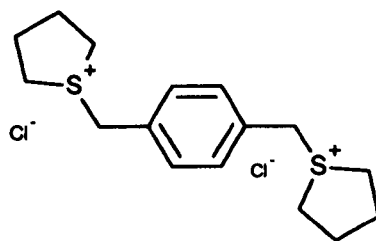


Step 3: Thermal elimination

The final step was the thermally induced elimination of the tetrahydrothiophene and hydrogen chloride to yield PPV by an E1 mechanism.³²

**3.3.2 Nuclear Magnetic Resonance (NMR)**

NMR was only carried out on the monomer using deuterated methanol as a solvent. Other techniques were used to characterise the polymers.



^1H NMR (400 MHz, METHANOL- d_4): δ 7.67 (s, 4H, Ar), 4.61 (s, 4H, ArCH_2), 3.39 - 3.60 (m, 8H, tetrahydrothiophene), 2.18 - 2.47 (m, 8H, tetrahydrothiophene) ppm.

^{13}C NMR (101 MHz, METHANOL- d_4): δ 133.0, 132.7, 46.6, 44.3, 29.8

3.3.3 Infrared Spectroscopy

The infrared spectrum of the monomer 1 confirmed the substitution reaction, (Figure 3.1). A stronger alkyl C-H stretching band at 2978 cm^{-1} due to the presence of the tetrahydrothiophene rings was observed. Furthermore the band around 755 cm^{-1} characteristic of the C-Cl bond had almost vanished whilst the strong band at 850 cm^{-1} due to the *para*-substituted ring was shifted towards higher energies (to 877 cm^{-1}) indicating the changes of the substituents on the ring. The peaks at 1511 and 1249 cm^{-1} are characteristic of the symmetric C=C stretching vibrations and the C-H in plane bending modes of the aromatic rings respectively. The monomer was highly hygroscopic; hence the strong peaks around 3500 and 1630 cm^{-1} , characteristic of water. After polymerisation had taken place, a shift in the peak indicating *para*-substitution, now at 827 cm^{-1} was observed, see Figure 3.2. In addition, partial conversion of the precursor polymer into PPV also occurred, as confirmed by the formation of a strong peak at 959 and 3021 cm^{-1} characteristic of the bending and stretching *trans*-vinylene C-H out of plane respectively.

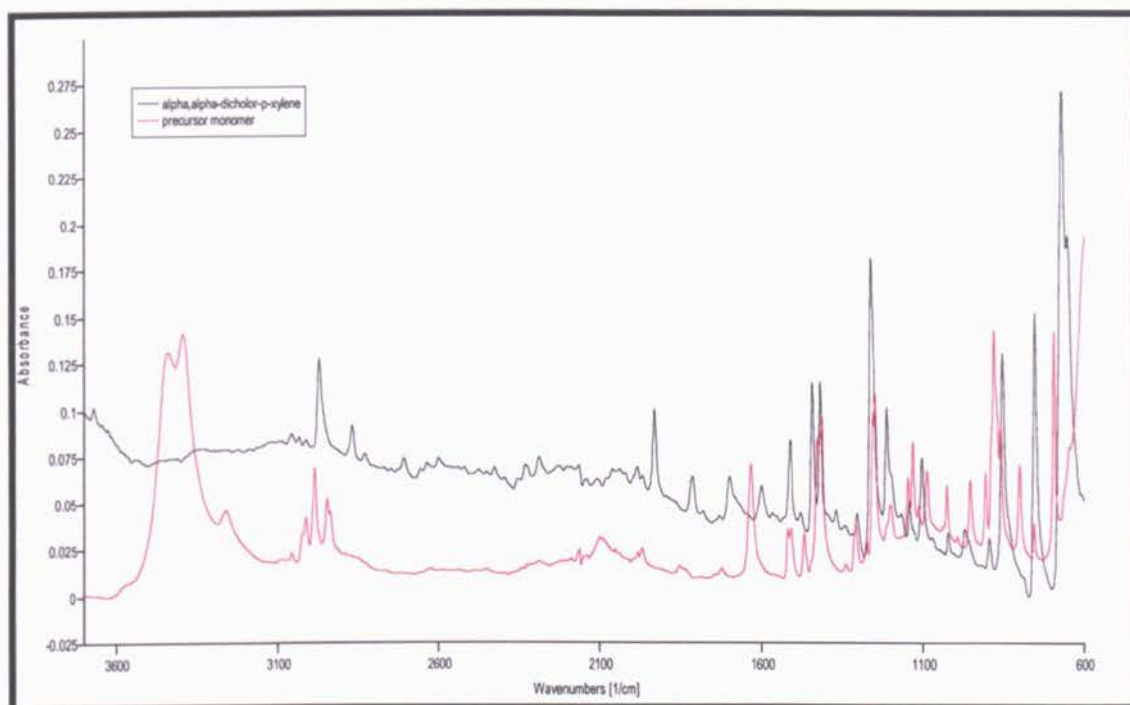


Figure 3 1: α,α' -Dichloro-p-xylene and p-xylene-bis(tetrahydrothiophenium chloride) (monomer 1) IR spectra in the region 3500- 500 cm^{-1}

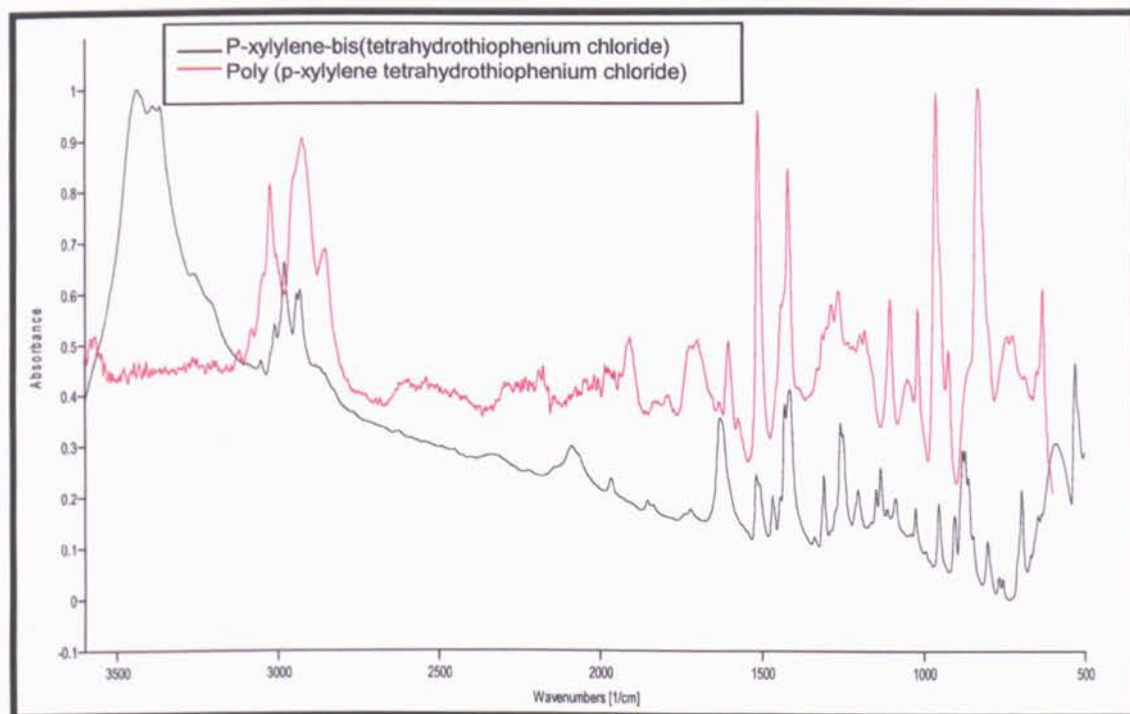


Figure 3 2: P-xylene-bis(tetrahydrothiophenium chloride) and Poly (p-xylene tetrahydrothiophenium chloride) IR spectra in the 3500-500 cm^{-1} region.

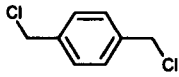
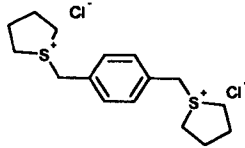
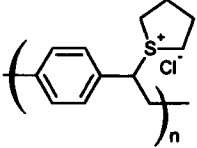
Vibrations			
Aromatic C-H stretching	3056 (w)	3056 (w)	3079 (w)
Trans-vinylene C-H stretching	-----	-----	3021 (s)
sp ³ C-H stretching (aliphatic)	2968(s)	2984 (s), 2945 (w)	2928 (s), 2847 (w)
Aromatic C=C stretching	1514 (m)	1511 (m)	1508 (s)
Aromatic C-H in plane bend	1266 (s)	1249 (s)	1269 (m)
Trans-vinylene C-H out of plane bend	-----	-----	959 (s)
Benzene Para-substituted	849(s)	877 (s)	827 (s)
C-Cl	755 (s)	758 (w)	735 (w)

Table 3.2. Experimental IR Vibrational frequencies (cm⁻¹) and assignments for α,α dichloro-p-xylene, monomer 1 and precursor polymer (PP). Note the strength of the band is assigned by w = weak, s = strong, m = medium.

3.3.4 UV-vis Absorption spectroscopy

This technique was used in order to gather information regarding the extent of π -orbital overlap, and hence the extent of the conjugation of the PPV backbone.

As reported by Halliday *et al* (1992),³³ the energy of the delocalised π - π^* transition in the absorption spectra depends on the conjugation length of the polymer backbone. Chemical defects, including saturated units and structural defects such as twisting on the polymer backbone can cause a reduction of the chain length due to the poor overlap of the p_z (π) orbitals.

The UV-visible spectrum of the sulfonium precursor polymer is shown in Figure 3.3. The λ_{\max} was around 345 nm (3.59 eV) and it was close to the values found in the literature.³³⁻³⁴ Other absorption peaks observed at lower energies (red shift) indicated that a small amount of conjugation was also present due to the partial conversion of the precursor polymer, under environmental conditions, into PPV; this explained the appearance of some of the PPV bands in the IR spectrum of the sample.

After the sulfonium precursor polymer had been thermally converted into PPV, a red shift in the λ_{\max} , to 400 nm (3.1 eV), was observed. This indicated lower energy π - π^* transitions, due to the formation of chain segments with longer conjugation.³⁵⁻³⁶ Studies on phenylenevinylene oligomers have shown that as the conjugated electron system elongates, the absorption maxima shifts towards the red part of the visible spectrum.³⁷ Moreover, Tian *et al* concluded that the effective conjugation length was no longer than 10 units.³⁷

An experimental energy band gap of 2.39 eV was calculated from the absorption edge of the π - π^* transition peak. Other small absorption shoulders were also observed at 458 (2.70 eV) and 497 nm (2.49 eV) characteristic of phenylene-based conjugated polymers which usually present multiple absorption features in the ultraviolet/visible region.³⁸

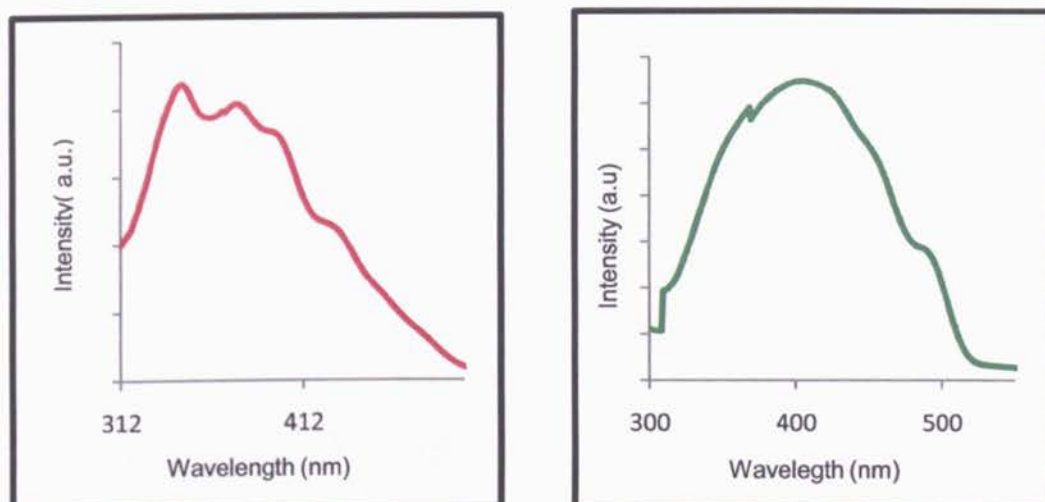


Figure 3.3: Sulfonium precursor polymer (left) and PPV (right) UV-visible showing λ_{\max} at 345 and λ_{\max} at 400 nm respectively.

Sample	λ_{\max} (nm)	E (eV)
<i>Precursor polymer</i>	345	3.59
	375	3.30
	401	3.09
	427	2.90
<i>PPV</i>	400	3.10
	458	2.71
	497	2.49

Table 3.3 UV-visible absorption wavelength of precursor polymer and PPV and the energy associated with it.

3.3.5 Fluorescence Spectroscopy

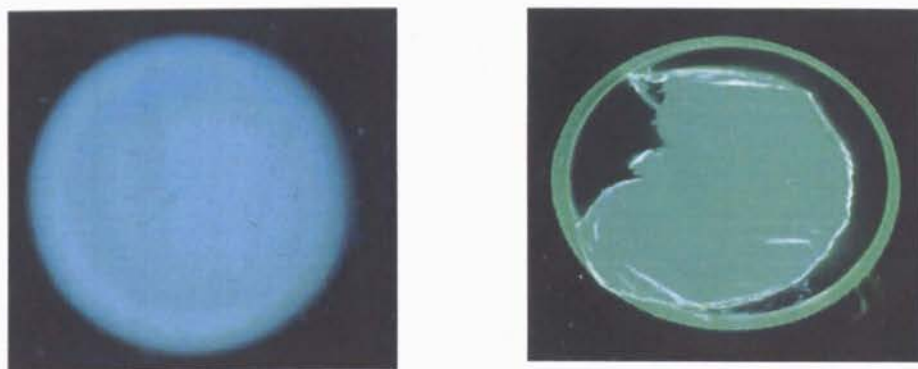


Figure 3.4: Fluorescence under a long range UV lamp of precursor polymer (left) and PPV (right).

The sulfonium precursor polymer was colourless and highly viscous, and when placed under UV light (long range UV lamp) it presented blue fluorescence (see Figure 3.4). When excited at 340 nm (UV-vis λ_{max}), the luminescence spectra displayed two emission peaks with maxima at 500 and 532 nm. The thermal elimination of the sulfonium groups led to a gradual red shift in luminescence with respect to the precursor polymer. Again, this was a confirmation of the formation of π -conjugation along the polymer backbone.

The three main features on the emission spectrum (Figure 3.5), 515, (2.40 eV), 544 (2.27 eV) and 593 nm (2.09eV), are associated with vibronic transitions 0-0, 0-1, and 0-2 respectively. These transitions are most commonly seen in the UV-visible spectrum at early stages of the conversion of the precursor polymer and are associated with the vibrational modes in the excited state;^{37,39} however, in this particular case, these transitions were more clear in the emission spectrum.

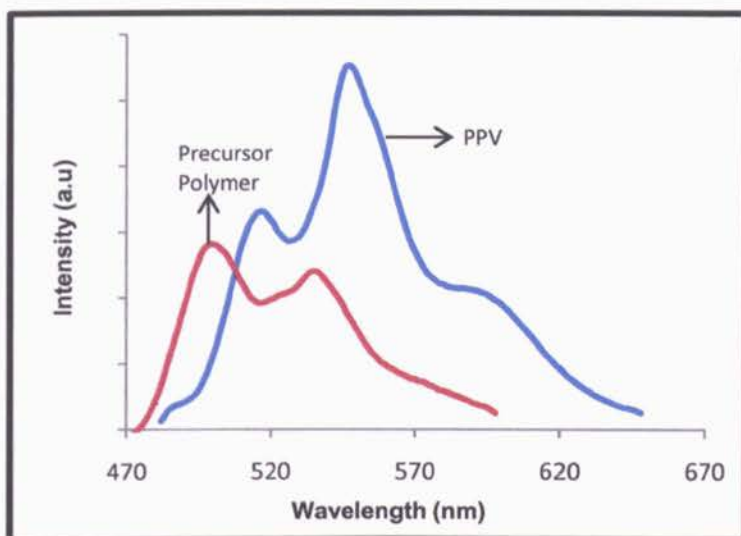


Figure 3 5: Emission spectrum of precursor polymer (red). Observed red shift on the emission spectrum after thermal conversion to PPV (blue).

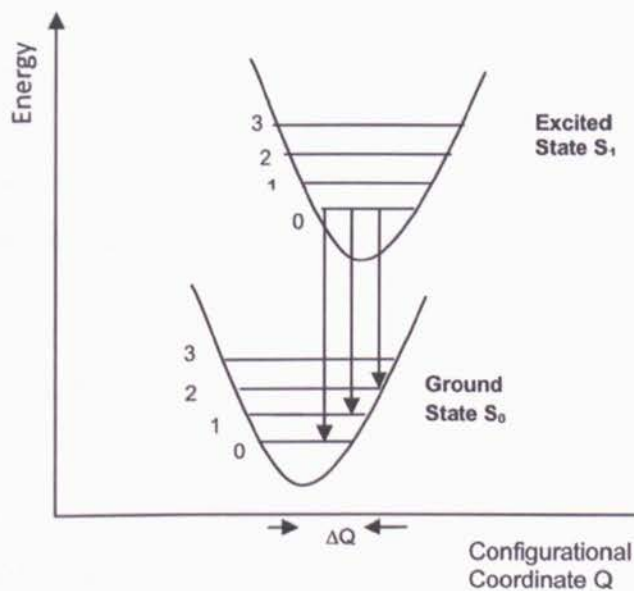


Figure 3 6: Configurational coordinate diagram for transitions between different states of PPV.

The separation between the 0-0 and the 0-1 peaks in the emission spectrum is about 0.141 eV (1137 cm^{-1}) and that of 0-1 and 0-2 peaks is (1443 cm^{-1}). These values of frequencies, can be associated with some of

the stretching and bending modes of the carbon backbone observed in the IR. Note that these values are only approximate because the vibronic transitions in the electronic spectra relate to vibrational modes of the molecule in the excited state which could differ in geometry from the molecule in the ground state, whereas transitions in the IR spectra relate to the molecule in the ground state.^{37,40}

According to Bradley *et al* (1987),⁴⁰ vibronic transitions are less visible for a well converted and well organised PPV. The fact that these transitions were so clearly defined in the emission spectrum could indicate that there were several forms of polymer present with different conjugation length due to an incomplete conversion. If true, the most likely reason for this is the temperature used to eliminate the sulfonium moieties. Many authors have quoted an optimum temperature value of 220⁰C for 12 hours to achieve full elimination.^{22,32-33,41} In this particular case, however, the temperature used was slightly lower and the times much shorter (6 hours). Additionally, even though the elimination was carried out under vacuum, there is still the possibility of oxygen being present during the formation of PPV, and this would result in the partial oxidation of the polymer, giving rise to shorter polymer chains and shorter wavelength emissions.³⁶

3.3.6 Estimation of the polymer molecular weight by viscometry

A range of concentrations of aqueous solutions of poly (p-xylylene tetrahydrothiophenium chloride) (0.25, 0.2, 0.1, 0.05 g dl⁻¹) were prepared. The flow times of pure solvent (water) t_0 and polymer solutions t were recorded using an Ubbelohde viscometer immersed in a thermostatic bath set at 30 ⁰C. The timing of the flow was repeated several times until at least 3 values were consistent within 0.3 seconds.

Theory

The ratio of the flow time of a polymer solution t to that of the pure solvent t_0 is equal to the ratio of their viscosity (η / η_0) if the densities are equal. This approximation is reasonable for dilute solutions and provides a measure of relative viscosity η_r .⁴²

$$\eta_r = (t / t_0) = (\eta / \eta_0) \quad \text{[Equation 3.1]}$$

As this has a limiting value of unity, then the specific viscosity η_{sp} can be obtain by

$$\eta_{sp} = \eta_r - 1 = (t - t_0) / t_0 \quad \text{[Equation 3.2]}$$

The viscosity average molecular weight M_v can be obtained by using the Mark-Houwink equation.⁴²

$$[\eta] = kM_v^a \quad \text{[Equation 3.3]}$$

where $[\eta]$ is the limiting viscosity number and k and a are constants for a particular polymer-solvent system at a specified temperature.⁴²

The limiting viscosity number $[\eta]$ is found by a linear extrapolation of the viscosity number $[\eta_{rel}]$ to zero:⁴²

$$[\eta_{rel}] = \eta_{sp} / C \quad \text{[Equation 3.4]}$$

where C is concentration in g dl^{-1}

Although Mark-Houwink parameters are not available for poly (p-xylylene tetrahydthiophenium chloride) estimates of the M_v were obtained using the parameters for poly(vinyl alcohol) (PVA) ($k = 6.5 \times 10^{-4} \text{ [dl/g]}$, $a = 0.628$, in

aqueous solution at 30 °C). Although k and a are dependent on the polymer-solvent system, the values of a for most flexible polymers are between 0.65 and 0.8, thus using the parameters of PVA could give a good estimate of the relative molecular weight of PPV.⁴²

The values for the specific viscosity and viscosity number of the different solutions are all shown in Table 3.4.

	H ₂ O	Solution 1	Solution 2	Solution 3	Solution 4
Concentration/ (g dl ⁻¹)	0	0.05	0.10	0.20	0.25
Flow time (t)/s	71.2	86.2	93.2	98.7	99.2
$\eta_{SP} = (t-t_0)/t_0$	0	0.21	0.31	0.38	0.39
$\eta_{rel} = \eta_{SP} / C$	-	4.2	3.1	1.9	1.6

Table 3.4 Values of specific viscosity and viscosity number of poly (*p*-xylene tetrahydrothiophenium chloride) solutions of different concentrations at 30°C.

Figure 3.7 is a plot of η_{rel} against concentration. The intercept value is the limiting viscosity number (intrinsic viscosity) $[\eta] = 4.6 \text{ dl g}^{-1}$ and the viscosity average molecular weight $M_v = 1.35 \times 10^6 \text{ Da}$. was found using the Mark-Houwink equation described above (Equation 3.3). The values found for both the intrinsic viscosity $[\eta]$ and the average molecular weight were both relatively low in comparison to the values reported for similar PPV precursors.^{37,39,40} The most likely reason for such low values is the fact that elimination of the sulfonium groups can take place even at room temperature leading to the formation of low molecular weight by-products that will certainly have an effect in the average molecular weight.

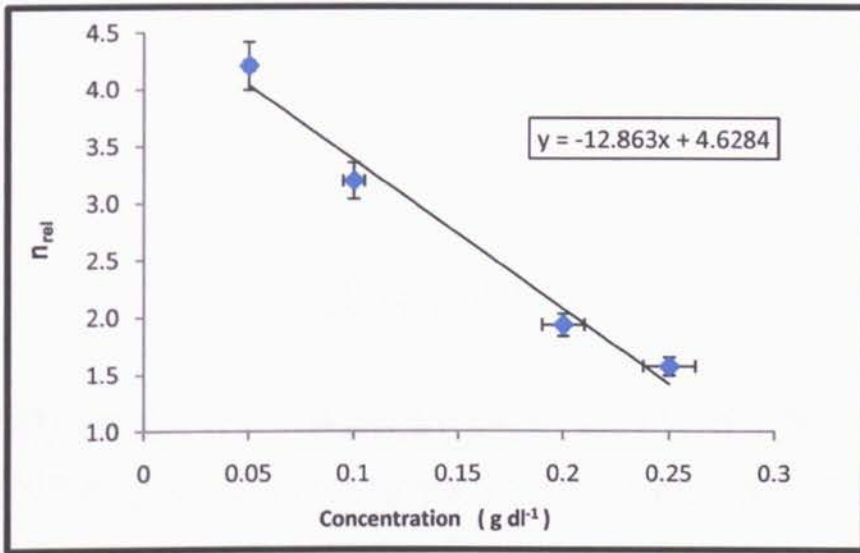


Figure 3 7: Plot of viscosity number (n_{rel}) against concentration (C). Inset: linear equation displaying the intercept $[n] = 4.6284$ when $C=0$.

Chapter 4:

SYNTHESIS, CHARACTERISATION AND INTERCALATION OF CRYSTALLINE METAL PHOSPHORUS TRISULFIDES

Over the years, MnPS_3 and CdPS_3 layer compounds have been studied by several research groups, mostly due to their ability to intercalate guest molecules and form organic-inorganic materials with improved magnetic and electronic properties. In addition to their intercalation properties, these materials have been chosen for the present work because they are optically transparent in the visible region which makes them ideal hosts for luminescent polymers; moreover they are non-oxidising host materials that can be easily prepared at both high and low temperatures (solid state and solution approach respectively).¹

4.1 Reagents and instruments used

The materials used for the synthesis of the layered inorganic compounds, their grades and suppliers are all given in Table 4.1 Most chemicals were used without further purification, in cases where they were purified this was specified during the synthetic procedure.

Material	Grade	Supplier
Manganese (II) sulfide	99.9 %	Alfa Aesar
Red phosphorus	99.9 %	Sigma-Aldrich
Sulphur	99.9 %	Alfa Aesar
Xylene	99.0 %	Sigma-Aldrich
Toluene	86.0 %	Sigma-Aldrich
Potassium chloride	99.5 %	BDH Chemicals
EDTA	99.4 %	Sigma-Aldrich

Table 4.1 Details of materials used for the synthesis of crystalline MPS_3 and PPV intercalated MPS_3 .

4.1.1 X-ray Diffraction

X-ray powder diffractometry (XRD) was carried out on all samples using a Bruker D8 Advance x-ray diffractometer, with Cu $K\alpha$ radiation ($\lambda = 1.542 \text{ \AA}$). In cases where the amount of the samples was too small, they were dispersed on clear sellotape. (The sellotape background was found in some of the x-ray diffractograms and was taken into account when assigning the peaks)

4.1.2 Scanning Electron Microscopy

SEM images were obtained from single crystals, polycrystalline material as well as thin films using a Zeiss EVO 50 with an Oxford Instruments INCA analytical suite.

4.1.3 Infrared Spectroscopy

Attenuated total reflection infrared (ATR-IR) spectroscopy was carried out on all samples using a Thermo Scientific Nicolet IS5 iD5 ATR, 16 scans, over the range 650-4000 cm^{-1}

4.1.4 Raman Spectroscopy

Raman spectroscopy was carried out on all samples using a Renishaw inVia Raman Microscope, using WiRE 3.3 software and Renishaw MS20 encoded Mechanical stage. (HeNe 633nm wavelength 500mW (typically 8mW at source) RED laser).

4.1.5 UV-vis Spectroscopy

UV-vis spectroscopy was carried out on single crystals (0.03 mm thick) mounted on cardboard substrates with small windows that permitted the passage of light, or in ethanolic suspensions (in the case of $\text{VOPO}_4 \cdot 2\text{H}_2\text{O}$ and derivatives), using a Cary 100 Bio, UV-visible spectrophotometer

4.1.6 Photoluminescence Studies

Photoluminescence studies were carried out on single crystals mounted in black cardboard substrates and on films coated on quartz slides. In both cases, the substrates were positioned at an angle of about 60 degrees to limit direct reflection from the quartz slides using a Varian Cary Eclipse Spectrophotometer

4.1.7 Elemental Analysis

Elemental analysis was carried out using a Jobin-Yvon Ultima 2C ICP AES instrument. All samples were dissolved in diluted hydrochloric acid.

4.2 Synthesis of metal phosphorus trisulphides (crystal growth)

Single crystals and polycrystalline material were obtained by a chemical vapour transport reaction. An excess of sulphur (~ 0.2% of the total sulphur) was used as transporting agent. The reactions were carried out in evacuated (10^{-4} Torr) quartz ampoules (200 mm length and around 15 mm diameter) in a Carbolite three zone tube furnace which was calibrated with a thermocouple probe prior to use. The temperature of the furnace and time of reaction varied depending on the metal used. Red phosphorus was washed with distilled water and Analar acetone to remove any oxide layer before it was used.

4.2.1 MnPS₃

General procedure A: Stoichiometric amounts of sulphur (2.12 g, 0.06 mol), red phosphorus (1.02 g, 0.03 mol), and manganese (II) sulphide (1.81 g, 0.02 mol) were combined in evacuated quartz tubes. The tubes were then heated at 720 °C with a temperature gradient to crystallise the products by sublimation at 680 °C, in the tube furnace for 4 weeks according to literature.^{13,43} Green single crystal platelets and polycrystalline material were obtained. The approximate size of the single crystals was 1.4 x 1.2 x 0.3 mm³, using a micrometer. Yield obtained; 4.383 g (73%)

4.2.2 CdPS₃

General procedure A was followed (using cadmium sulphide instead) with a minor modification of the growth temperature (680 °C down to a sublimation temperature of 630 °C) and time (7 days). White polycrystalline material was obtained.

All samples were cleaned by Soxhlet extraction for several hours using either xylene or toluene to remove any unreacted sulphur or phosphorus. The samples were then rinsed with acetone and water to remove any organic residues. Dilute hydrochloric acid (2 M) was used to remove any metal phosphides or sulphides. Finally the samples were washed with water and dried in a vacuum oven at 80 °C for 24 hours.

4.3 Synthesis of composites by intercalation

The MnPS₃ lattice is made up of Mn²⁺ complexes held together by P₂S₆⁴⁻ bridging ligands. The ions occupy all the octahedral sites in every other layer. When intercalation occurs, a chemical transformation takes place, that is, as intercalated cations enter the interlayer space, some of the Mn²⁺ species leave the lattice to maintain the overall charge balance. Attempts to intercalate the cationic precursor polymer directly into the MnPS₃ were unsuccessful, probably due to the slow kinetics for the transport of the polymer.⁵⁻⁶ On the other hand small cations such as K⁺ are well known to be easily intercalated; hence a two-step intercalation mechanism was chosen to form the PPV intercalated MPS₃ composites. During the first step, potassium ions (K⁺) were intercalated to pre-expand the layers. This facilitated the second step during which the sulfonium precursor polymer was intercalated by cation exchange.^{9,13}

4.3.1 MnPS₃

4.3.1.1 Intercalation of potassium ions (K⁺) (K_MnPS₃)

Single crystals of MnPS₃ (0.04 g, 2.14 x10⁻⁴ mol) were added to an aqueous solution of KCl (5.0 ml, 2M). The mixture was stirred for 1 hour at ambient temperature. The product was filtered off and washed with distilled water and dried under vacuum for 24 hours at 80 °C. The product obtained was K_MnPS₃. Yield obtained: 0.02 g (44 %)

4.3.1.2 Intercalation of precursor polymer by cation exchange (PP_MnPS₃)

General procedure B: Polycrystalline K_MnPS₃ (0.01 g, 4.94 x10⁻⁵) was added to a methanolic solution of precursor polymer (10 ml, 0.2 M). The solution was stirred at room temperature for 2 weeks, protecting it from light. The product was then collected by centrifugation and washed several times with methanol. The product was then dried in air and protected from light.

Conversion of intercalated precursor polymer into PPV

PP_MnPS₃ was placed under nitrogen and heated to 230°C for 5, 30 and 60 minutes.

4.3.1.3 In situ formation and intercalation of precursor polymer inside MnPS₃

K_MnPS₃ crystals (0.06 g, 2.73 x10⁻⁴ mol) were added to a methanolic solution containing monomer 1 (11 ml, 0.2 M). The mixture was left stirring for 24 h under nitrogen. Then it was cooled down to 0 °C and NaOH (11 ml, 0.2 M, 0 °C) was added, after which it was stirred for a further hour. HCl (1M) was then added to neutralise it, and stirring was carried on for

two more hours, keeping the mixture at 0 °C throughout the reaction. A green-yellow suspension was formed, containing the intercalated crystals. This suspension was then dialysed against water (3 x 2 L) for 3 days. After this, the crystals were filtered off and washed with methanol several times, then dried and kept protected from light.

Conversion of intercalated precursor polymer to PPV

Some crystals of PP_MnPS₃ were heated under nitrogen to 230 °C for 5 and 10 minutes. It was observed that if the crystals were heated for longer times at this temperature, they turned black; hence, lower temperatures (150 °C) were used for further experiments.

4.3.2 CdPS₃

4.3.2.1 Intercalation of potassium ions (K⁺)

Aqueous EDTA (3.0 ml, 0.1 M), aqueous K₂CO₃/KHCO₃ (5.0 ml, 1M) and CdPS₃ (0.05 g, 2.13 x 10⁻⁴) were added to aqueous KCl (10 ml, 2M). The mixture was stirred at room temperature for 2 days. The product was then filtered off and washed several times with distilled water, and then it was dried in air and under vacuum for 24 hours. Product obtained: K_CdPS₃. Yield obtained: 0.03 g (53 %)

4.2.2.2 Intercalation of precursor polymer by cation exchange

General procedure B was followed using K_CdPS₃ instead, with aqueous instead of methanolic solutions.

Conversion of intercalated precursor polymer to PPV

The samples were heated under nitrogen to 230 °C for 90 minutes.

4.4 Results and Discussion

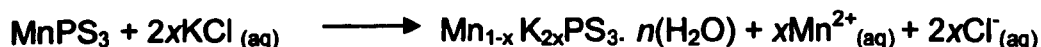
4.4.1 MnPS₃ and MnPS₃ intercalates

4.4.1.1 Elemental Analysis

4.4.1.1.1 MnPS₃

A green polycrystalline material and thin platelet-like crystals were obtained from the crystal growth ampoule. The average size of the single crystals was 1.4 x 1.2 x 0.3 mm³. ICP analysis of the sample (single crystal) led to the formula Mn_{1.04}P_{1.12}S_{3.76} (Mn, 57.24 mg L⁻¹, P, 34.88 mg L⁻¹, S, 120.53 mg L⁻¹).

4.4.1.1.2 K⁺ intercalated MnPS₃



Pale green crystallites were obtained upon intercalation of potassium ions (K⁺). ICP analysis suggested the formula to be K_{0.5}Mn_{0.5}P_{0.93}S_{3.14} (K, 19.84 mg L⁻¹, Mn, 30.67 mg L⁻¹, P, 28.69 mg L⁻¹, S, 100.5 mg L⁻¹)

4.4.1.2 X-ray Diffractometry

The series of (*h k l*) peaks obtained from the XRD are characteristic of layered compounds. The strong intensity and sharpness of the peaks as well as their regularity indicate the highly crystalline structure of the inorganic hosts.

The angle (θ) was calculated using Bragg's law equation:

$$2d \cdot \sin \theta = \lambda, \quad \text{hence} \quad \theta = \sin^{-1}(\lambda/2d) \quad [\text{Equation 4.1}]$$

where, d = interlayer spacing in Å and $\lambda = 1.542$ Å (wavelength of the anode material, Cu)

4.4.1.2.1 MnPS₃

The layered structure of MnPS₃ was confirmed through the XRD pattern shown in Figure 4.1. The first reflection was observed at 13.58° (2θ) corresponding to an interplanar space (d) of 6.52 Å followed by a 2nd order reflection at 27.52° (2θ) with an interplanar space of 3.24 Å. Other peaks also present (see Table 4.2) were all typical reflections of the MnPS₃ monoclinic space group, in agreement with values in the literature.

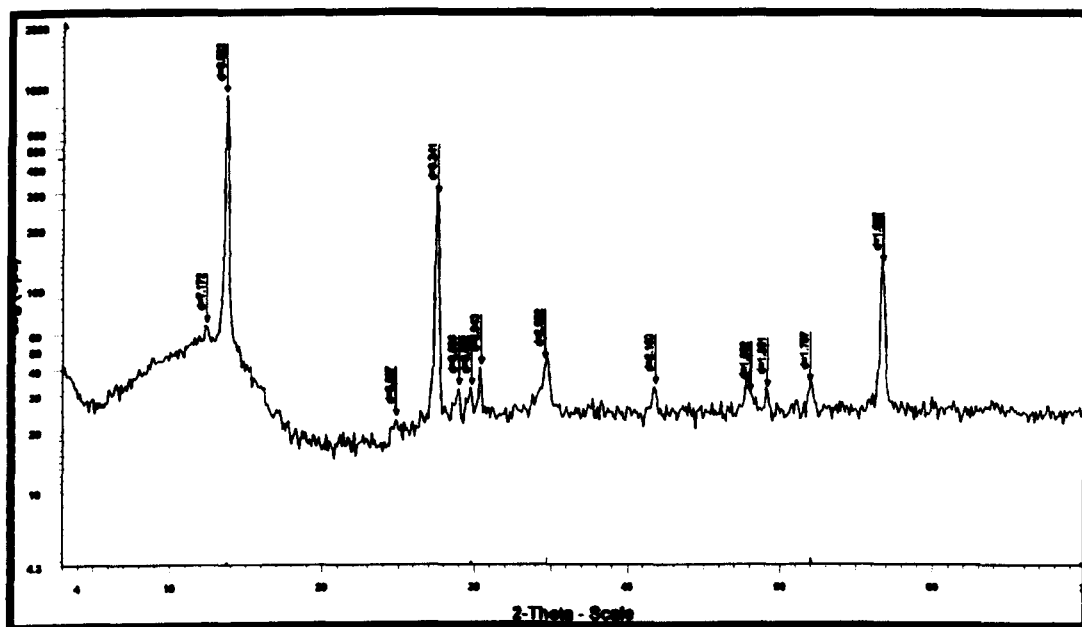


Figure 4 1: X-ray diffractogram of polycrystalline MnPS₃

θ (2 θ) ^o	d / (Å)	Calculated Interlayer Spacing (Å)	(h k l) parameters	d / (Å) literature Yang <i>et al</i> (2000) ⁴⁴
13.58	6.522		0 0 1	6.51
27.53	3.241	6.482	0 0 2	3.244
29.78	3.002		1 3 0	3.000
34.61	2.592		1 3 1	2.576
41.82	2.16	6.480	0 0 3	-
48.09	1.892		2 0 2	1.897
52.06	1.757		0 6 0	1.754
56.76	1.622	6.488	0 0 4	1.621

 Table 4.2 Assignment of XRD data for MnPS₃ including literature values.

4.4.1.2.2 K⁺-Intercalated MnPS₃ (K₂MnPS₃)

The product retained its layered structure and crystallinity as evidenced by the sharp, clear peaks observed in the XRD pattern (Figure 4.2). An interlayer expansion of 2.47 Å along the c axis was achieved and a new (0 0 l) peak was observed at 9.84^o (2 θ) with an interlayer spacing of 8.99 Å. This expansion is due to the intercalation of K⁺ into the empty interlayer space of the MnPS₃ and is consistent with values found in the literature for this kind of intercalation compound.^{8,45} In some cases bigger expansions (Figure 4.2 b) were observed due to the intercalation of water molecules as well as K⁺. These water molecules were easily lost upon heating and

thorough drying of the samples. The XRD characteristic peaks of the original host were not observed in most cases; however in some samples reflections of 2nd and 3rd order characteristic of the pure host were observed indicating traces of unintercalated MnPS_3 .

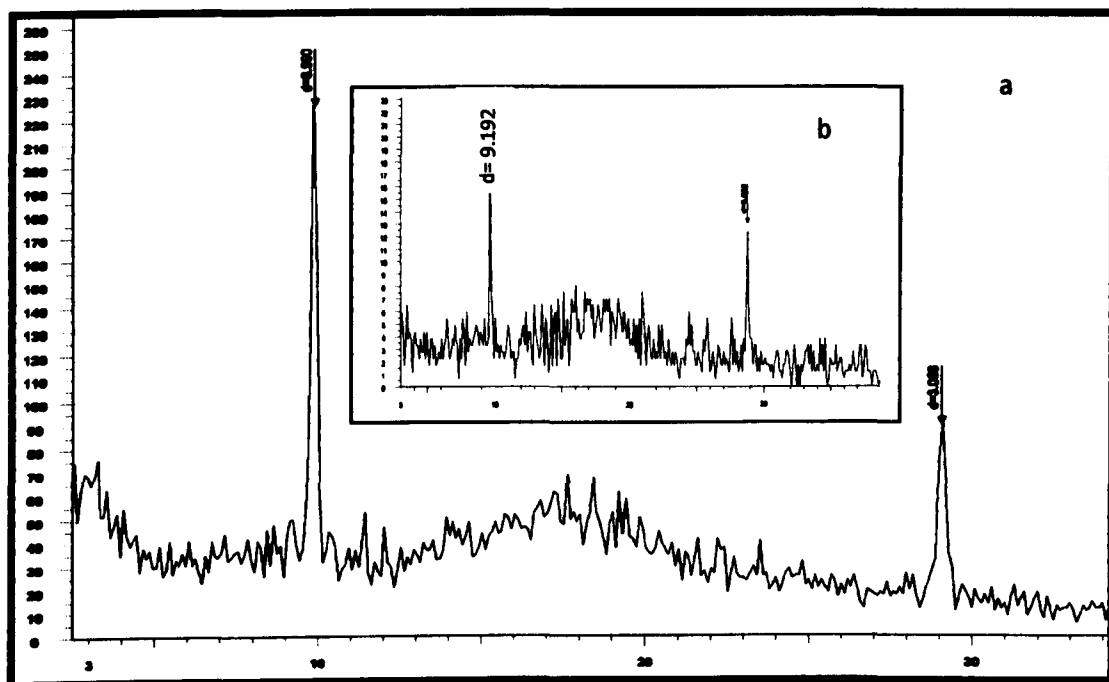


Figure 4 2: Powder X-ray diffractogram of (a) dried K^+ intercalated MnPS_3 and (b) K^+ and H_2O intercalated MnPS_3 showing a reduction of the layer space after the removal of water.

4.4.1.2.3 Polymer intercalated MnPS_3 (cation exchange) PPV_MnPS_3

The powder XRD of the polymer intercalate MnPS_3 is shown in Figure 4.3 and for comparison the XRD pattern of the original host material is also shown (inset). A new 0 0 1 reflection was observed with a d spacing of 10.33 Å corresponding to a lattice expansion of 3.81 Å. This value suggested that the orientation of the polymer was parallel to the layer of the inorganic host.⁴⁶ Traces of the original sample were observed at

13.95⁰ (2 θ) indicating only partial intercalation. Apart from the layer expansion, the pattern also showed peak broadening, indicating breaking up of the crystallites upon exfoliation and insertion of larger molecules. Intercalation usually occurs in stages, and it is possible that several phases were formed in the process, which may explain the splitting of the peaks in the new xrd pattern. No other changes were observed in the pattern, and therefore it is reasonable to assume that only the c-axis was affected by the intercalation process.

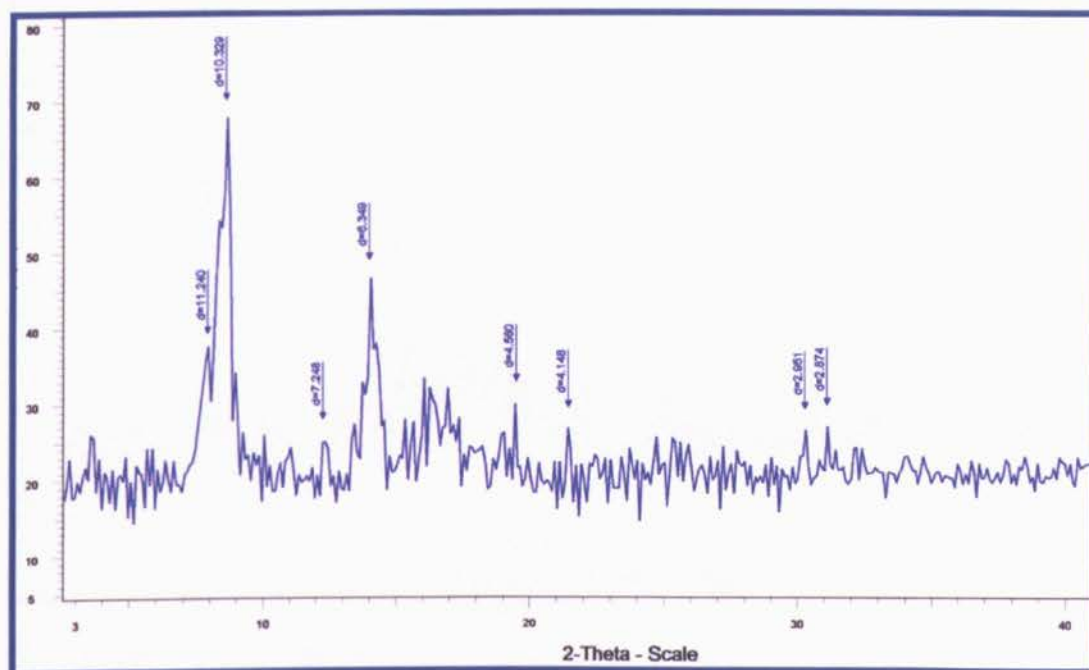


Figure 4 3: X-ray diffractogram showing intercalation of PPV precursor in MnPS_3 showing a new d-spacing of 10.33 Å.

4.4.1.2.4 Polymer intercalate MnPS_3 (In situ polymerisation) (PPV2_ MnPS_3)

The achievement of cation exchange intercalation was confirmed by the x-ray pattern (Figure 4.4) The diffraction patterns of the pre-intercalated KMnPS_3 as well as pristine MnPS_3 were no longer observed; instead new (0 0 l) lines corresponding to an interlayer spacing of 11.58 Å were detected. The 5.13 Å increase in d-spacing was attributed to the

intercalation of the precursor polymer chains parallel to the host layer but with the benzene rings adopting a perpendicular rather than parallel arrangement.⁴⁷ No other peaks were observed. The fact that the K^+ ions were exchanged first by the monomer and that the polymer was formed *in situ* between the layers, permitted the formation of a single phased structure that was more organised and retained its crystallinity throughout the process.

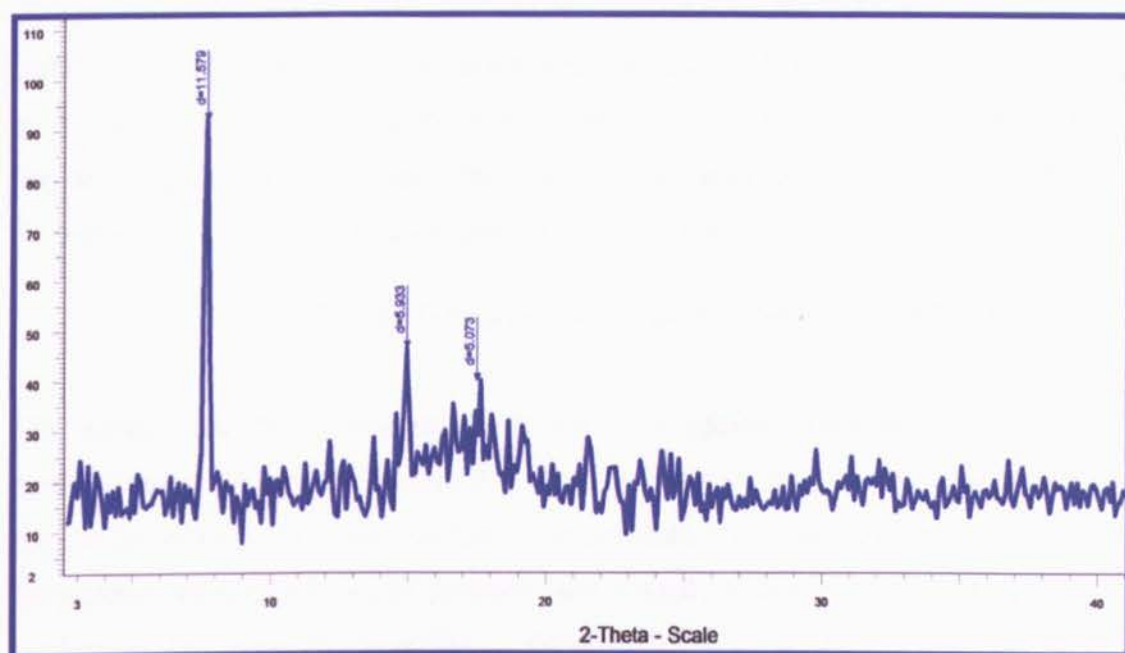


Figure 4 4: X-ray diffractogram of intercalated PPV precursor prepared by in situ polymerisation. The sharp lines indicated that the crystallinity of the host was kept after intercalation of the polymer had taken place.

Sample	d / Å	Layer expansion/ Å	(h k l) parameters
MnPS ₃	6.52	-----	0 0 1
K_MnPS ₃	8.99	2.47	0 0 1
PPV_MnPS ₃	11.58	5.05	0 0 1

Table 4.3 d-spacing expansion of MnPS₃ upon intercalation of K^+ and PPV

4.4.1.3 Thermogravimetric analysis

4.4.1.3.1 K^+ -Intercalate $MnPS_3$ (K_MnPS_3)

TGA analysis of K^+ -intercalated $MnPS_3$ showed a weight loss of 12 % at about 120 °C (see appendix E). This was attributed to the elimination of K^+ ions and water molecules that were present in the lamellar space. The elimination of these species would normally take place at lower temperature; however, as they were intercalated and more strongly bound to the lattice, their removal from the interlayer space is more difficult and requires higher temperatures. The sample was relatively stable up to 450 °C when the inorganic lattice started to decompose.

4.4.1.3.2 Precursor polymer intercalated $MnPS_3$ (PP_MnPS_3)

The weight loss of the precursor polymer intercalated sample occurred in several steps as seen in Figure 4.5. The first weight loss of 1% was in the region previously observed for the K^+ intercalated samples which indicated that these species were still present and therefore that only partial cation exchange between K^+ and the sulfonium polyelectrolyte took place. A sudden weight loss was observed between 130 and 380 °C, this was due to the loss of tetrahydrothiophene groups and xylene moieties and was consistent with the boiling point of these groups which are within that temperature range (bp:119 and 254 °C respectively). Moreover, considering that the polymer had been partially converted into PPV (which can occur over the time under environmental conditions) then that would account for the thermal degradation that started taking place above 380 °C.

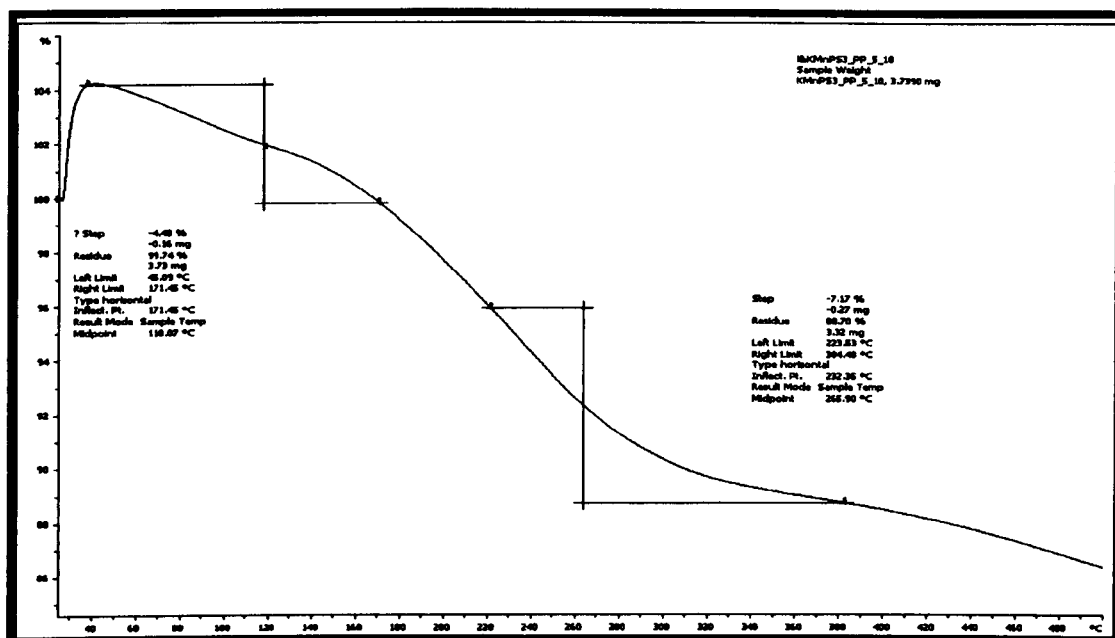


Figure 4 5: TGA curve of precursor polymer intercalated MnPS₃ showing several weight loss steps due to the presence of more than one species.

4.4.1.3.3 PPV intercalated MnPS₃ (PPV_MnPS₃)

In the case of PPV-intercalated MnPS₃, the TGA diagram showed that the sample was stable up to 200 °C (Figure 4.6). This indicated that during the thermal conversion, in addition to the of sulfonium groups, the intercalated K⁺ and solvent molecules were also removed. The first weight loss of 11 % took place between 200 and 300 °C; this was most likely due to the removal of uneliminated sulfonium groups which suggested that the precursor polymer was only partially converted into PPV. The final step took place between 350 and 400 °C and it was attributed to the degradation of PPV.

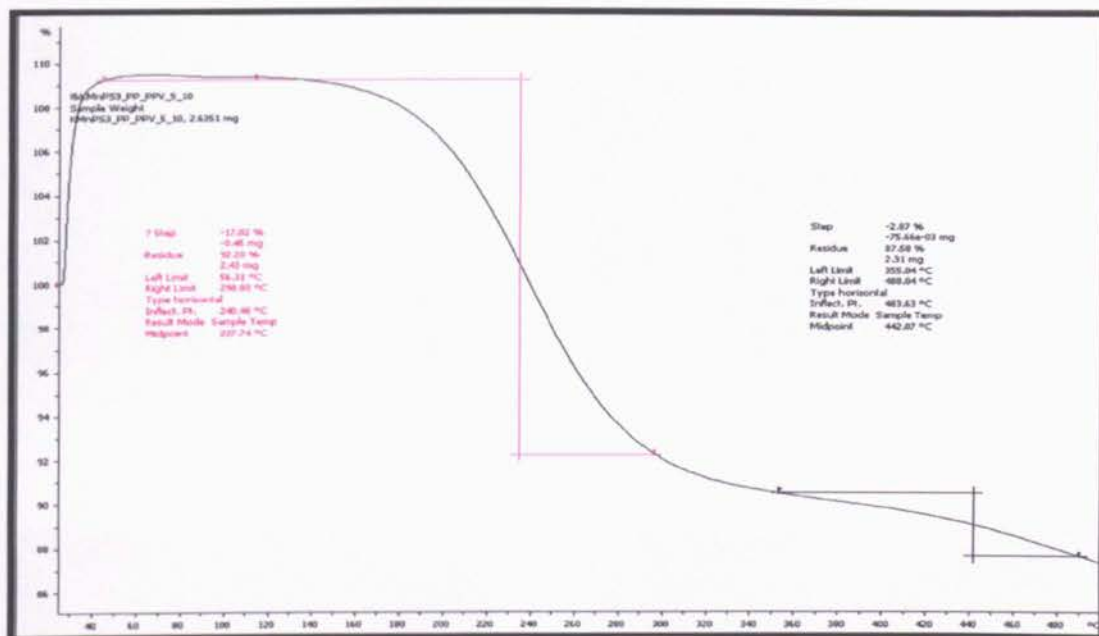


Figure 4 6: TGA curve of PPV-intercalated MnPS_3 showing thermal stability up to 200 °C.

4.4.1.4 Scanning Electron Microscopy (SEM)

The morphology of the samples was studied by SEM. Clear lamellar structures were observed on the pristine MnPS_3 indicating the regular stacking of the compound (Figure 4.7). The morphology of the crystals was slightly affected by the intercalation process. As can be seen on the SEM images below, after inclusion of the K^+ ions the samples retained their lamellar structure but defects such as cracks and uneven corners resulted on the surfaces of the crystals due to the mechanical stress that the samples underwent during the insertion of guest molecules. Furthermore in some cases insertion of the polymer resulted in partial exfoliation of the layers.

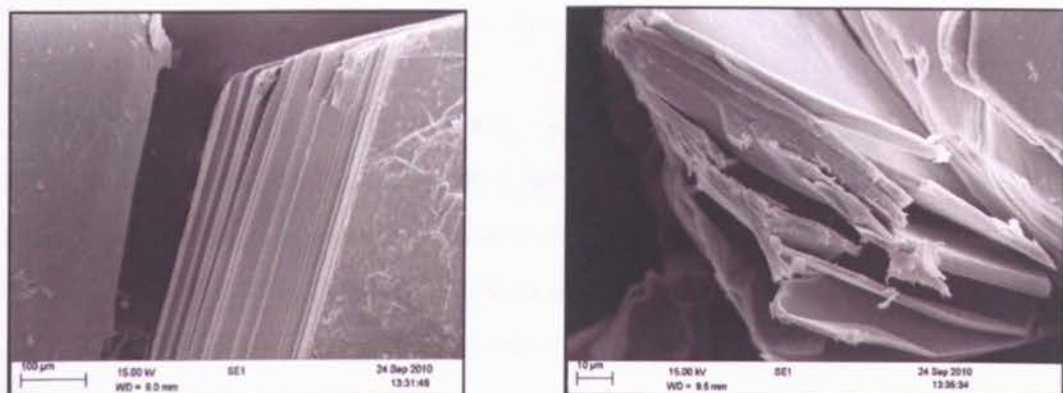


Figure 4 7: SEM images of MnPS₃ showing the lamellar structure.

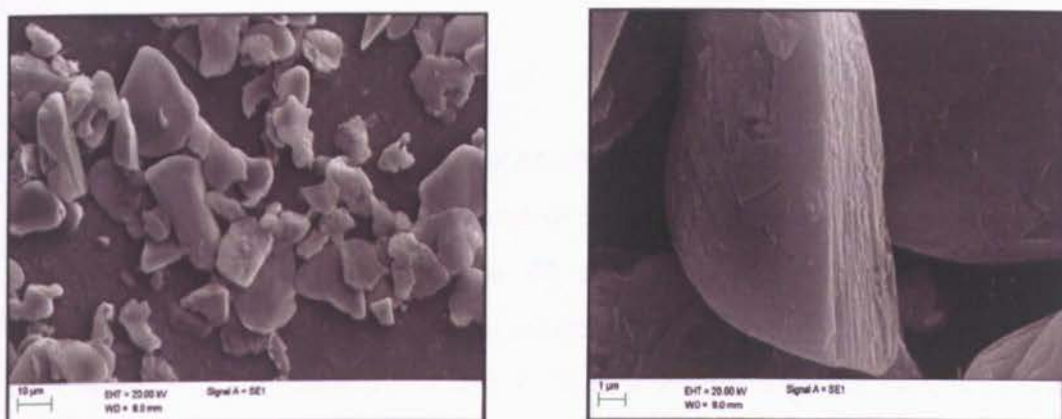


Figure 4 8: SEM images of K_xMnPS₃. After intercalation with K⁺ cracks started to appear on the surface of the crystal due to mechanical stress.

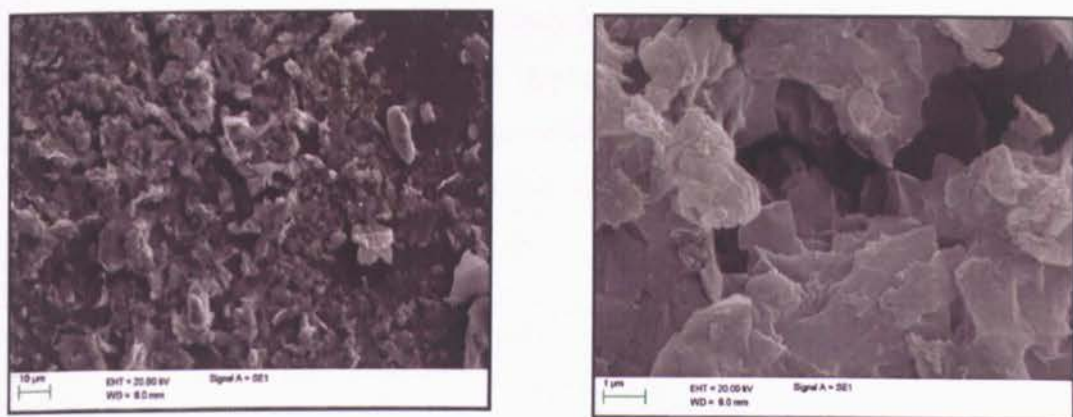


Figure 4 9: SEM images of PP_xMnPS₃. After intercalation of the polymer, the lamellar structure of MnPS₃ was preserved.

4.4.1.5 Infrared and Raman Spectroscopy

Vibrational studies were carried out on the host lattices and on intercalated samples, in order to gather new information regarding any structural changes upon intercalation and the dynamics of the intercalated molecules. It is important to mention that Raman spectroscopy was used as a complementary technique to the infrared which allowed us to observe vibrations at lower frequencies.

4.4.1.5.1 MnPS₃

The infrared and Raman spectra of MnPS₃ are shown below (Figures 4.10, 4.11) The main features of this sort of compound are generally found in the region below 600 cm⁻¹. The IR spectrum showed the vibrational features characteristic of the MPS₃ compounds at 572 cm⁻¹ assigned to the P-S stretching frequencies of the P₂S₆ unit of the M₂P₂S₆ lattice.⁴⁷ The internal modes of P₂S₆⁴⁻ are represented by the sharp lines at 275 and 383 cm⁻¹ in the Raman spectrum. The first one (275 cm⁻¹) is attributed to the S-P-S and S-P-P modes and the second one (383 cm⁻¹) can be assigned to the mixed symmetric P-P and P-S stretching modes.⁴⁸ The low frequency Raman bands are usually metal-sensitive; therefore the weak peak arising at about 154 cm⁻¹ was attributed to the M-S bond.⁴⁹⁻⁵⁰

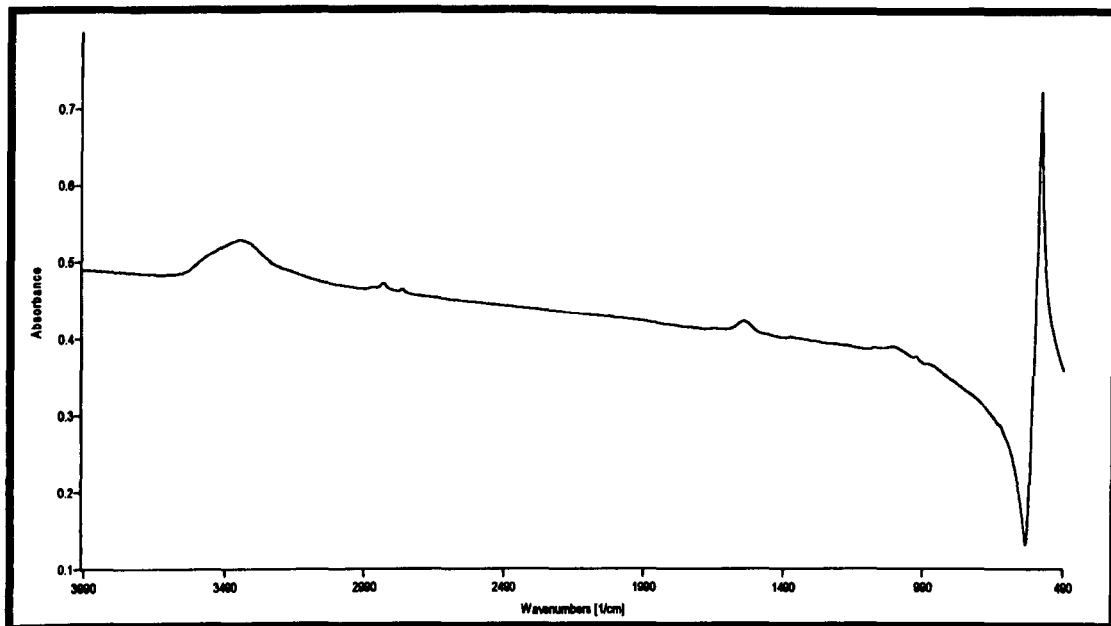


Figure 4 10: Single crystal of MnPS₃ IR Spectrum.

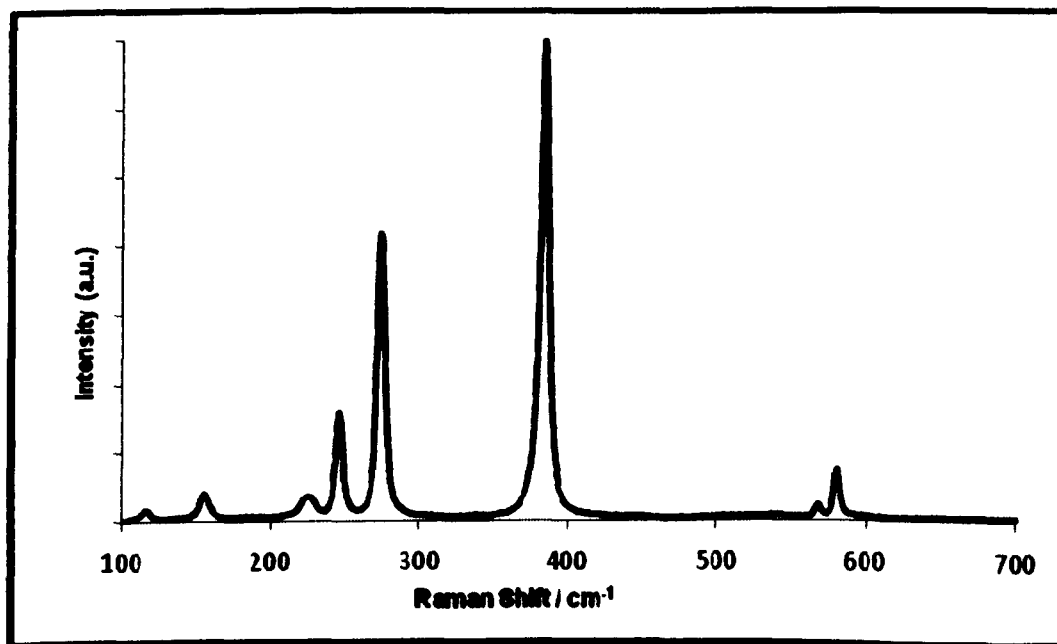


Figure 4 11: MnPS₃ Raman Spectrum.

4.4.1.5.2 K^+ intercalated $MnPS_3$ (K_MnPS_3)

The evidence for the intercalation of K^+ is the splitting of the $\nu(\text{PS}_3)$ asymmetric deformation band that occurred at 572 cm^{-1} in the IR spectrum. The two new peaks that were observed at 553 and 607 cm^{-1} (see Figure 4.12) are characteristic of intercalated MPS_3 compounds.⁴⁵ The main intercalation mechanism of the MPS_3 group is a cation exchange reaction, where M^{2+} are released and cation vacancies are formed.^{45,49} According to Lagadic *et al* (1997)⁴⁵ the splitting of this band is due to the formation of these vacancies which produce a mixture of P-S bonds surrounded by vacancies and others still bound to a metal ion (Mn^{2+} or Cd^{2+}). Other features in the IR spectrum are a broad band at 3438 cm^{-1} and a weak peak around 1620 cm^{-1} attributed to the water molecules present in the interlayer gap; these water molecules were easily removed by drying the sample thoroughly in a vacuum oven. Apart from an increase in the intensity of the peaks, the Raman spectra of the intercalated compound did not show any particular change as the internal modes of the $P_2S_6^{4-}$ units in the host were not affected by the intercalation.

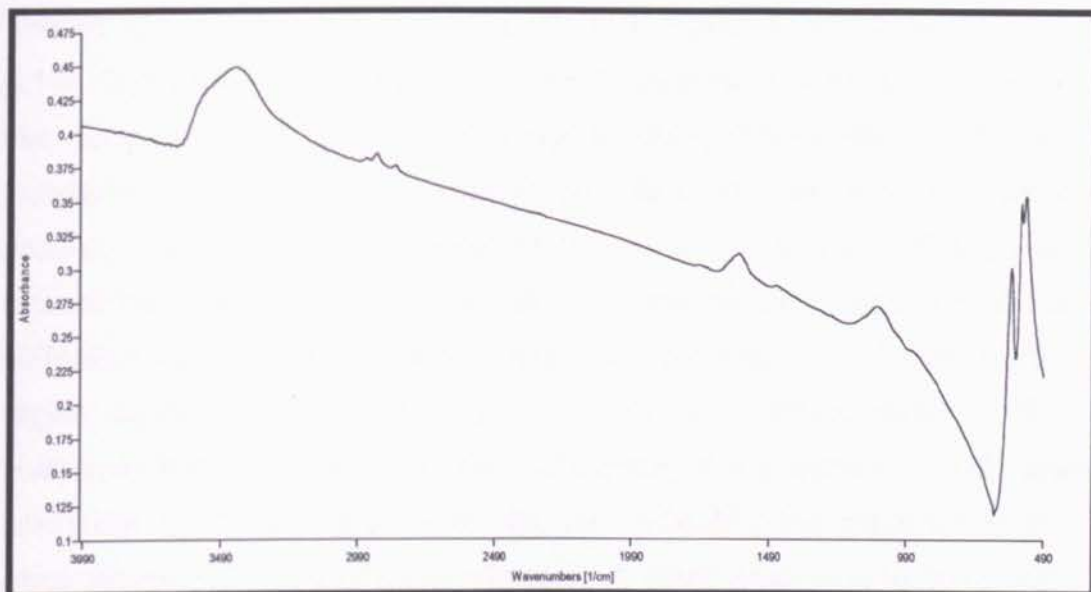


Figure 4 12: K₂MnPS₃ IR spectrum.

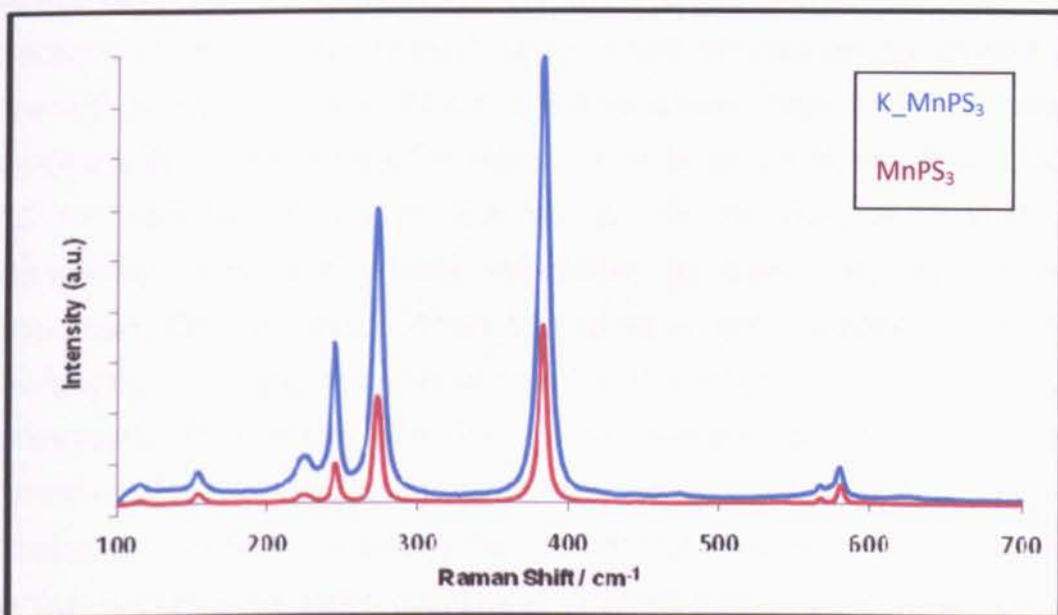


Figure 4 13: K₂MnPS₃ and MnPS₃ Raman spectra.

4.4.1.5.3 Polymer-intercalated MnPS₃

The IR spectra indicated the presence of the precursor polymer (Figure 4.14). The peaks are less intense than those observed in the infrared of the pure precursor, due to the polymer being intercalated inside the inorganic hosts. The broad peak around 3500 cm^{-1} and the sharp peak around 1600 cm^{-1} were attributed to the presence of water. The peaks around 2921 and 2850 cm^{-1} correspond to the sp^3 C-H stretching of the sulfonium leaving groups of the precursor polymer.⁵¹⁻⁵³ Peaks in the region between 1450 and 1050 cm^{-1} are also characteristic of the sulfonium salts. Additionally, the elimination of the sulfonium salt was confirmed by the strong peak at 980 cm^{-1} indicating the presence of the *trans*-vinylene C-H out of plane vibration. A small peak around 3013 cm^{-1} was starting to form, which corresponds to the *trans*-vinylene C-H stretch characteristic of the conjugated PPV.⁵¹⁻⁵³ No further changes were observed in the IR of the inorganic host. The presence of the metal vacancies was observed throughout the whole process as confirmed by the split peaks at 607 and 553 cm^{-1} (inset spectrum). Attempts to eliminate thermally the intercalated precursor polymer at temperatures above $200\text{ }^\circ\text{C}$ for extended periods of time resulted in the samples appearing completely burnt and it was impossible to carry out any further characterisation on them. When the samples were exposed to such temperatures for only a couple of minutes, the polymer was only partially eliminated. After heating the intercalated samples at $150\text{ }^\circ\text{C}$ it was observed that the samples started to change from green to light brown. This may have been caused by the presence of small amounts of oxygen in the vacuum oven, which could have oxidised parts of the polymer chain at such high temperature. Therefore, lower elimination temperatures were used.

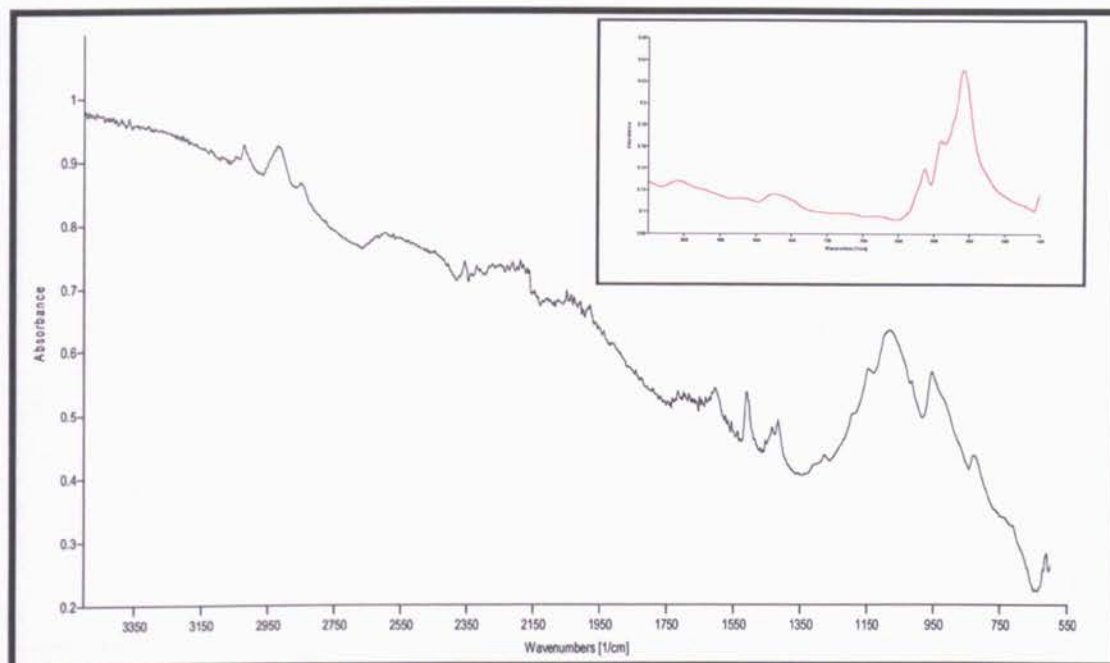


Figure 4 14: PPV intercalated MnPS₃ IR spectra. Inset the spectrum below 600 cm⁻¹

The Raman spectrum of the intercalated precursor polymer confirmed the conversion of the precursor polymer into PPV. According to Aarab *et al* (2005)³⁶ the new group of peaks arising at 1174, 1325, 1566, 1592 and 1635 cm⁻¹ is characteristic of the vibrations of PPV, only the small peak arising at 1414 cm⁻¹ is associated with the precursor polymer which is infrared and Raman active indicating that there were some traces of uneliminated sulfonium salt. No changes associated with the inorganic host were observed in the spectrum.

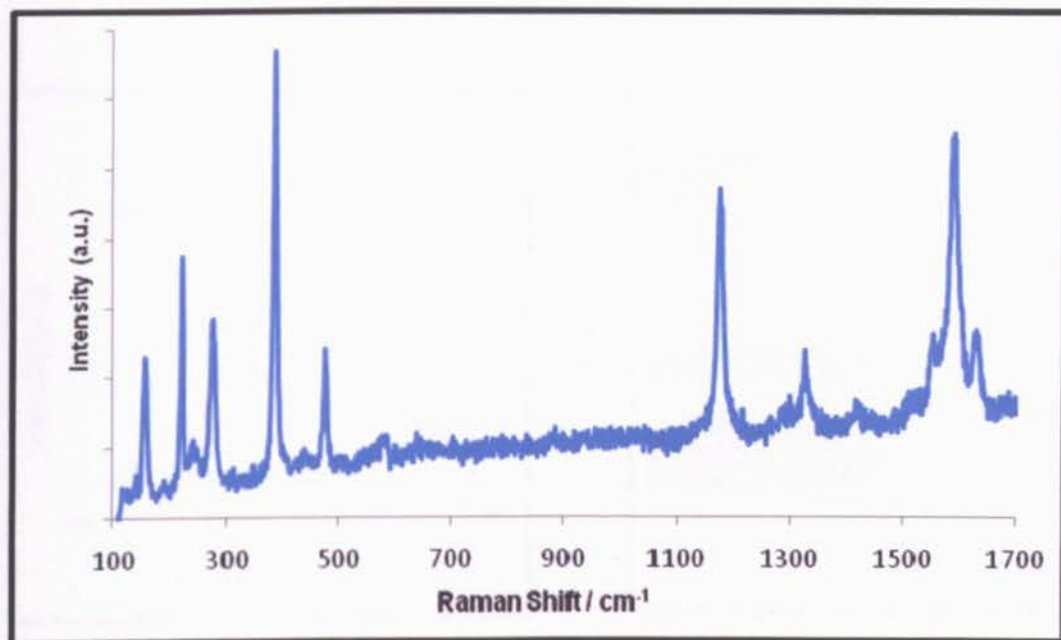


Figure 4 15: PPV-intercalated MnPS₃ Raman spectrum

4.4.1.6 UV-visible Spectroscopy

According to Grasso *et al* (1989),¹⁴ the valence and conduction band states originate from the P₂S₆⁴⁻ orbitals while the 3d states of the metal are positioned in the gap near the Fermi level and do not play a significant role in bonding.

The optical absorption spectrum of single crystals of MnPS₃ is shown in figure 4.16. The positions of the bands have all been assigned by several authors.^{14,47,54} The spectrum consists of a low intensity peak at 638 nm (1.94 eV) and a small shoulder at 536 nm (2.31 eV) followed by a steep absorption beginning at 487 nm (2.54 eV). The first two bands are low energy d-d absorption bands, due to the forbidden transitions of the M²⁺ d⁵ electrons whilst the fundamental absorption band at 2.54 eV is due to the ligand to metal charge transfer (see Figure 4.16).

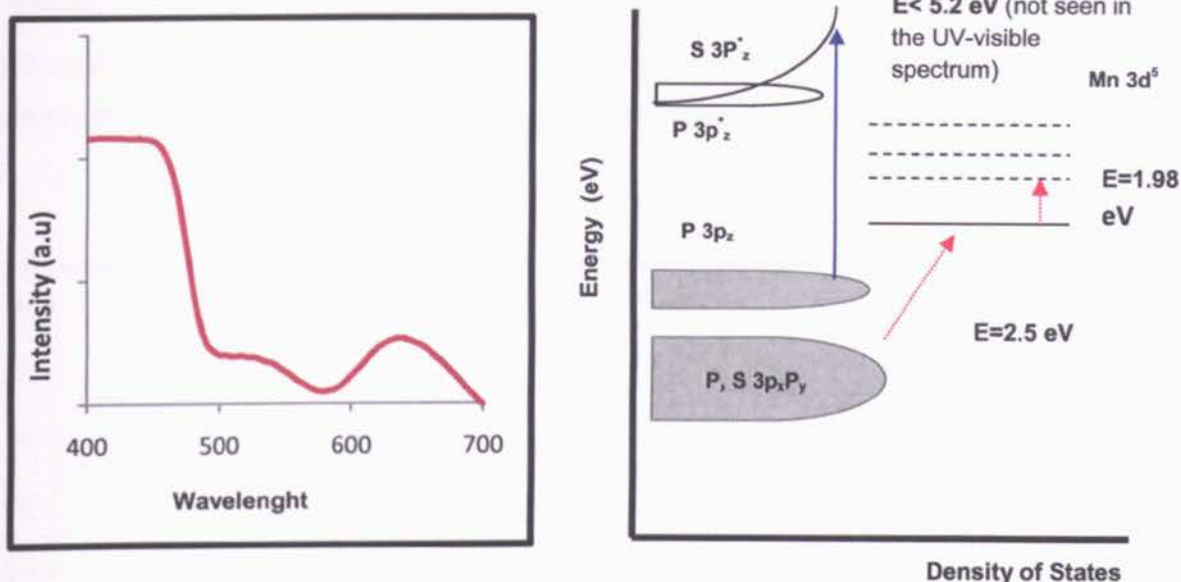


Figure 4.16: UV-visible spectrum of a MnPS₃ single crystal (left) and a graphical representation of the energy levels of MnPS₃ with the appropriate energy values¹⁴ (right)

4.4.2 CdPS₃

4.4.2.1 Elemental analysis

A white polycrystalline material was obtained from the synthesis of CdPS₃. Elemental analysis (EDX) of the sample suggested the formula to be Cd₂P₂S₆ (Cd, 45.70%, P, 12.00%, S, 39.32 %)

4.4.2.2 X-ray Diffractometry

4.4.2.2.1 CdPS₃

In the XRD pattern of CdPS₃ (Figure 4.17) the first reflection peak was observed at 13.37 (2θ) with a d spacing equal to 6.62 Å. This peak represented the (0 0 l) plane and was in good agreement with the values found in the literature.^{13,44} The 2nd, 3rd and 4th order reflections are given

in the Table 4.4. Due to the polycrystalline nature of the sample, reflections of the h and k planes were also observed; however their intensities were a lot lower, indicating preferred orientation of the plate-like crystallites. These reflections were assigned according to the literature.⁴⁴

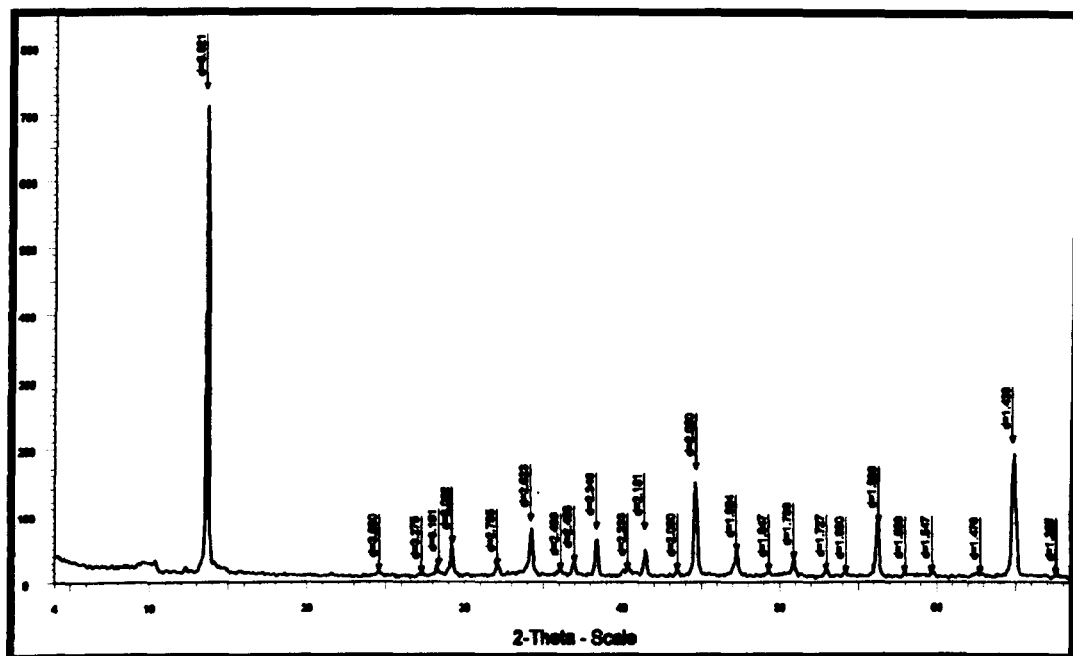


Figure 4 17: X-ray diffractogram of Polycrystalline CdPS₃

θ (2 θ) ^o	d / (Å)	Calculated Interlayer Spacing (Å)	(h k l) parameters	d / (Å) Literature Yang et al (2000) ⁴⁴
13.37	6.621	6.61	0 0 1	6.548
27.23	3.275	6.55	0 0 2	-
29.17	3.062		1 3 0	3.071
34.19	2.623		2 0 2	2.633
36.95	2.433		2 0 1	2.435

θ (2θ) ^o	d / (Å)	Calculated Interlayer Spacing (Å)	(h k l) parameters	d / (Å) Literature Yang et al (2000) ⁴⁴
41.40	2.181	6.543	0 0 3	-
50.93	1.793		0 6 0	1.794
56.346	1.633	6.532	0 0 4	-
59.78	1.547		2 0 3	1.549
64.84	1.438		2 6 1	1.446

 Table 4.18 Assignment of XRD data of CdPS₃ including literature values

4.4.2.2.2 K⁺-Intercalated CdPS₃ (K₂CdPS₃)

The x-ray diffractogram is shown in Figure 4.18. As expected, a new reflection peak appeared upon intercalation of K⁺. An interlayer expansion of 2.41 Å was observed at 9.80^o. The crystallinity of the sample was not affected, as evidenced by the sharp peaks on the XRD. Reflections of 2nd, 3rd and 4th order were also present but with lower intensities.

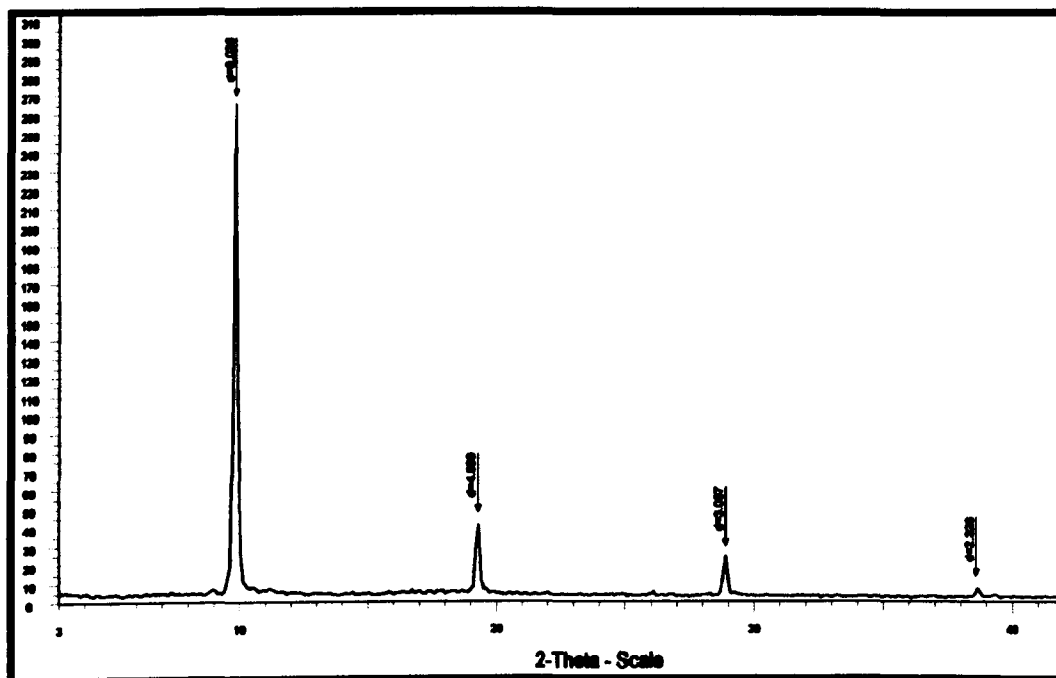
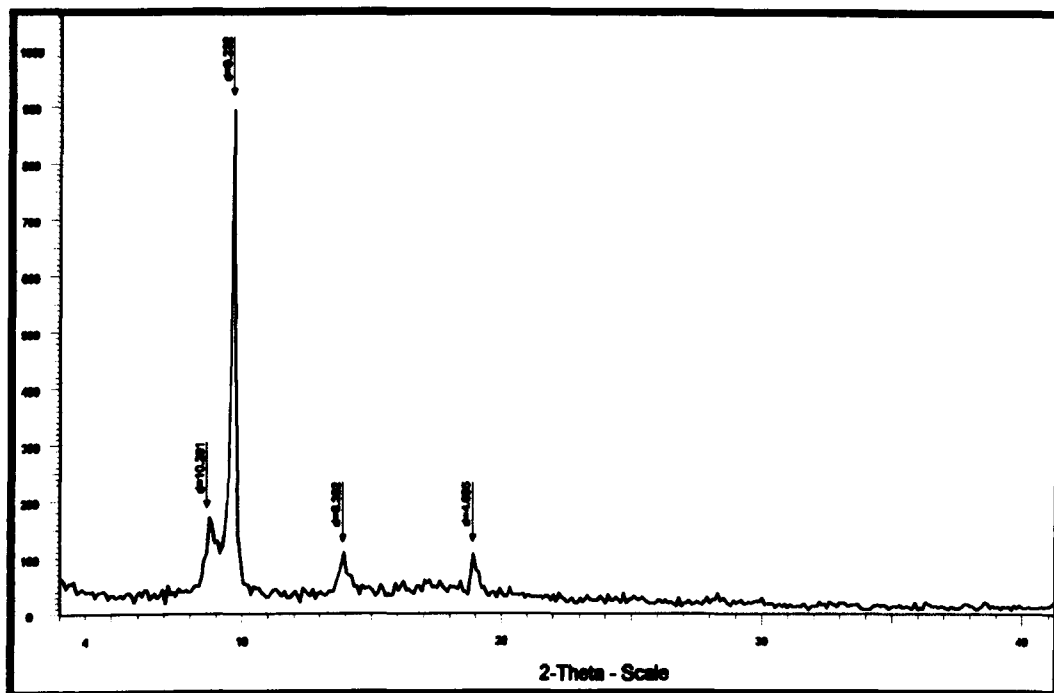


Figure 4 18: X-ray diffractogram of K^+ Intercalated $CdPS_3$ showing an interlayer expansion of 2.41 Å.

4.4.2.2.3 Polymer-intercalated $CdPS_3$ (PPV_CdPS_3)

The XRD pattern in figure 4.14 showed a new (0 0 l) reflection corresponding to a lattice expansion of 3.67 Å along the c-axis. This indicated that the polymer chains were lying flat, with the aromatic rings parallel to the host layers. A more intense peak at 9.58° ($d = 9.232$ Å) was also observed, indicating that the sample was only partially intercalated and that a significant amount of K^+ was still between the layers. Traces of unintercalated $CdPS_3$ were also seen, suggesting that the intercalation reaction was reversible. The sharpness of the sample peaks was an indication of the crystallinity of the sample which was not affected by the intercalation of the polymer.


 Figure 4 19: X-ray diffractogram of precursor polymer-intercalated CdPS₃

Sample	d / Å	Layer expansion/ Å	(h k l) parameters
CdPS ₃	6.62	-----	0 0 1
K_CdPS ₃	9.02	2.40	0 0 1
PPV_CdPS ₃	10.29	3.67	0 0 1

 Table 4.5 d-spacing expansion of CdPS₃ upon intercalation of K⁺ and PPV

4.4.2.3 Thermogravimetric Analysis (TGA)

The TGA data of the precursor polymer-intercalated CdPS₃ gave a 4% weight loss below 100 °C; this weight loss was attributed to the loss of weakly bound water molecules and intercalated K⁺. After 120 °C a steady weight loss was observed to due to the elimination of sulfonium groups.

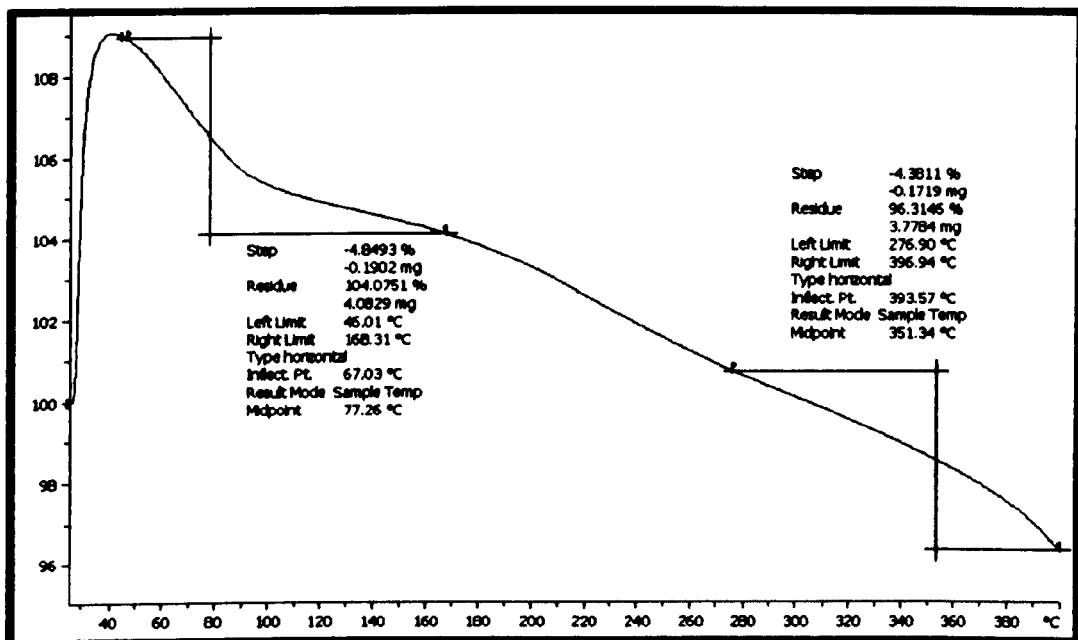


Figure 4 20: TGA diagram of precursor polymer intercalated CdPS₃ showing several weight loss steps.

The TGA diagram of PPV intercalated CdPS₃ gave a small percent weight loss below 100 °C. Considering the temperatures used during the conversion step, it was unlikely that there were any water molecules intercalated; hence, this loss was most likely due to any moisture picked up while the samples were left on the open bench. The sample was relatively stable up to 350 °C, but above this temperature another transition was observed and this was attributed to the degradation of PPV.

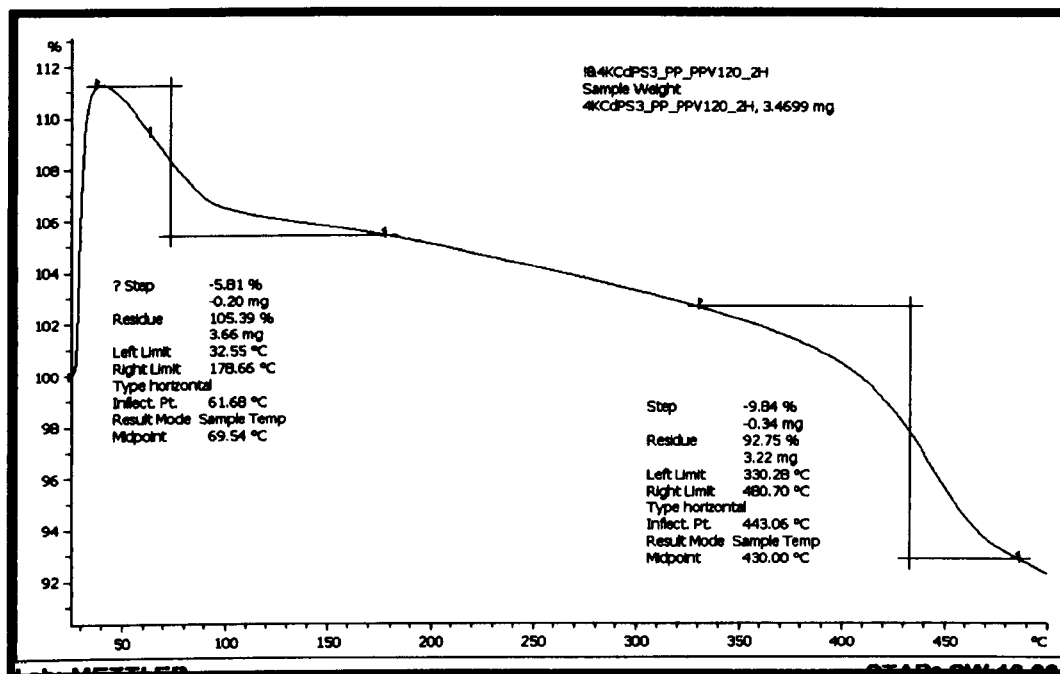


Figure 4 21: TGA diagram of PPV-intercalated CdPS₃ showing relatively good stability below 350 °C.

4.4.2.4 Scanning Electron Microscopy

The lamellar structure of CdPS₃ was also confirmed by SEM imaging. Similarly to MnPS₃, after intercalation of K⁺ there were some defects formed on the surfaces and edges of the samples. After addition of the polymer, the sample had a powder-like consistency, but at higher magnification it was possible to confirm that the layer structure had been maintained.

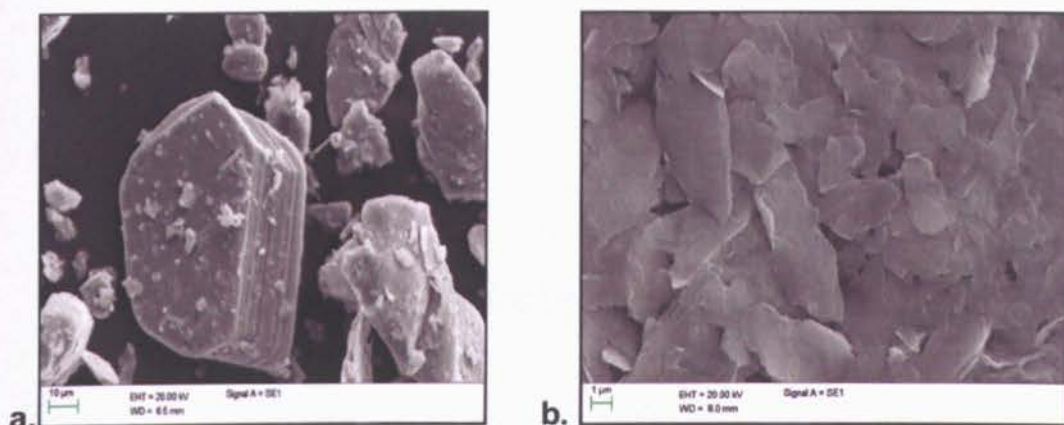


Figure 4 22: a.SEM image of lamellar CdPS₃ and b.SEM image of K⁺intercalated CdPS₃

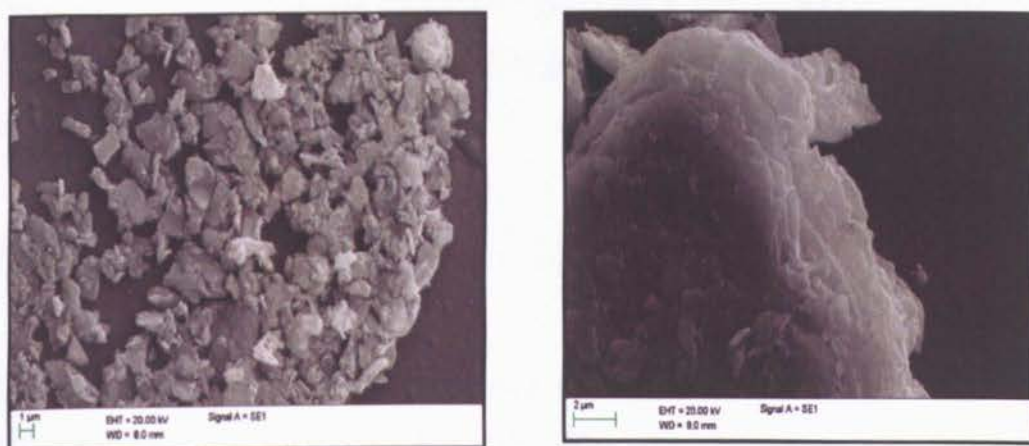


Figure 4 23: SEM image of precursor polymer-intercalated CdPS₃

4.4.2.5 Infrared and Raman spectroscopy

The spectra of the CdPS₃ were very similar to those of MnPS₃, with only small differences in their intensities; therefore only the spectra corresponding to the MnPS₃ samples have been shown. (See Appendixes A and B for CdPS₃ IR and Raman spectra).

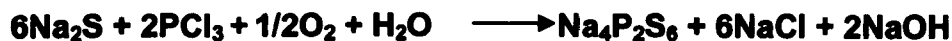
Chapter 5:

SYNTHESIS, CHARACTERISATION AND INTERCALATION OF AMORPHOUS THIOHYPOPHOSPHATES AND THIOORTHOPHOSPHATES

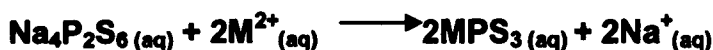
Thiohypophosphates ($M^{II}PS_3$ or $M^{II}_2P_2S_6$)

Even though MPS_3 are usually prepared as macroscopic crystals by high temperature techniques, they can also be produced as colloidal nanoparticles in aqueous solutions at room temperature. This was first successfully achieved by Foot *et al* (1986)⁵⁵ by mixing together a source of hexathiohypophosphate (P_2S_6)⁴⁻ anion and a solution of M^{2+} cation. This resulted in the production of large quantities of amorphous MPS_3 with properties very similar to those made by the solid state reaction at high temperatures. Moreover, their crystallinity could be readily improved by annealing the samples at about 300°C for about 2 to 4 hours.⁵⁵ This method permits the synthesis of thin film coatings and is much more convenient for the purpose of scaling up, particularly for photovoltaic or photo-electrochemical applications.

The source of (P_2S_6)⁴⁻ used by Foot and co-workers was the hexathiohypophosphate $Na_4P_2S_6$ first prepared by Falius (1968)⁵⁶ The reaction mechanism is given below:



Colloidal MPS_3 compounds are formed by reacting aqueous solutions of $\text{Na}_4\text{P}_2\text{S}_6$ with aqueous solutions of the metal in the M^{2+} state and the reaction mechanism can be written as follows:⁵⁵

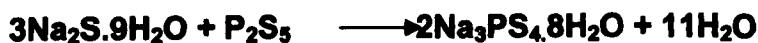


This approach was also used for the purpose of this project.

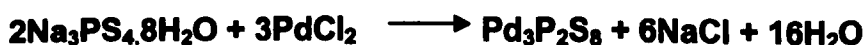
Thioorthophosphates [$\text{M}_3^{\text{II}} (\text{PS}_4)_2$]

In the case of palladium thiophosphate, $\text{Pd}_3(\text{PS}_4)_2$, its crystal structure consists of Pd^{2+} cations coordinated to thiophosphate groups $(\text{PS}_4)^{3-}$ in a square planar arrangement. Therefore it was necessary to find a suitable source of (PS_4) anions that could easily be prepared in aqueous solutions, and furthermore that could easily be reacted with a source containing Pd^{2+} , similarly to the synthesis of MPS_3 compounds.

Sodium tetrathiophosphate, Na_3PS_4 , was first prepared by E. Glatzel (1905)⁵⁷ by reacting sodium sulphide and phosphorus pentasulphide as follows:



Aqueous solutions of PdCl_2 or $\text{Pd}(\text{CH}_3\text{COO})_2$ were used as the source of Pd^{2+} and the reaction was expected to take place as follow:



5.1 Reagents and instruments used

The materials used for the synthesis of the amorphous $\text{MPS}_3\text{-Sn}$, their grades and suppliers are all given in Table 5.1. All chemicals were used without further purification. For information regarding the equipment used for the characterisation, please refer to chapter 4.

Material	Grade(%)	Supplier
Sodium sulphide nonahydrate	98.0	Sigma-Aldrich
Phosphorus trichloride	99.0	Sigma-Aldrich
Phosphorus pentasulphide	99.0	Sigma-aldrich
Manganese (II) chloride tetrahydrate	98.0	BDH Chemicals Ltd.
Manganese (II) acetate	99.9	Sigma-Aldrich
Palladium (II) chloride	99.0	Sigma-Aldrich
Palladium (II) acetate	98.0	Sigma-Aldrich

Table 5.1 Details of materials used for the synthesis of amorphous $\text{MPS}_3\text{-Sn}$

5.2 Synthesis of amorphous MPS_3

5.2.1 Synthesis of sodium hexathiohypophosphate $\text{Na}_4\text{P}_2\text{S}_6 \cdot 6\text{H}_2\text{O}$

$\text{Na}_4\text{P}_2\text{S}_6 \cdot 6\text{H}_2\text{O}$ was synthesised according to the literature.⁵⁵ $\text{Na}_2\text{S} \cdot 9\text{H}_2\text{O}$ (77.30 g, 0.2 mol) was dissolved in distilled water (100 ml), then PCl_3 (6.8 ml) was added dropwise, making sure that the temperature did not go above 25 °C. After all the PCl_3 had been added, the solution was stirred on an ice bath for 20 minutes, and then at room temperature for 1 hour. Air was bubbled through the mixture during the whole reaction to facilitate the oxidation process. The solution was then placed in the refrigerator (5 °C) for 48 hours. A white crystalline precipitate was obtained. The crude product was recrystallised from a hot mixture of water/ethanol (75:25) to remove the P-O impurities present. The pure product was a white polycrystalline powder. This reaction was repeated several times in attempt to improve the yield. It was observed that the longer the solution was left at temperatures below 5 °C the more precipitate was formed; however the products contained a lot of impurities. It was necessary to recrystallise the samples several times and once purified it was necessary to keep them in a desiccator under vacuum to prevent further oxidation. It was also possible to obtain further crops from the filtrate by addition of ethanol (100 ml); the mixture was left standing in air and the precipitate formed was filtered and washed with ethanol. The white powder was then recrystallised from hot water/ethanol (25:75). In order to remove all the impurities it was necessary to recrystallise the sample twice. Yield obtained: 8.23 g (30 %.)

5.2.2 Synthesis of $\text{Na}_3\text{PS}_4 \cdot 8\text{H}_2\text{O}$

$\text{Na}_3\text{PS}_4 \cdot 8\text{H}_2\text{O}$ was prepared according to the literature.⁵⁷ $\text{Na}_2\text{S} \cdot 9\text{H}_2\text{O}$ (80.32 g, 0.3 mol) was ground into small pieces. P_2S_5 (8.03g, 0.03 mol) was added slowly and the powders were mixed together until a fine mixture was obtained. The mixture was then placed in a beaker and heated until the powders melted. Keeping the temperatures at about 200 °C the mixture was stirred for 25 minutes until a bright orange solution was obtained. Then distilled water was added (80 ml) and the solution was heated for 15 more minutes. The solution was filtered while hot to remove any unwanted solid impurities, and the filtrate was left standing in air for 24 hours to form a white crystalline precipitate. The product was then filtered off, dried in air and recrystallised from an aqueous Na_2S solution as follows: $\text{Na}_2\text{S} \cdot 9\text{H}_2\text{O}$ (16 g, 0.06 mol) was dissolved in distilled water (32 ml), then the crude product (8.0 g) was added and the solution was heated up to 60 °C, and when the product was completely dissolved, the hot solution was filtered and left to cool down for 24 h. The precipitate was filtered off and dried in air for several hours. The product obtained was colourless and crystalline. Yield obtained after recrystallisation: 5.77 g (70%)

5.2.3 Synthesis of amorphous $\text{MnPS}_3 \cdot \text{Sn}$

In a typical reaction two solutions were prepared separately, one of them containing $\text{MnCl}_2 \cdot 4\text{H}_2\text{O}$ (0.40 g in 2.0 ml H_2O), the other one containing $\text{Na}_4\text{P}_2\text{S}_6 \cdot 6\text{H}_2\text{O}$ (0.09 g in 2.0 ml H_2O). When the two solutions were mixed, a pale green precipitate was formed almost immediately. This precipitate was then collected by centrifugation, washed several times with water and dried in air. Finally a green fine powder was obtained. Yield obtained: 0.09 g (95%) Alternatively $\text{Mn}(\text{CH}_3\text{COO})_2$ (0.08 g in 2.0 ml H_2O) was also used as the Mn^{2+} source using a solution of aqueous $\text{Na}_4\text{P}_2\text{S}_6 \cdot 6\text{H}_2\text{O}$ (0.05 g in 2.0 ml H_2O).

5.3 Synthesis of intercalated MnPS₃_Sln

5.3.1 Intercalation of Potassium Ions (K⁺)

MnPS₃_Sln (0.03 g, 9.3×10^{-5} mol) was immersed in an aqueous solution of KCl (15 ml, 0.5 M) for 1 hour. The precipitate formed was then collected and washed several times with distilled water.

5.3.2 Intercalation of precursor polymer

Two micellar solutions were prepared separately according to reference.^{58,63} One of them contained Brij-97 surfactant (3.2 g) in cyclohexane (40 ml), aqueous MnCl₂ (0.02 g in 1.5 ml H₂O) and precursor polymer solution (5 ml). The other solution contained Brij-97 (4.0 g) in cyclohexane (50 ml) and Na₄P₂S₈.6H₂O (0.03 g in 3 ml H₂O). The two solutions were mixed and left stirring for 48 hours; ethanol was then added to break the emulsion and the precipitate formed was collected and washed several times with ethanol and dried in air for 24 hours.

Thermal elimination to form PPV

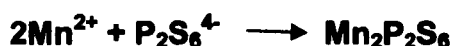
The samples were heated under nitrogen for 10 minutes at 220 °C at first, and then they were heated for an hour more under the same conditions.

5.4 Results and Discussion

5.4.1 Elemental Analysis

5.4.1.1 *MnPS₃Sln*

The preparation is based on an ion exchange method; the chemical reaction is given below:



The direct combination of aqueous solutions containing $\text{Na}_4\text{P}_2\text{S}_6 \cdot 6\text{H}_2\text{O}$ and MnCl_2 resulted in the immediate formation of a cloudy pale green suspension. The sample was left to precipitate, and after centrifugation a fine pale-green powder was collected.

Elemental analysis (ICP) led to the formula $\text{Mn}_{0.5}\text{P}_1\text{S}_3$ (Mn 20.5 g L⁻¹, P 24.5 g L⁻¹, S 84.8 g L⁻¹) which suggested that only partial exchange of the Na atoms had taken place.

5.4.2 X-ray Diffractometry

5.4.2.1 *Na₄P₂S₆·6H₂O*

The XRD pattern of $\text{Na}_4\text{P}_2\text{S}_6 \cdot 6\text{H}_2\text{O}$ is shown in Figure 5.1. All distinctive diffraction peaks of the sample are observed and are in good agreement with the literature values.⁵⁹ The sharpness of the peaks suggested the formation of highly crystalline $\text{Na}_4\text{P}_2\text{S}_6 \cdot 6\text{H}_2\text{O}$.

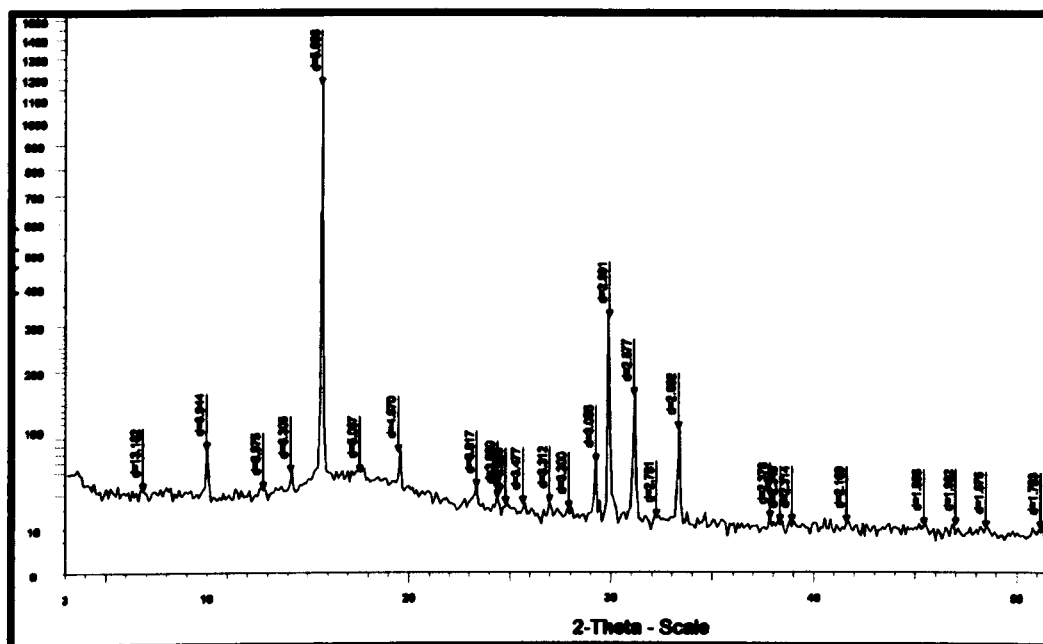


Figure 5 1: X-ray diffractogram of $\text{Na}_4\text{P}_2\text{S}_6 \cdot 6\text{H}_2\text{O}$.

5.4.2.2 $\text{MnPS}_3_{\text{Sln}}$

The samples obtained by this approach presented similar structural features to the MnPS_3 prepared by the solid state process; however, the crystallinity of these samples was much lower than the high temperature synthesised phase, as can be observed in the XRD pattern of the $\text{MnPS}_3_{\text{Sln}}$, Figure 5.2

Even though the broadness of the peaks suggested that the material was less ordered, it was possible to see the [0 0 l] reflections, which indicated that the preferred orientation of the layers was parallel to the substrate and thus it was possible to estimate the interlayer distance which was 6.46 Å, a value very similar to that of the high temperature synthesised MnPS_3 .⁴⁵ Other peaks present were at 29.6 and 32.1° (2θ) which according to Li *et al* (2005)⁶⁰ corresponded to the crystal planes of [130] and [131] respectively. After annealing the sample, the crystallinity was slightly improved; the peaks became sharper and clearer and it was possible to see the [001], [002] and [003] planes at 13.9, 28.2 and 41.4° (2θ)

respectively. The interlayer space was slightly smaller (6.40 Å) due to the reorganisation of the crystal sites.

The broad peak seen around 17° (2θ) in all the XRD patterns of the amorphous samples was due to the background of the sellotape used to hold the samples in place during examination.

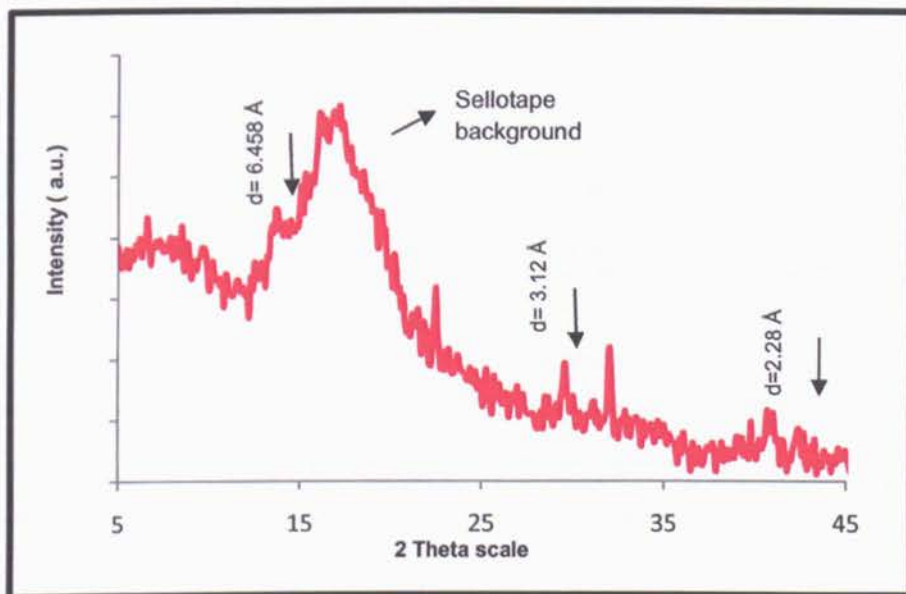


Figure 5 2: XRD pattern of amorphous MnPS₃_SIn before annealing.

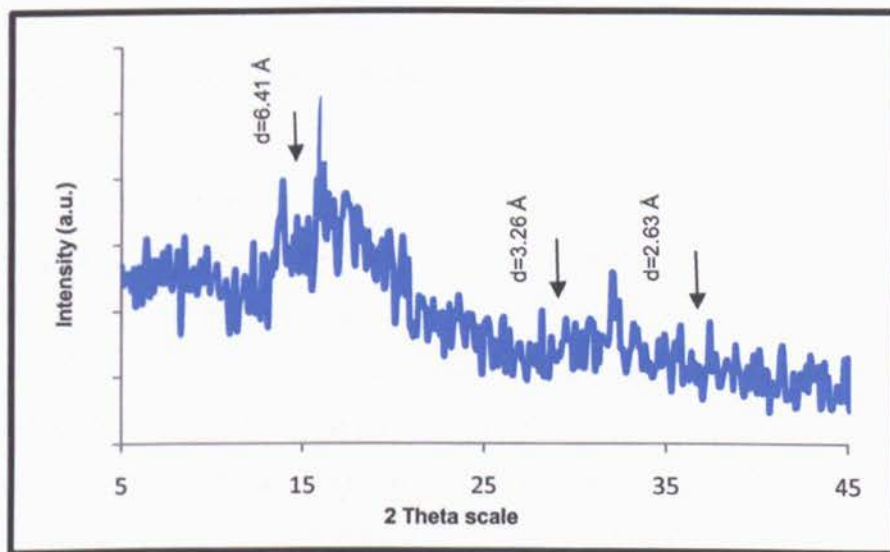


Figure 5 3: XRD pattern of amorphous MnPS₃_SIn after annealing.

Sample	θ (2 θ)	d/(Å)	Calculated Interlayer spacing/(Å)	(h k l) parameters	θ (2 θ) literature Li <i>et al</i> (2005) ⁶⁰	d/(Å) literature Li <i>et al</i> (2005) ⁶⁰
Mn₂P₂S₆	13.7	6.46	6.46	0 0 1	13.64	6.53
	28.7	3.21	6.42	0 0 2	27.48	3.34
	29.6	3.12	-----	1 3 0	29.74	3.10
	32.1	2.90	-----	1 3 1	34.79	2.70
	42.4	2.28	6.84	0 0 3	Not given	Not given
Mn₂P₂S₆ Annealed	13.9	6.41	6.41	0 0 1	13.64	6.53
	16.1	5.56	-----	-----	Not given	Not given
	28.2	3.26	6.52	0 0 2	27.48	3.34
	31.9	2.91	-----	1 3 0	29.74	3.10
	35.8	2.63	-----	1 3 1	34.79	2.70
	41.3	2.33	6.99	0 0 3	Not given	Not given

Table 5.2 Assignment of XRD data of MnPS₃_Sln before and after annealing, including literature values.

5.4.2.3 K⁺ intercalated MnPS₃_Sln

The intercalation of K⁺ was confirmed by an increase of 2.75 Å in the interlamellar distance of the amorphous Mn₂P₂S₆ as seen in the x-ray diffraction pattern shown in Figure 5.4. A small amount of the original phase (0 0 1, d ~ 6.5Å) of the pure MnPS₃_Sln was still observed, which suggested that the intercalation occurred only partially. The reasons behind the partial intercalation are not very clear, but perhaps this was due to the short time the sample was left to react, however, K⁺ ions are one of the most common and easy cations to intercalate in short periods of time (1 h). Attempts to form a homogeneous phase by prolonging the stirring

time to 24 h resulted in the complete removal of Mn^{2+} from the lattice, and thus, the formation of unwanted compounds

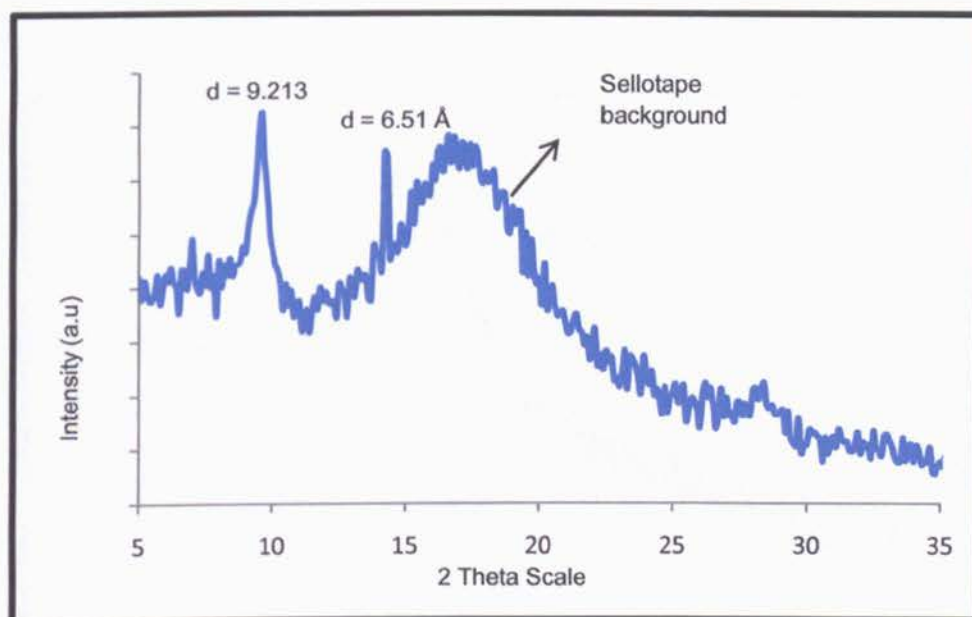


Figure 5 4: X-ray diffractogram of K^+ intercalated $MnPS_3_Sln$ showing traces of unintercalated $Mn_2P_2S_6$

5.4.2.4 PPV intercalated $MnPS_3_Sln$

The intercalation of the polymer was confirmed by a new peak at 6.1° (2θ) in the xrd pattern shown in Figure 5.5 corresponding to an interlayer expansion of almost 8 Å. This expansion may have been due to the insertion of water molecules as well as well as the polymer; however, the IR spectra did not show any sign of water being present in the compound. Furthermore, the formation of a double layer of polymer parallel to the layers of the host material (based on the results of the intercalation of PPV into the layers of polycrystalline $MnPS_3$) seems a more reasonable reason for such a big interlayer expansion. The peaks corresponding to the pristine amorphous $Mn_2P_2S_6$ all disappeared, indicating that the mutual

organisation of the planes had been lost as a result of the polymer intercalation.

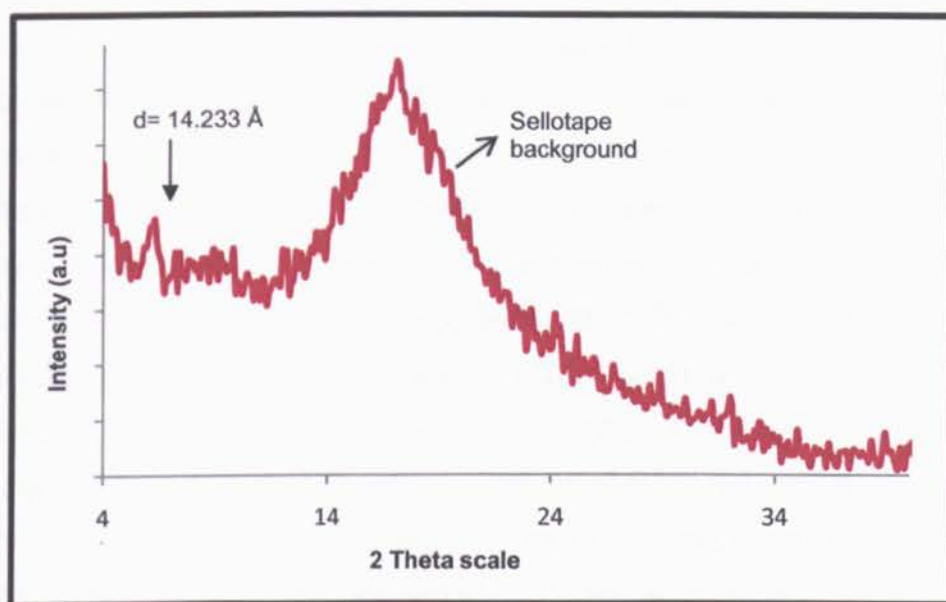


Figure 5 5: X-ray diffractogram of PPV-intercalated MnPS_3Sln .

Sample	d / Å	Layer expansion/ Å	(h k l) parameters
$\text{Mn}_2\text{P}_2\text{S}_6$	6.46	-----	0 0 1
$\text{K}_\text{Mn}_2\text{P}_2\text{S}_6$	9.21	2.75	0 0 1
$\text{PPV}_\text{Mn}_2\text{P}_2\text{S}_6$	14.23	7.77	0 0 1

Table 5.3 d-spacing expansion of MnPS_3Sln upon intercalation of K^+ and PPV

5.4.3 Infrared and Raman Spectroscopy

5.4.3.1 $\text{Na}_4\text{P}_2\text{S}_6 \cdot 6\text{H}_2\text{O}$

In the case of the crude product, a strong peak around 1116 cm^{-1} was observed in the IR spectrum of the sample. This peak was attributed to the presence of P-O impurities that were expected to be formed during the oxidation process. This peak disappeared completely after recrystallisation. Other peaks also present were a broad band at 3350 cm^{-1} and a less strong but sharp peak at 1620 cm^{-1} , both of them characteristic of water molecules. In the region below 600 cm^{-1} , the absorbance bands are mostly due to the $\text{P}_2\text{S}_6^{4-}$ group with a broad and strong band arising at 579 cm^{-1} due to the P-S stretching frequencies.⁶¹ Furthermore, the Raman spectrum of the pure compound presented the characteristic peaks of the isolated $(\text{P}_2\text{S}_6)^{4-}$ unit. According to Prouzet *et al* (1999)⁶² the high frequency peak localised at 550 cm^{-1} and its shoulder at 570 cm^{-1} are due to the PS_3 antisymmetric degenerate stretching modes, $\nu_{\alpha}(\text{PS}_3)$, whereas the strong sharp peak at 379 cm^{-1} was attributed to the symmetric stretching mode $\nu_{\text{sym}}(\text{PS}_3)$. The PS_3 bending modes were observed at 264 cm^{-1} in agreement with the literature value.⁶²

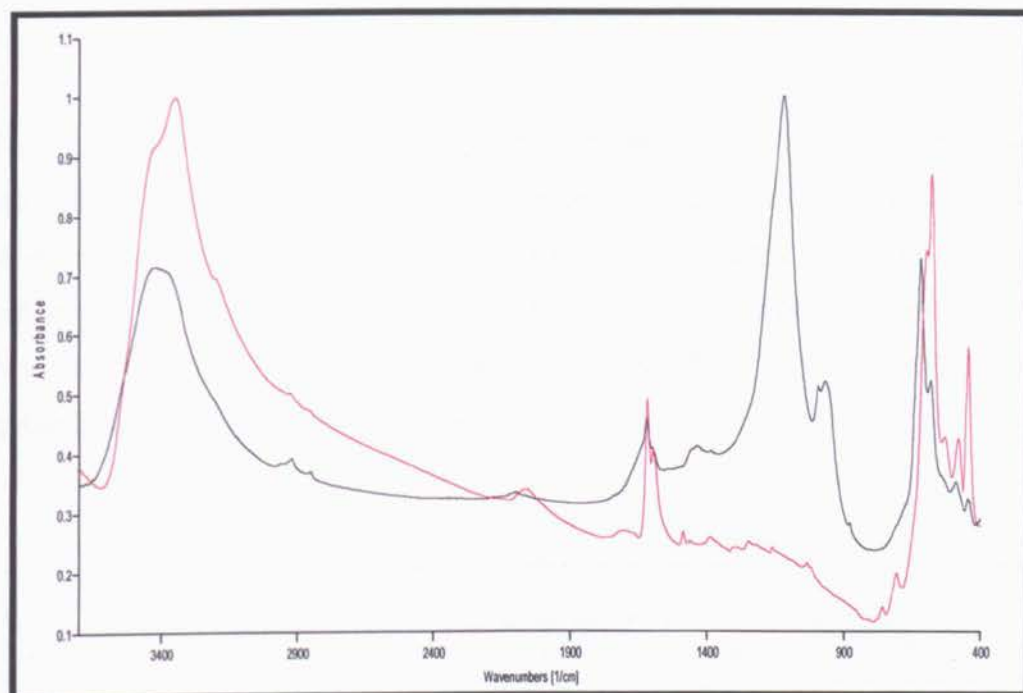


Figure 5 6: Infrared Spectra of crude (black) and recrystallised (red) $\text{Na}_4\text{P}_2\text{S}_6 \cdot 6\text{H}_2\text{O}$.

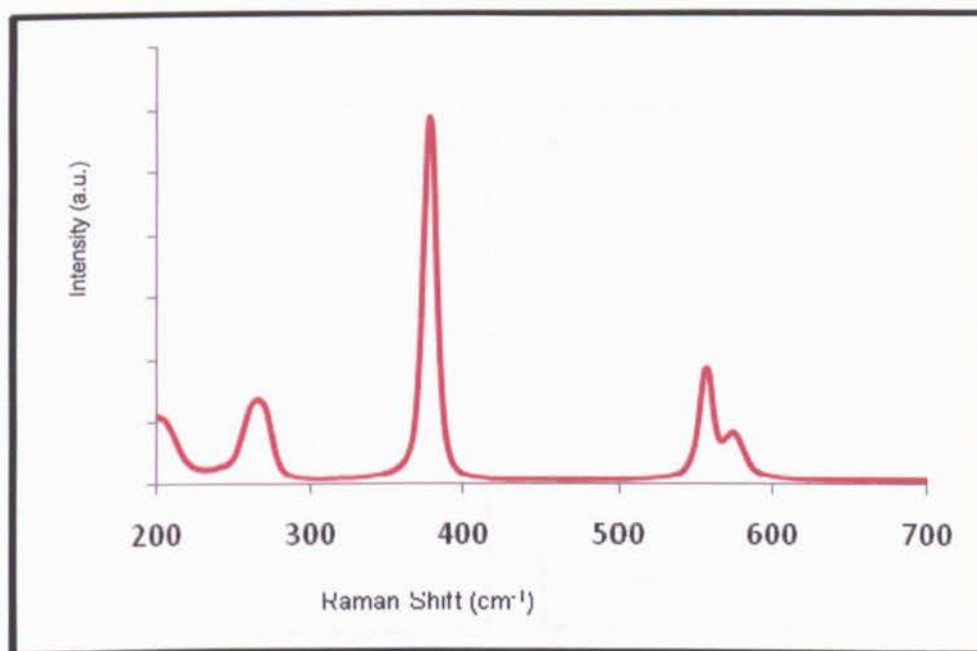


Figure 5 7: $\text{Na}_4\text{P}_2\text{S}_6 \cdot 6\text{H}_2\text{O}$ Raman spectrum.

5.4.3.2 MnPS₃_Sln

The infrared spectrum of MnPS₃_Sln did not show major changes with respect to the Na₄P₂S₆ spectrum; there was only a small shift of the absorption peaks towards lower energies. Similarly, in the Raman spectrum, there was a small shift on the (P₂S₆)⁴⁻ vibrational peaks due to the change in the structural environment. The Raman shifts and assignments are given in the table below.

Assignment	Na ₄ P ₂ S ₆ .6H ₂ O	MnPS ₃ _Sln
$\nu_{\text{sym}} \text{PS}_3$	570 cm ⁻¹	573 cm ⁻¹
$\nu_{\text{sym}} \text{P-P}$ and $\nu_{\text{sym}} \text{P-S}$	379 cm ⁻¹	379 cm ⁻¹
$\delta \text{S-P-S}$ and $\delta \text{S-P-P}$	264 cm ⁻¹	270 cm ⁻¹

Table 5.4 Assignment of the Raman shifts observed for Na₄P₂S₆.6H₂O and MnPS₃_Sln

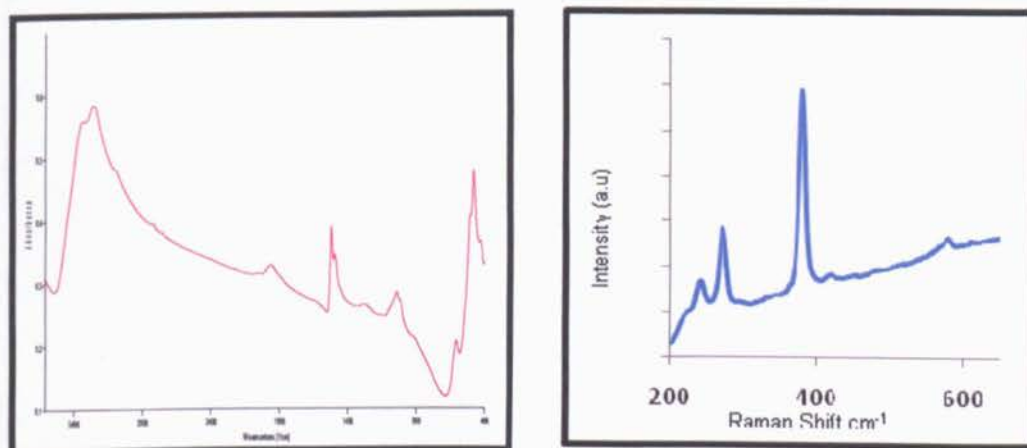


Figure 5.8: MnPS₃_Sln IR (left) and Raman (right) spectra.

5.4.3.3 K^+ Intercalated $MnPS_3_Sln$

The infrared spectrum of the intercalated sample is shown in Figure 5.9. The absorbance band at 581 cm^{-1} corresponding to the asymmetric stretching $\nu(PS_3)$ has been split into two components (610 and 558 cm^{-1}) in the intercalated sample. This splitting of the band, as mentioned before (refer to the intercalation of crystalline $MnPS_3$, page 71), is due to the formation of intralamellar Mn^{2+} vacancies that create different environments on the P-S bond. The two bands (3400 cm^{-1} broad, 1600 cm^{-1} sharp) show the presence of water, whereas the small band around 1100 cm^{-1} indicates the formation of P-O impurities due to the hydrolysis of the intralamellar ($P_2S_6^{4-}$) according to the following proposed equation:⁴⁵

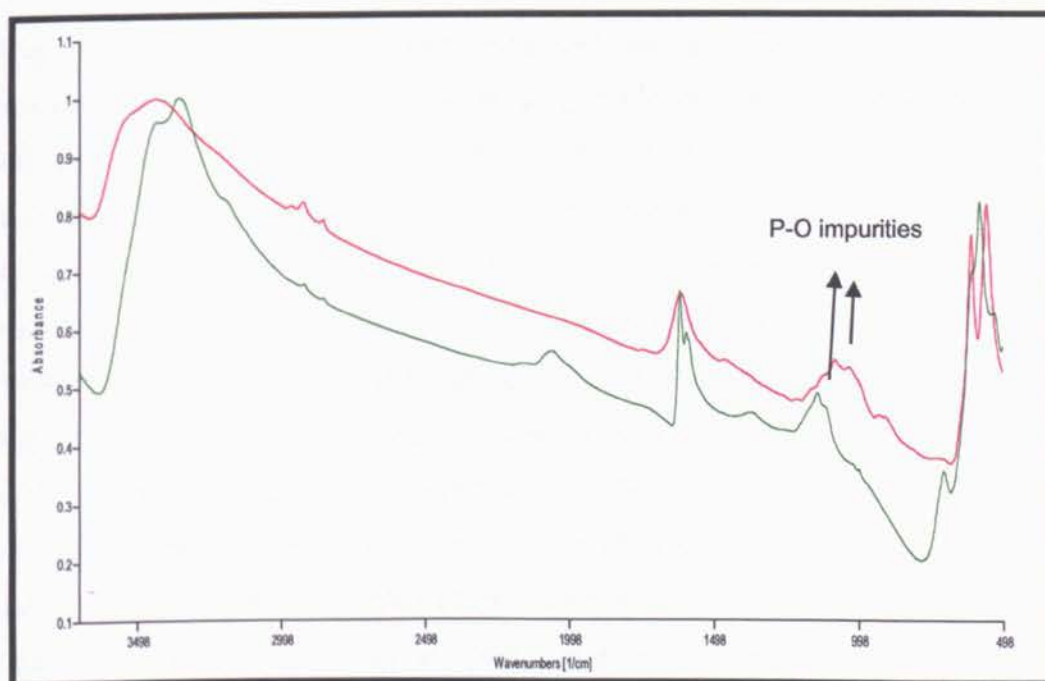
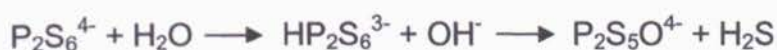


Figure 5.9: $MnPS_3_Sln$ and K^+ -intercalated $MnPS_3_Sln$ IR spectra.

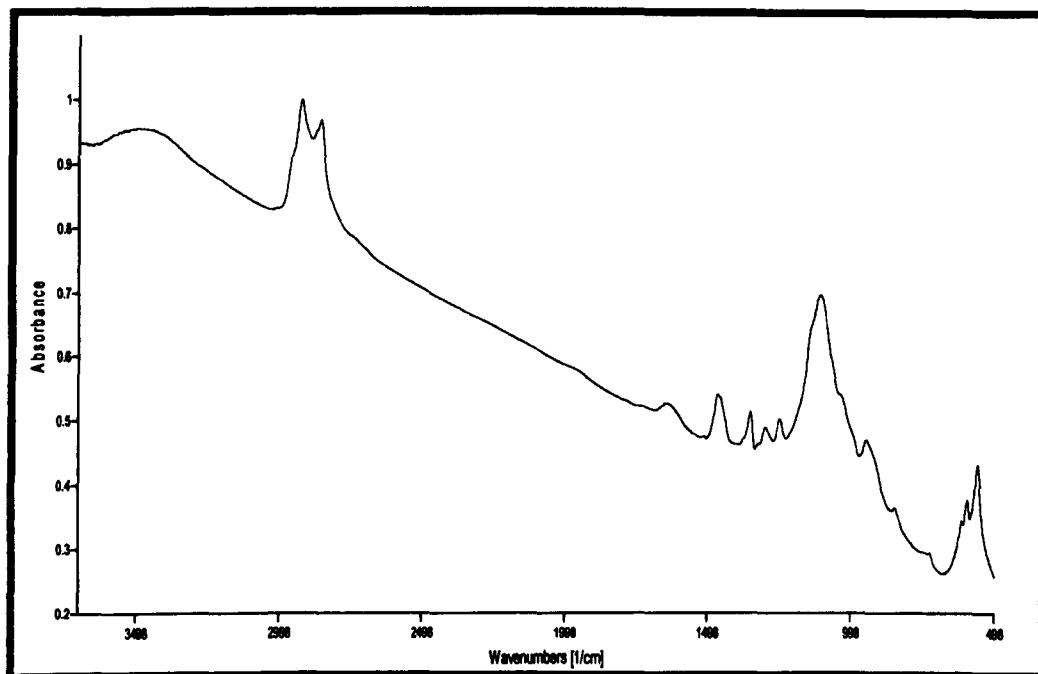


Figure 5 10: PPV-intercalated MnPS₃·5Sn IR spectra.

5.4.3.4 PPV intercalated MnPS₃·5Sn

The intercalation of PPV was achieved by an alternative and more convenient procedure used by Yi *et al* (2005)⁶³ that did not require several ion exchanges. The strong peak at 2929 cm⁻¹ are due to the sp³ C-H stretching of the sulfonium leaving groups of the precursor polymer which suggests that only partial conversion was achieved after heating the samples for 10 minutes. The bands between 1450 and 1050 cm⁻¹ are also characteristic of the sulfonium salts. A small peak at 980 cm⁻¹ started to appear indicating the presence of the trans-vinylene C-H out of plane of PPV, however no peaks corresponding to the trans-vinylene C-H stretch was observed. Additionally, a strong band around 1100 cm⁻¹ was observed due to the formation of phosphates during the intercalation process. The peaks corresponding to the inorganic phase were also present with the typical "band split" which is the signature of intercalated MPS₃ compounds.

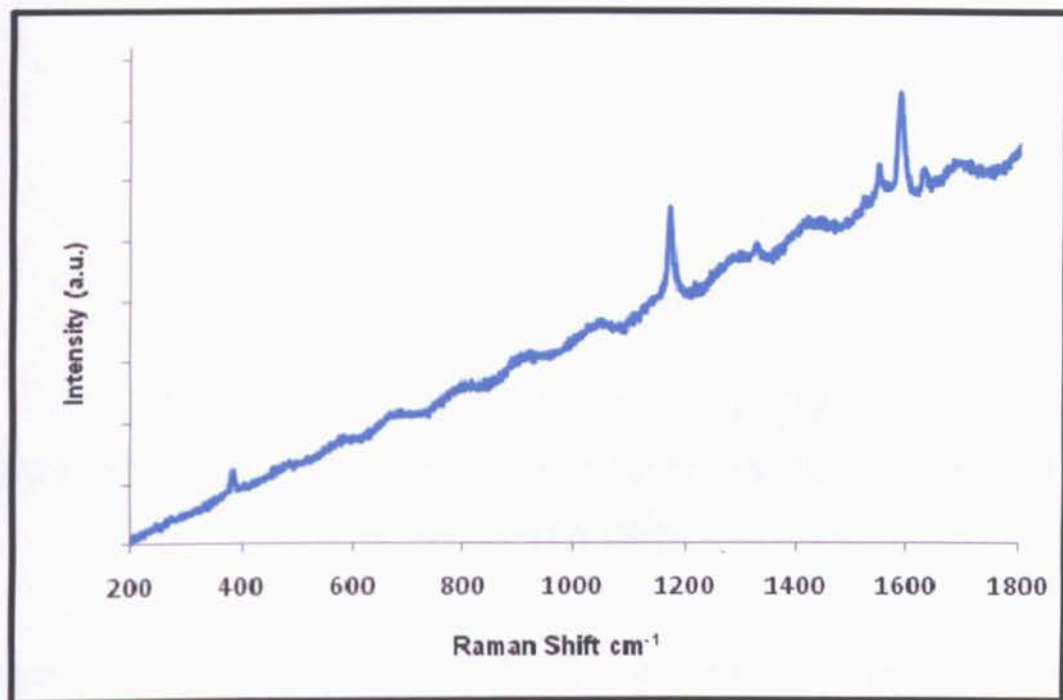


Figure 5.11: Raman spectrum of PPV-intercalated MnPS₃_SIn.

The Raman spectra of the PPV intercalated MnPS₃_SIn is shown in Figure 5.11. The characteristic PPV vibrations at 1174, 1548, 1585 and 1630 cm⁻¹ are all present. The featured peaks belonging to the host MnPS₃_SIn are all overcast by the intense peaks of the conjugated PPV, however; it is still possible to see a small peak at 384 cm⁻¹ due to the $\nu_{\text{sym}}(\text{PS}_3)$ mode.

Chapter 6:

SYNTHESIS, CHARACTERISATION AND INTERCALATION OF LAMELLAR OXOVANADIUM PHOSPHATES

Oxovanadium phosphate ($\text{VOPO}_4 \cdot 2\text{H}_2\text{O}$) is a well known layered system that can intercalate polymers by several routes, particularly by *in situ* intercalation/polymerisation. This technique of intercalation is suitable for lamellar structures that are highly oxidizing, where simultaneous intercalation of monomers and polymerisation takes place.¹⁶ The intercalation of polyaniline for example, has been successfully achieved by this method because the polymerisation reaction requires an oxidising agent and $\text{VOPO}_4 \cdot 2\text{H}_2\text{O}$ is ideal. However, for the purpose of this research, the oxidising properties of $\text{VOPO}_4 \cdot 2\text{H}_2\text{O}$ could eventually lead to the degradation of PPV and the formation of unwanted products.

To overcome this problem; $\text{VOPO}_4 \cdot 2\text{H}_2\text{O}$ was first treated with a suitable reducing agent. During the reduction, a charge compensating cation was introduced into the interlayer space of VOPO_4 ,⁶ and consecutively exchanged for the precursor polymer cations.

In addition to the layer structure and the variety of intercalation pathways; this compound was chosen as an alternative inorganic host because it can be easily prepared at relatively low temperatures. The reaction yields are reasonably high and the material obtained is highly crystalline with good optical properties.

6.1 Reagents and instruments used

The materials used for the synthesis of $\text{VOPO}_4 \cdot 2\text{H}_2\text{O}$ their grades and suppliers are all given in Table 6.1. All chemicals were used without further purification. For information regarding the equipment used for the characterisation please refer to Chapter 4.

Material	Grade (%)	Supplier
Vanadium pentoxide	99.6	Sigma Aldrich
Phosphoric acid	85	VWR International
Hydrochloric acid	37	Fisher Scientific
Potassium iodate	99.8	BDH Chemicals
Acetone	99.5	VWR International
Ethanol	99.9	Fisher Scientific

Table 6.1 Details of materials used for the synthesis of $\text{VOPO}_4 \cdot 2\text{H}_2\text{O}$ and intercalates

6.2 Synthesis of $\text{VOPO}_4 \cdot 2\text{H}_2\text{O}$

$\text{VOPO}_4 \cdot 2\text{H}_2\text{O}$ was prepared according to the literature⁶⁴ by refluxing V_2O_5 (2.42 g, 13.2×10^{-3} mol), H_3PO_4 (13.5 ml) and distilled water (58.9 ml) for 3 days. The reaction mixture was allowed to cool down and the precipitate was filtered off and washed, first with distilled water, then with acetone. A yellow-green crystalline material was obtained. The sample was dried in air for 24 hours. Yield obtained: 3.52 g (68%)

6.3 VOPO₄.2H₂O intercalation

6.3.1 Intercalation of Lithium ions (Li⁺) (Li_VOPO₄)

General procedure C: VOPO₄.2H₂O (0.50 g, 2.52x10⁻³ mol) and Lil (5.00 g, 37.3x10⁻³ mol) were added to a mixture containing water and acetone (2:14 ml ratio). The mixture was refluxed for 5 days at 40^oC. The precipitate was then filtered off, washed with a solution of water /acetone (1:1) and left to dry in air for 24 hours. The product was a pale green crystalline powder.

6.3.2 Intercalation of Potassium ions (K⁺) (K_VOPO₄)

General procedure C was followed. KI (1.03 g, 6.20x10⁻³ mol) was used instead of Lil and the mixture was refluxed for 10 days instead of 5.

6.3.3 Intercalation of precursor polymer

A mixture containing K_VOPO₄ (0.03 g, 2.0x10⁻⁴ mol) and ethanol (10 ml) was prepared and bubbled with nitrogen for 1 hour. To this mixture, a degassed ethanolic solution of monomer 1 (1.00 g in 14.5 ml of ethanol) was added and refluxed for 24 hours under nitrogen. The mixture was then cooled down to 0 ^oC and a cooled ethanolic solution of KOH (14.5 ml, 0.2 M) was added to it. This mixture was stirred at 0 ^oC for 2 hours and then at room temperature for 6 days. After this time a gel-like mixture was formed which was then sonicated with a bit of precursor polymer solution until the gel was completely dissolved. The solution was then placed in aluminium dishes and the solvent was left to evaporate.

6.4 Results and Discussion

6.4.1 Elemental Analysis

6.4.1.1 $\text{VOPO}_4 \cdot 2\text{H}_2\text{O}$

A green-yellowish crystalline powder was obtained. Elemental analysis (EDX) of the compound led to the formula $\text{V}_{0.17} \text{O}_{0.86} \text{P}_{0.16}$ (V, 23.10%, O, 28.56%, P, 13.34 %).

The water content was determined by thermogravimetric analysis. The final composition was found to be $\text{V P}_{0.94} \text{O}_{3.88} 1.9\text{H}_2\text{O}$

6.4.1.2 K^+ intercalated VOPO_4

Green polycrystalline powders were obtained. The amount of intercalated ions was calculated by titration as described by Chauvel *et al* (1995)⁶⁵ and led to the formula $\text{K}_{0.6} \text{VOPO}_4 \cdot 1.8\text{H}_2\text{O}$

6.4.2 Powder x-ray diffraction

6.4.2.1 $\text{VOPO}_4 \cdot 2\text{H}_2\text{O}$

The identity of the synthesised layered compound was confirmed by the XRD pattern shown in Figure 6.1 The interlayer space was found to be 7.48 Å at about 11.82° (2 θ). This value was consistent to the literature.⁶⁴⁻⁶⁵ A second order reflection was also observed at 23.90° with an interlayer spacing of 7.45 Å. No other peaks were observed.

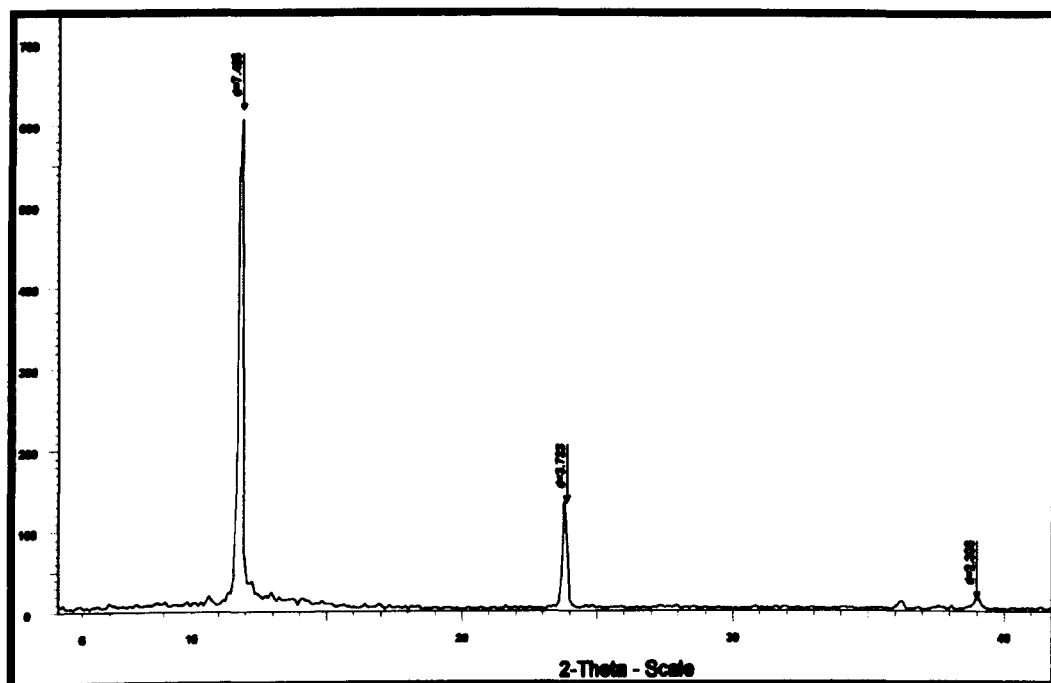


Figure 6 1: X-ray diffractogram of $\text{VOPO}_4 \cdot 2\text{H}_2\text{O}$.

6.4.2.2 Li^+ and K^+ intercalated VOPO_4

The xrd patterns of the compound K_VOPO_4 showed that after intercalation, the samples remained highly crystalline, Figure 6.2. A contraction of the interlayer space was observed, due to electrostatic attraction between the intercalated cations and the vanadyl phosphate layers which became negatively charged as the vanadium (V) was reduced. Furthermore the observed decrease in the d-spacing is also evidence of the replacement of the weakly-bonded water molecules between the layers by cationic species.⁶⁵ It is very likely that the intercalation only affected the *c*-axis as no peaks apart from (0 0 l) were observed in the xrd pattern. The new d values for the intercalated samples depended on the intercalated cation: for Li^+ $d = 6.035 \text{ \AA}$ and for K^+ $d = 6.187 \text{ \AA}$.

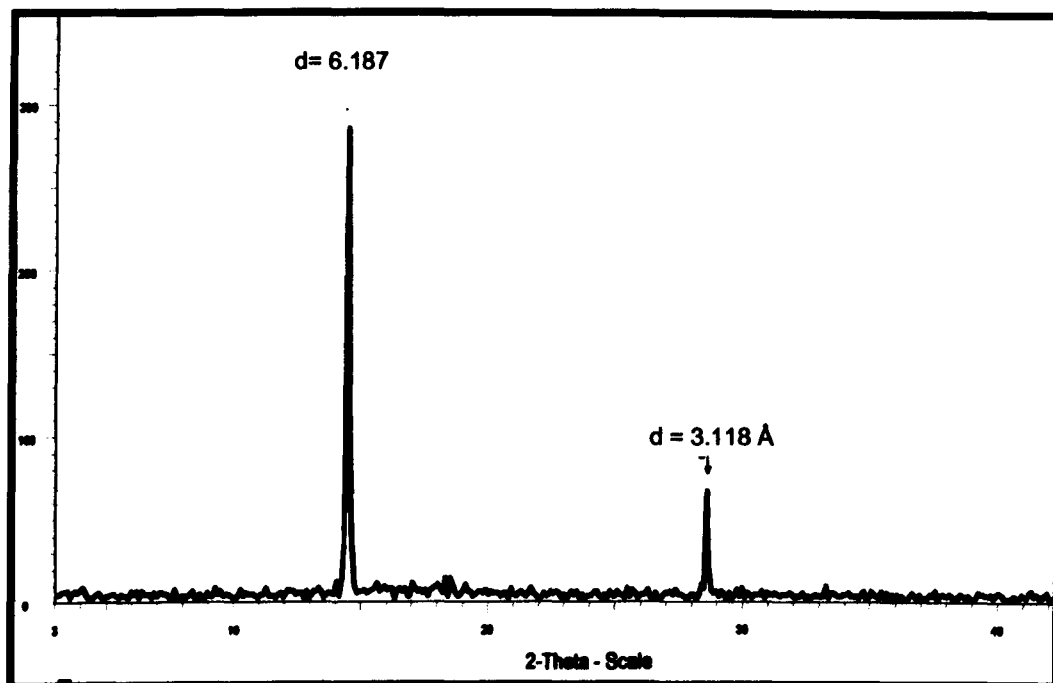


Figure 6 2: X-ray diffractogram of K^+ -intercalated $VOPO_4 \cdot 2H_2O$.

6.4.2.3 Precursor polymer intercalated $VOPO_4$

The XRD pattern (Figure 6.3) shows a significant decrease in the intensity of the lines and broadening of the peaks, indicating a loss of crystallinity of the samples. Additionally, intercalation of the precursor polymer caused an increase of 3.849 Å in the interlayer spacing compared with the original host. This value is consistent with the one observed for the $MnPS_3$ and $CdPS_3$ samples, indicating that the polymer chains are lying horizontally parallel to the sample layers. A 3rd order peak was also observed at about 26.523° corresponded to an interlayer space of 10.08Å. Other peaks observed had no clear attribution.

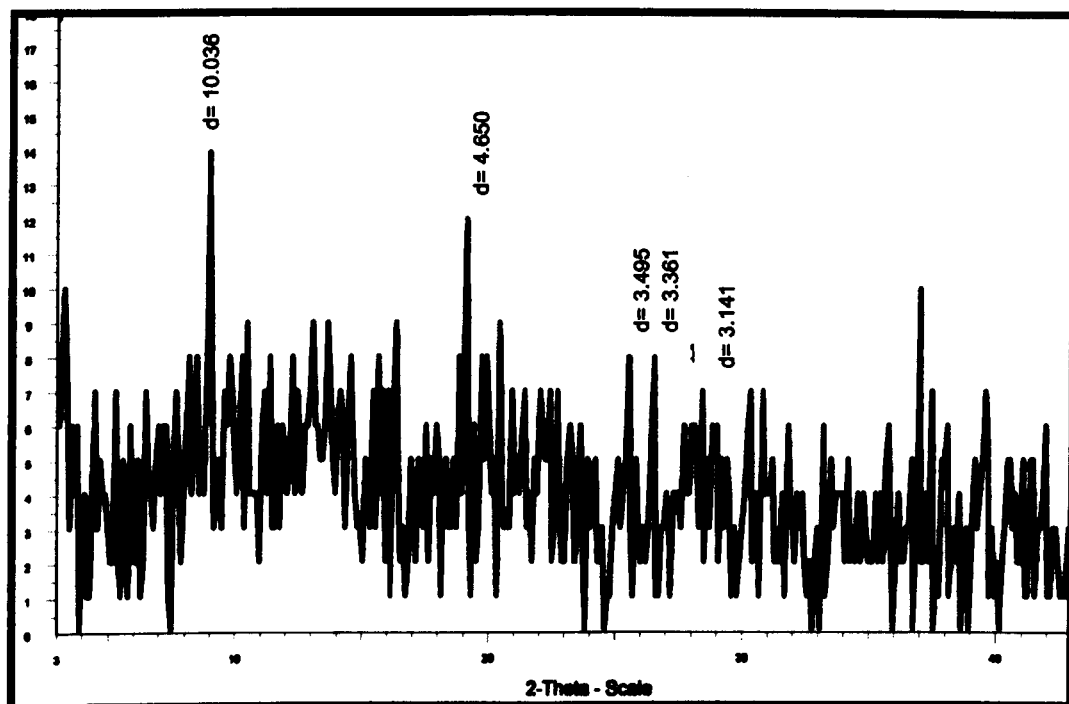


Figure 6 3: X-ray diffractogram of Precursor polymer intercalated VOPO_4

6.4.3 Scanning Electron Microscopy (SEM)

The SEM images of the samples are shown in Figure 6.4 and correspond to $\text{VOPO}_4 \cdot 2\text{H}_2\text{O}$ and they show that this material consisted of irregular plate-like crystallites stacked vertically, perpendicular to the a,b-plane (which is consistent with the XRD pattern). For the intercalated samples Figures 6.5 and 6.6 the SEM images show that the samples retained their lamellar structure; however they underwent some morphological changes: there were cracks on the surface of the crystallites; mainly due to mechanical stress. Moreover, intercalation of the polymer resulted in partial exfoliation of the sample and a decrease in the long-range organisation of the layer structure.

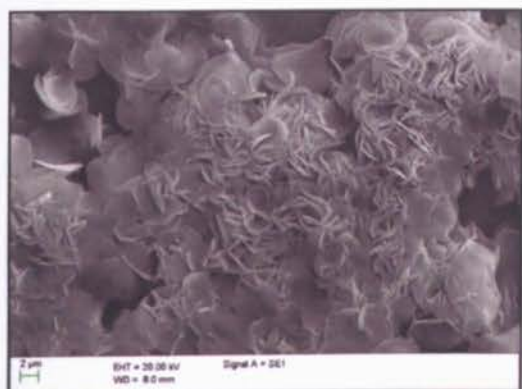


Figure 6 4: $\text{VOPO}_4 \cdot 2\text{H}_2\text{O}$ SEM image.

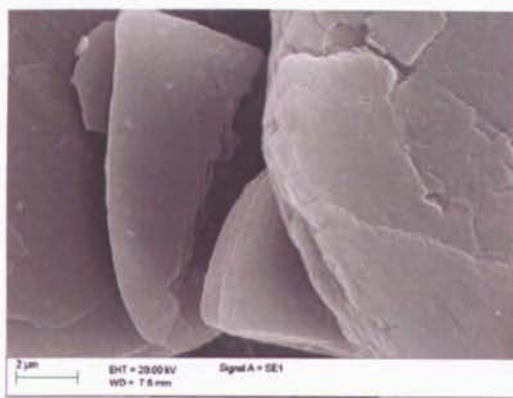
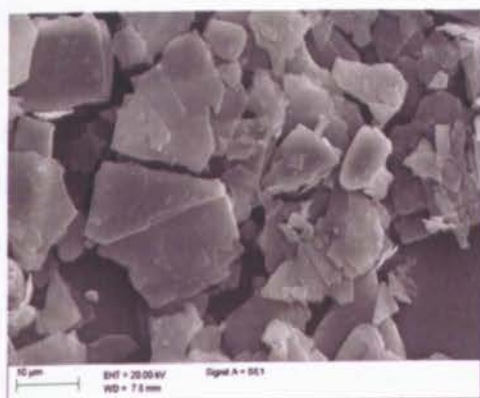


Figure 6 5: K^+ intercalated VOPO_4

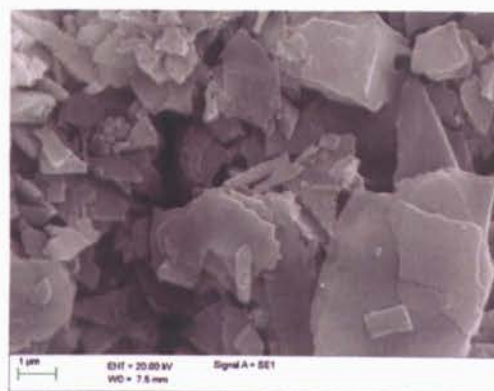
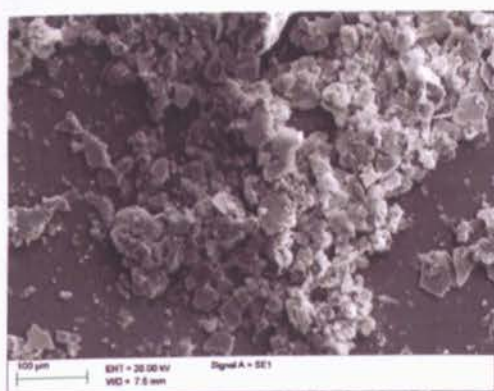


Figure 6 6: PPV intercalated VOPO_4

6.4.4 Infrared Spectroscopy and Raman Spectroscopy

6.4.4.1 VOPO₄·2H₂O

The IR spectrum is shown in Figure 6.7. The main bands observed at about 3500 and 1600 cm⁻¹ are attributed to the $\nu(\text{OH})$ and $\delta(\text{HOH})$ modes of the water molecules. The intense peaks at 1085 and 945 cm⁻¹ correspond to the symmetric $\nu(\text{P-O})$ vibrations of the phosphate tetrahedron in the VOPO₄·2H₂O whereas the antisymmetric $\nu(\text{P-O})$ vibrations were only observed as a small shoulder at 1160 cm⁻¹. The V-O stretching modes of the vanadyl group were also observed only as small shoulders at 1033 and 995 cm⁻¹. The less intense peaks at 680 and 570 cm⁻¹ are the bending V-O-P and O-P-O respectively. All these frequencies are in good agreement with the values found in the literature.⁶⁴⁻⁶⁶

The stretching vibrations were also observed in the Raman spectrum of vanadyl phosphate and are consistent with the values reported by Griesel *et al* (2004).⁶⁷ The intense peak at 955 cm⁻¹ corresponds to the symmetric $\nu(\text{P-O})$ vibrations. The stretching vibrations of the V-O in the vanadyl were observed at 988 and 1037 cm⁻¹ which are very close to the values observed in the IR spectrum. According to the literature the higher energy peak (1037 cm⁻¹) is characteristic of the $\nu(\text{V-O})$ of the anhydrous form of the VOPO₄ compound whilst the lower energy shift at 988 cm⁻¹ is due to the coordination of the water molecules to the vanadium atom; the appearance of both peaks suggested the formation of two phases.⁶⁷⁻⁶⁸

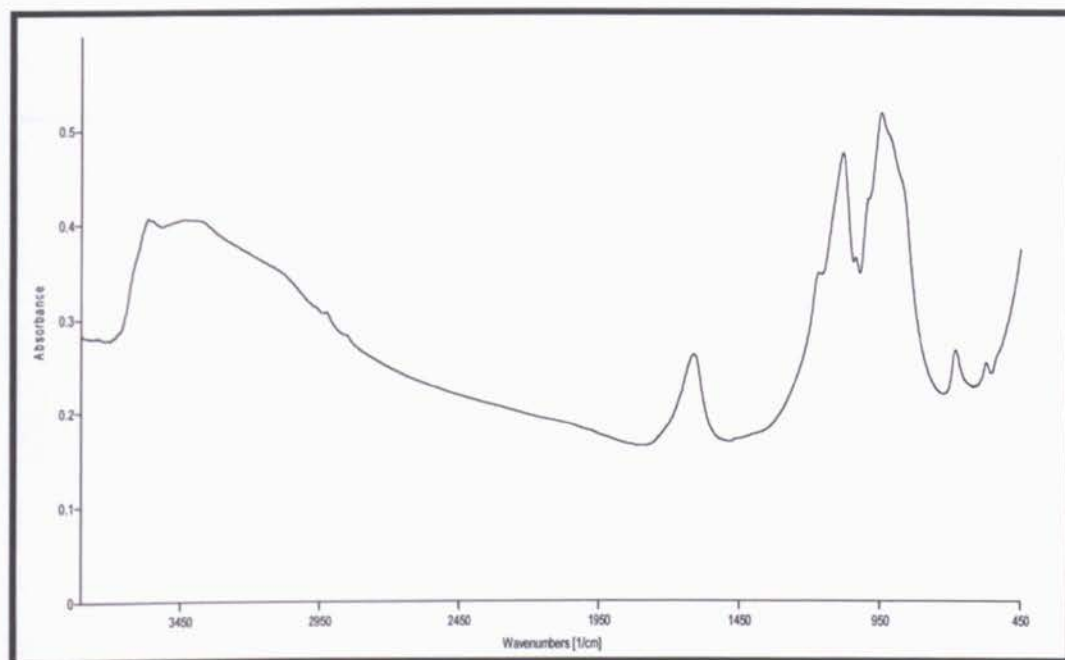


Figure 6 7: VOPO₄·2H₂O IR spectrum.

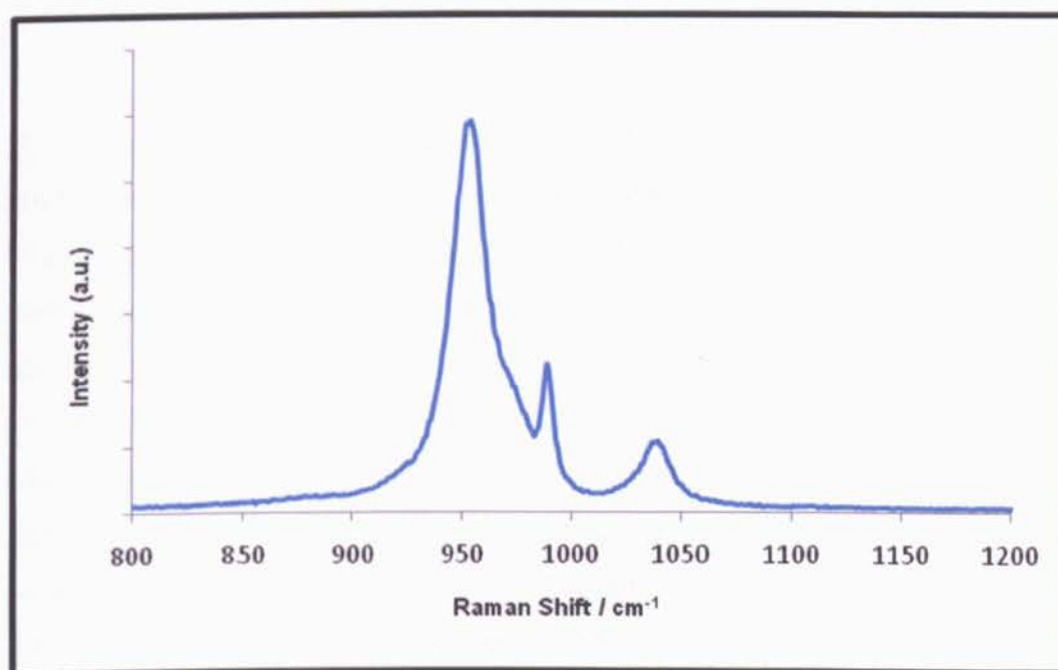


Figure 6 8: VOPO₄·2H₂O Raman spectrum.

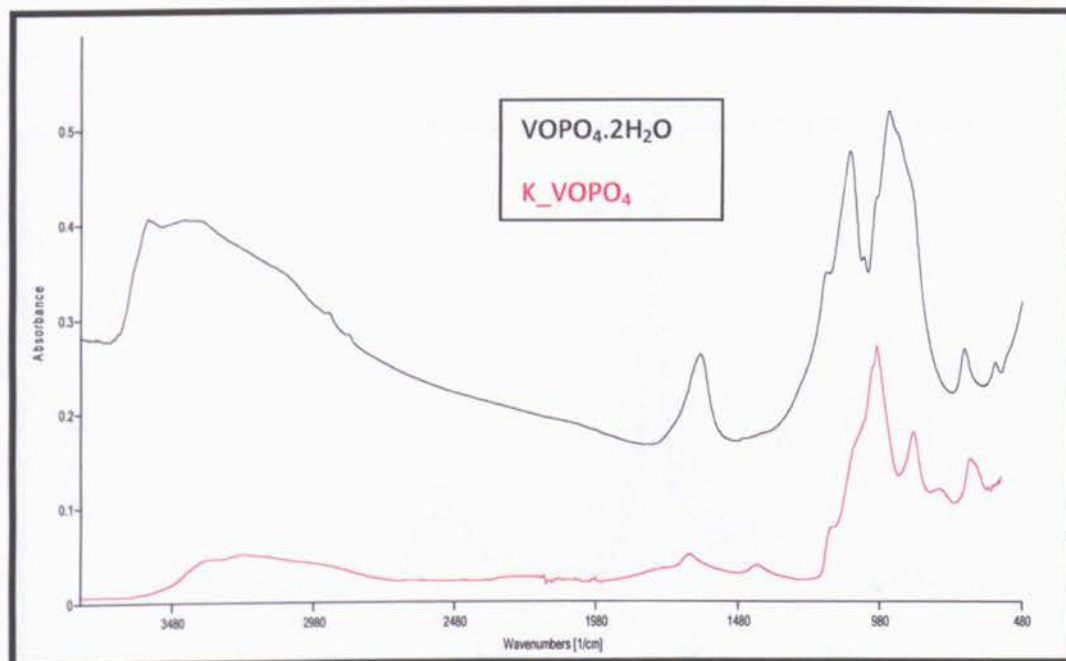
6.4.4.2 K^+ intercalated $VOPO_4$ 

Figure 6 9: K^+ -intercalated $VOPO_4$ (black) and $VOPO_4 \cdot 2H_2O$ (Red) IR spectra.

No major changes were observed in the IR spectrum of the intercalated compounds which suggested that the inorganic lattice retained its integrity. The bands corresponding to the $\nu(\text{PO})$, $\nu(\text{VO})$ and $\nu(\text{OH})$ modes were all shifted towards lower energies whereas the angular deformations (bending modes) were all shifted towards higher energies. A plausible explanation for this behaviour could be the redox intercalation mechanism of the $VOPO_4 \cdot 2H_2O$ in which the reduction of the vanadium (V) to vanadium (IV) increases the ionic character of the bonds inside the lattice resulting in the weakening of the V-O bond and subsequently affecting the P-O bonds. Additionally, the bands corresponding to the water molecules were clearly weakened, as a result of the displacement of the inter-planar water molecules by the potassium ions.⁶⁵ Energy shifts were also observed in the Raman spectrum of the intercalated samples, particularly the symmetric stretching vibrations of the PO_4^{3-} which were shifted to 867 cm^{-1} . The band at 998 cm^{-1} corresponding to the V=O stretching vibrations

was intensified, whereas the band at 1037 cm^{-1} of the anhydrous sample disappeared almost completely.

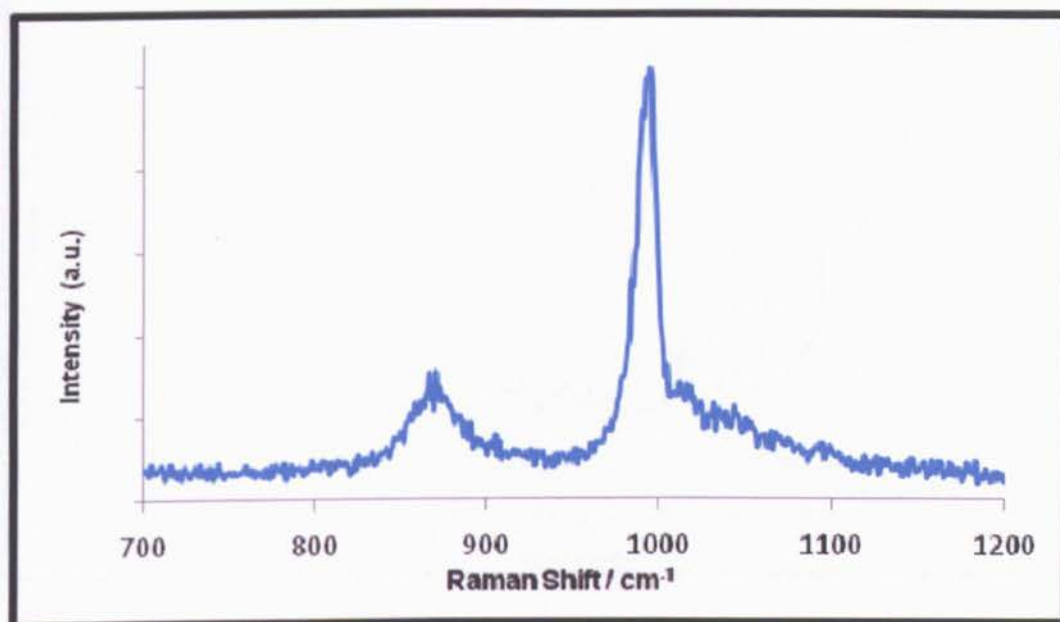


Figure 6 10: K⁺-intercalated VOPO₄ Raman spectrum.

6.4.4.3 Precursor Polymer intercalated VOPO₄

Some of the characteristic bands of the sulfonium polymer backbone appeared below 1600 cm^{-1} . An additional broad peak appeared around 1700 cm^{-1} ; this peak may correspond to C=O groups which are known to occur as a result of the oxidation of the polymer under ambient conditions; in this particular case, however, the formation of the carbonyl moieties are most likely due to the oxidising character of the inorganic host which at this stage contained a mixture of both vanadium (V) and (IV). The region below 1000 cm^{-1} was a bit difficult to allocate due to overlap between the polymer and the lattice vibrations. The five main bands typical of PPV were observed in the Raman spectrum, at 1175 , 1331 , 1556 , 1589 and 1631 cm^{-1} ; as well as a less intense band at 1421 cm^{-1} associated with the precursor

polymer.³⁶ The bands related to the vanadyl phosphate were diminished by the strong intensity of the polymer bands; however, it was still possible to see the peaks at their corresponding wavelengths.

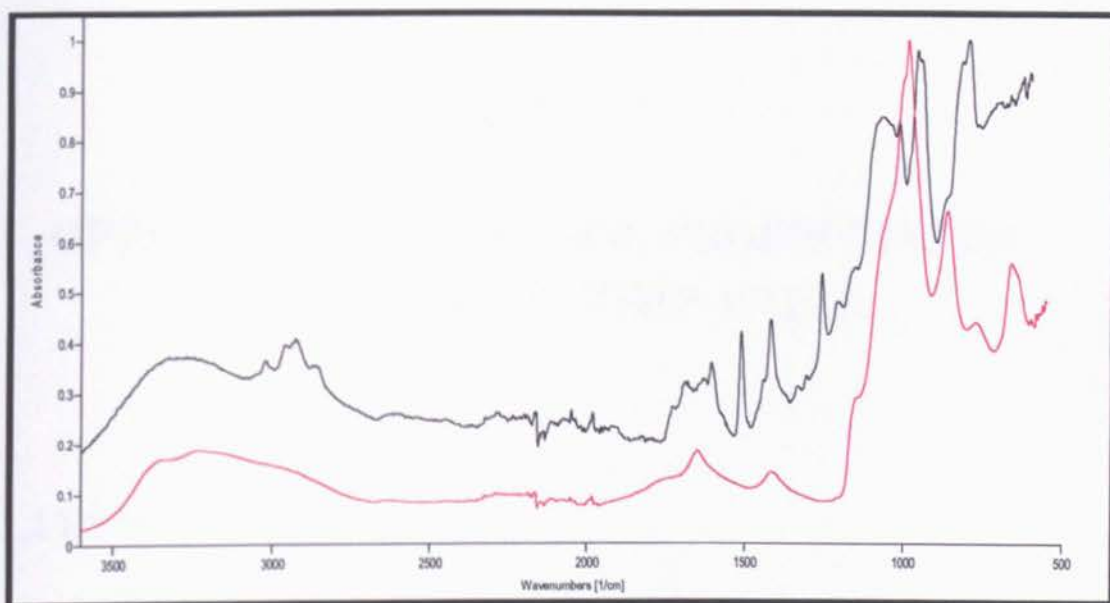


Figure 6 11: K^+ intercalated (red) and partially converted sulfonium polymer intercalated (black) $VOPO_4$ IR spectra.

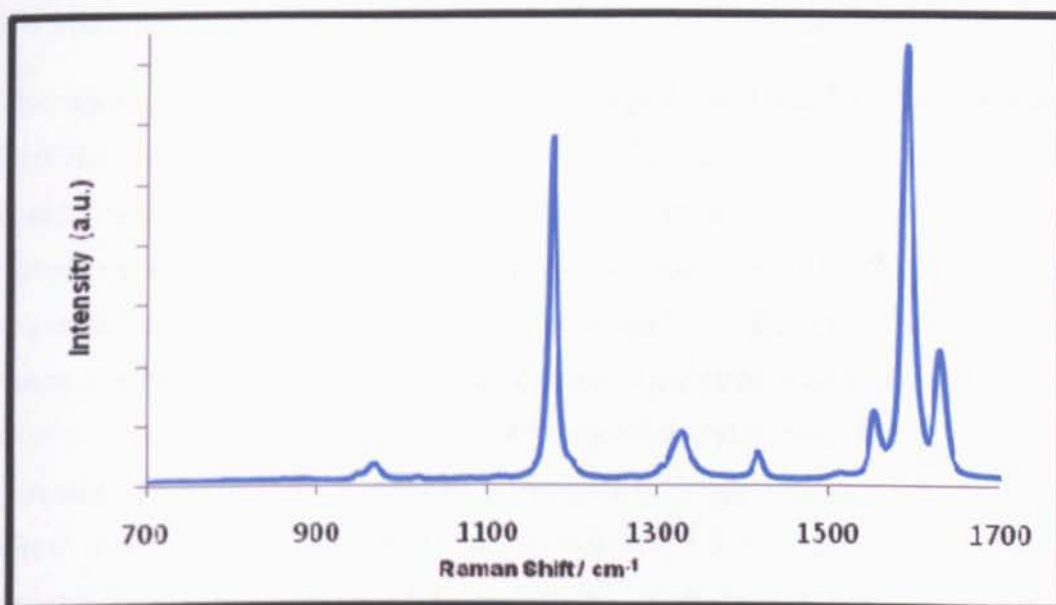


Figure 6 12: Sulfonium precursor polymer intercalated $VOPO_4$ Raman spectrum.

Chapter 7:

OPTICAL AND ELECTRONIC PROPERTIES OF INTERCALATED COMPOSITES

7.1 UV-vis absorption

7.1.1 PPV intercalated MnPS₃ and CdPS₃

The optical absorption measurements were carried out on thin films on all the intercalated samples.

The absorption spectra of the precursor polymer and the PPV-intercalated MnPS₃ are displayed in Figure 7.1. The spectra are simply the combination of absorptions of the individual constituents of the composites. The broad band that peaked at about 350 nm (3.5 eV) in the precursor-intercalated MnPS₃ was red shifted to 400 nm (3.1 eV) after thermal elimination of the sulfonium groups. This peak was assigned to the π - π^* transitions of the conjugated PPV formed inside the MnPS₃ and the wavelength indicated a similar conjugation length to that of the un-intercalated PPV. The insertion of the polymer inside the inorganic cavity did not modify the position of its absorption band (see Figure 7.1). On the other hand, the peaks that corresponded to the MnPS₃ were shifted towards lower energies. Grasso *et al* (1986-1989)^{14,56} proposed that the

main excitation process in MnPS_3 is for electrons in the valence band generated by the p_x and p_y orbitals of the P and S atoms to the levels that originate from the d orbitals in the Mn^{2+} ions, thus, the formation of vacancies (during the intercalation process) in the manganese phase changes the energy states that are responsible for the absorptions generated by the transitions that involved the manganese ions.⁶⁹ In the case of the PPV intercalated CdPS_3 the absorption edge was seen around 550 nm. CdPS_3 is basically transparent in the visible region; its main absorption band takes place in the UV region.⁷⁰ Contrary to the MnPS_3 , CdPS_3 does not present the low energy d-d absorption band because it has a closed shell electronic configuration ($\text{Cd}^{2+} = d^{10}$). The main absorption band of CdPS_3 is due to the excitation of electrons from the valence band, formed by the sulphur non-bonding orbitals, to the conduction band, mainly formed by the bonding phosphorus and the anti-bonding sulphur orbitals;⁶⁹⁻⁷¹ hence, the absorption taking place in the spectrum of the PPV-intercalated CdPS_3 is purely due to the polymer.

The energy gap of each sample was obtained by extrapolating the absorption edge to zero. The corresponding wavelengths were then placed in the following equation for energy:

$$E=hc/\lambda \quad \text{[Equation 7.1]}$$

where h is Planck's constant, c is the speed of light and λ is the wavelength at zero absorption.²¹

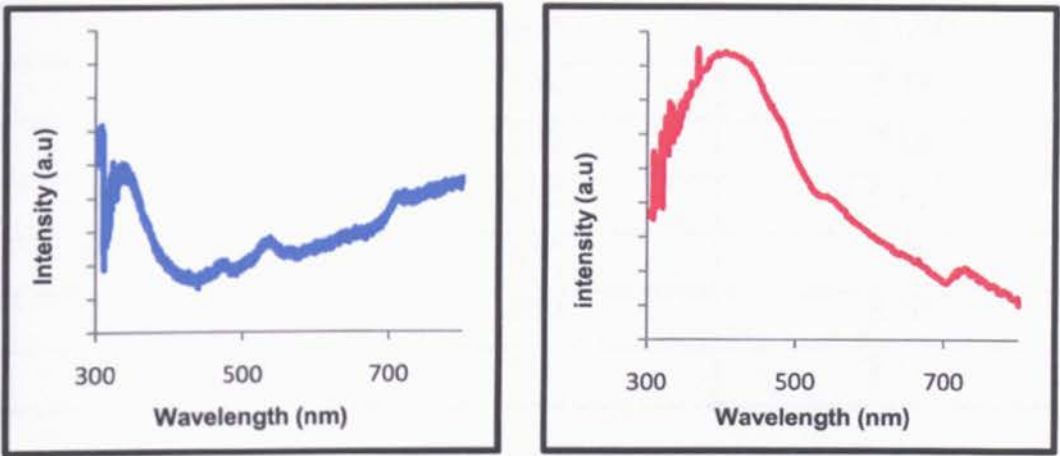


Figure 7 1: UV-visible spectra of precursor polymer-intercalated MnPS₃ (left) and PPV-intercalated MnPS₃ (right)

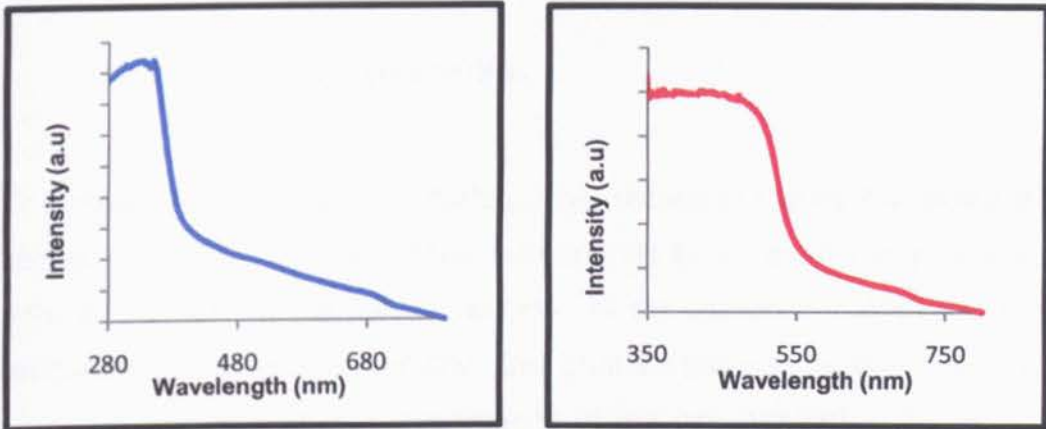


Figure 7 2: UV-visible spectra of precursor polymer-intercalated CdPS₃ (left) and PPV-intercalated CdPS₃ (right)

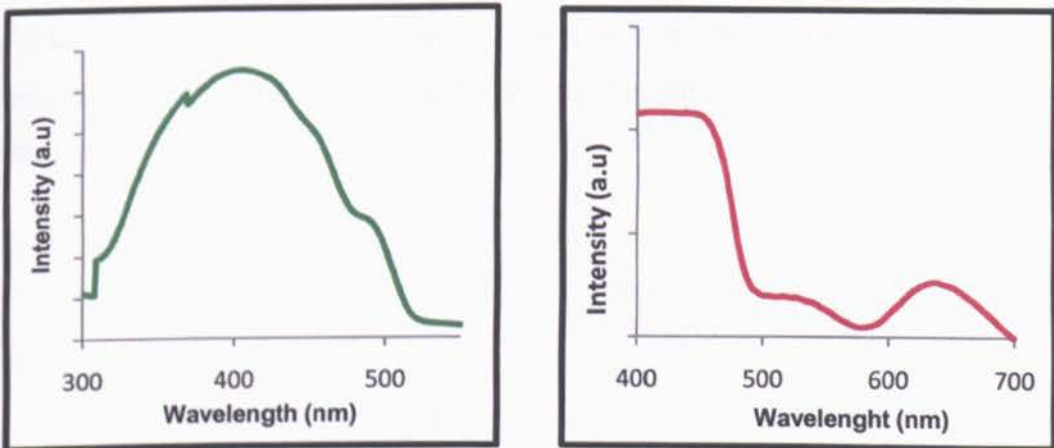


Figure 7 3 UV-visible spectra of PPV (left) and pristine MnPS₃ (right)

Compound	$\lambda(\text{nm})$	E_g (eV)
PPV	532	2.33
MnPS ₃	500	2.48
PP_MnPS ₃	450	2.75
PPV_MnPS ₃	615	2.02
PP_CdPS ₃	400	3.10
PPV_CdPS ₃	570	2.17

Table 7.1 Calculated band gap of individual organic and inorganic components and intercalated composites.

7.1.2 PPV intercalated VOPO₄

The absorption spectrum of VOPO₄.2H₂O shown in Figure 7.4 presents a shoulder at about 313 nm. This corresponds to an energy gap of about 3.96 eV, similar to the values reported in the literature.⁷² After the PPV precursor had been intercalated, the bands observed in the absorption spectrum corresponded to absorptions of the polymer with a λ_{max} at 323 nm. Also observed were some apparent vibronic transitions of the uneliminated precursor. These transitions became less noticeable as conversion into PPV took place. The original absorption of the vanadyl phosphate had been obscured by the absorption of PPV which was more intense.

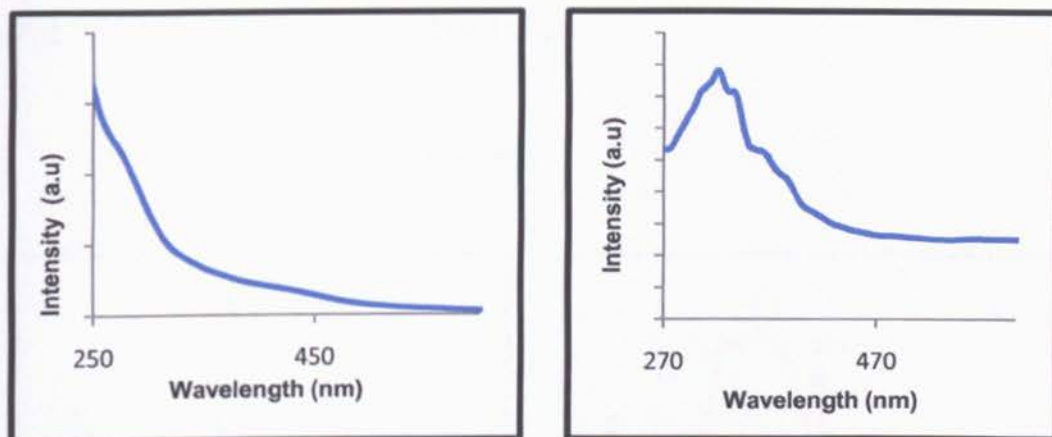


Figure 7 4: UV-visible spectra of $\text{VOPO}_4 \cdot 2\text{H}_2\text{O}$ in ethanol (left) and precursor polymer-intercalated VOPO_4 in ethanol (right).

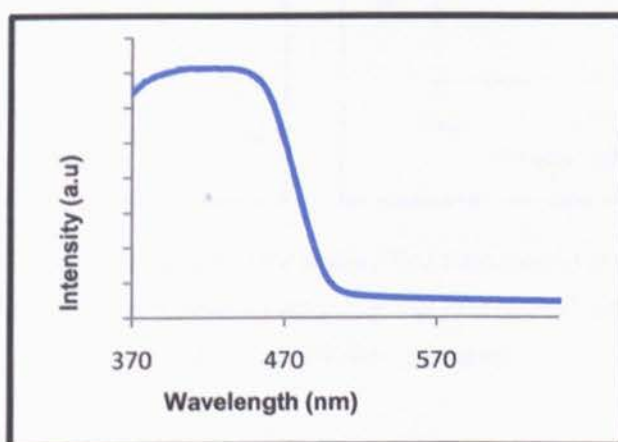


Figure 7 5: UV-visible spectrum of PPV intercalated VOPO_4 . Vibronic transitions were less apparent as the conversion into PPV took place.

Compound	$\lambda(\text{nm})$	E_g (eV)
$\text{VOPO}_4 \cdot 2\text{H}_2\text{O}$	313	3.96
K_ VOPO_4	323	3.83
	340	3.65
	362	3.42
	389	3.18
PPV_ VOPO_4	512	2.42

Table 7.2 Calculated band gap of individual $\text{VOPO}_4 \cdot 2\text{H}_2\text{O}$ and its intercalates.

7.2 Photoluminescence Studies

7.2.1 PPV-intercalated MnPS₃

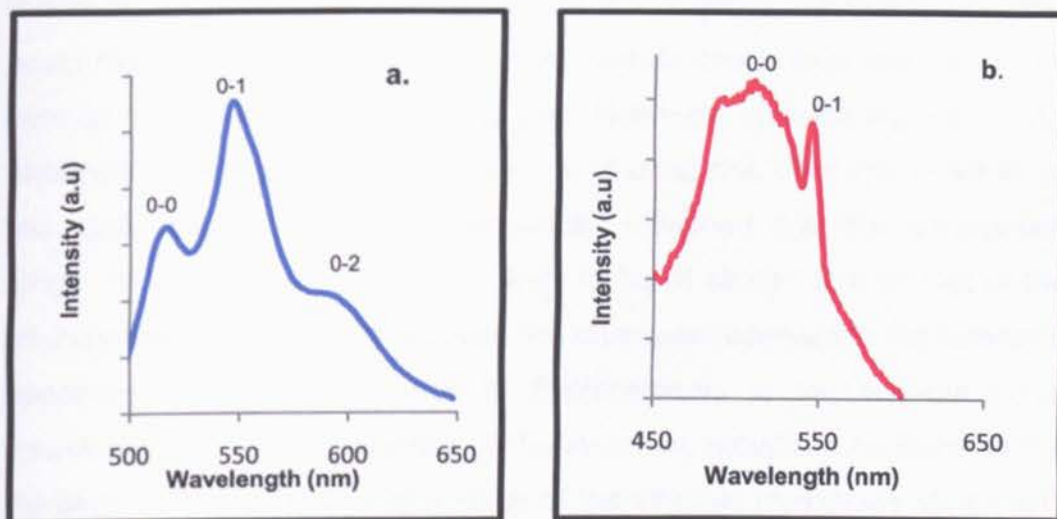


Figure 7.6: Emission Spectra of a. PPV and b. PPV intercalated in MnPS₃. The 0-0, 0-1 and 0-2 transitions were observed for PPV. For the intercalated polymer only the 0-0 and the 0-1 transitions were seen.

The emission spectra of PPV and PPV-intercalated MnPS₃ are shown in Figure 7.6. Both samples were excited at 400 nm. After elimination of the sulfonium residues, the extent of π -conjugation in the intercalated polymer (and un-intercalated as well) was increased and led to a red shift in the emission band with respect to the precursor polymer. PPV emitted green light with a λ_{max} around 550 nm and vibronic bands at 515 nm and 587 nm assigned to the 0-0 and 0-2 transitions respectively.⁷³ The emission spectrum of the intercalated PPV was very similar to that of the pure PPV film, except the intensity of the 0-0 peak which increased relative to pure PPV, whilst that of the 0-1 was reduced, thus, the emission maximum was blue-shifted to around 505 nm compared to that of the un-intercalated polymer. Two possible reasons can explain the changes observed in the emission spectrum: First of all, bathochromic (red shift) or hypsochromic

(blue shift) shifts in the emission spectra are usually related to changes in the conjugation length of the polymer chain. In this case, the blue shift observed in the λ_{max} of intercalated PPV could indicate that the short segments of polymer are responsible for the emission process. This would therefore mean that the intercalation of the polymer inside the inorganic hosts resulted in the scissioning of the polymer chain, thus reducing the π overlap and increasing the energy gap. However, considering the results obtained in the UV-visible spectroscopy studies, this does not seem to be the case; on the contrary these results indicated that the conjugation length of the intercalated PPV is likely to be of similar size to that of the un-intercalated polymer. Moreover, the changes observed in the emission spectrum are most likely due to displacements in the configurational coordinate due to the presence of the inorganic moieties. As found in the literature,⁷³⁻⁷⁵ the relative intensities of the vibronic transitions varies with the configurational displacement (ΔQ), that is, as ΔQ decreases, the position of the peak in the vibronic spectrum will shift to a lower vibrational state; hence, the relative intensity of the 0-0 transition increases.^{74,75} In this case, the confined spaces created by the inorganic matrix permitted the formation of polymer chains with less conformational disorder aligned inside the layers of the inorganic host.⁷³⁻⁷⁴ As the planarity of the polymer is enhanced, the configurational coordinate displacement (ΔQ) is reduced, and the relative intensity of the 0-0 (515 nm) transition of the intercalated PPV is increased.^{73,76-77}

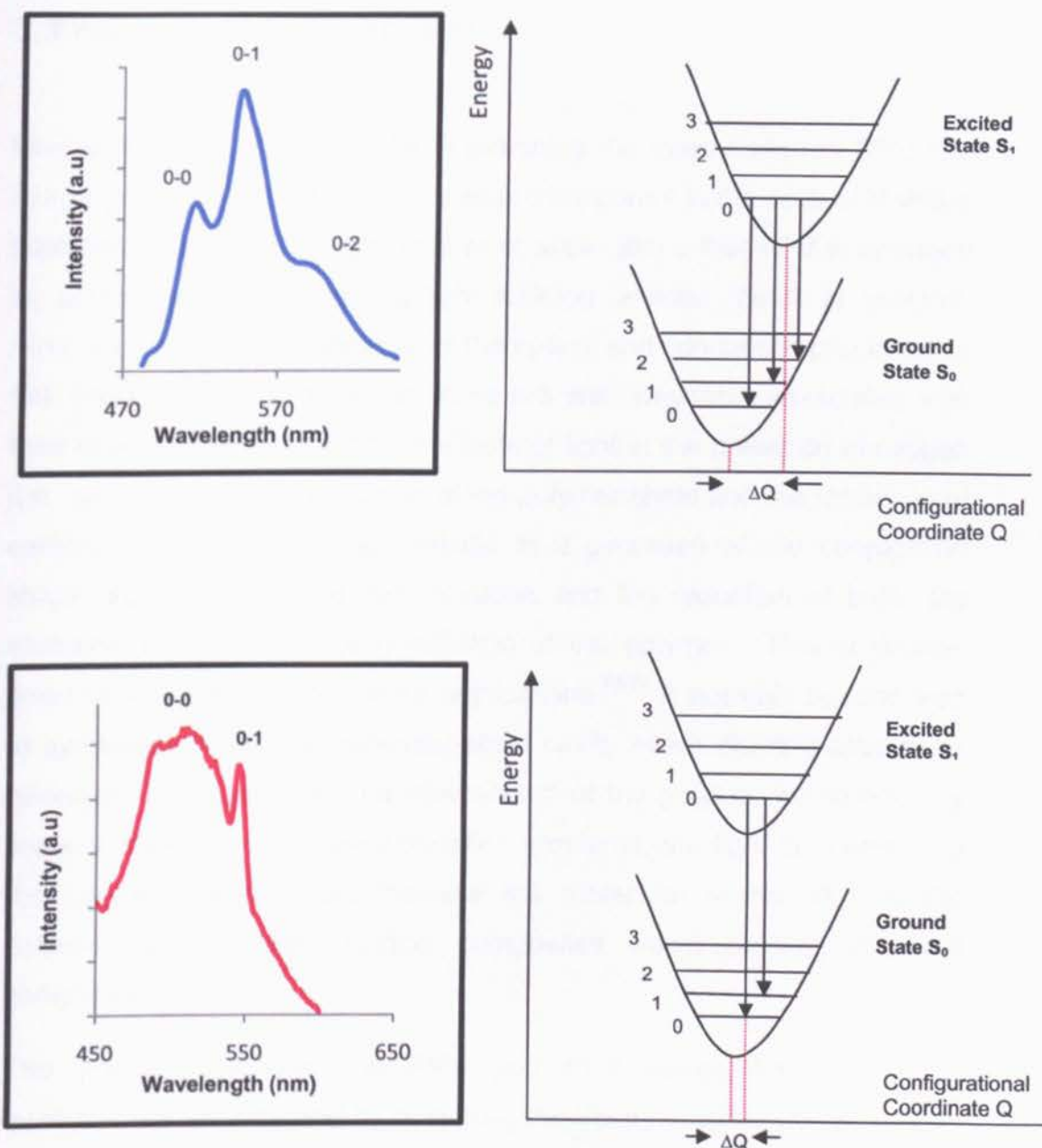


Figure 7.7: Left: PPV (above) and PPV intercalated (below) emission spectra showing vibronic transitions. Right configurational coordinate diagram for transitions between different states of PPV (above) and intercalated PPV (below)

7.3 Photodegradation Studies

One of the main incentives for researching the intercalation of PPV into inorganic, optically transparent (or semi-transparent in the case of MnPS_3), host matrices was the large number of applications that PPV is engaged in, particularly those involving light emitting devices. Years of research have led to many improvements of the optical and conducting properties of this class of polymer; however, there are still drawbacks associated with their environmental stability; the effects of light in the presence of oxygen are scission of the double bond of the polymer chain and the formation of carbonyl groups, which then results in a decrease of the conjugation length leading to loss of delocalisation and the reduction of both, the emission intensity and the conduction of the polymer. This of course, limits their use for optoelectronic applications.⁷⁸⁻⁷⁹ A possible solution was to synthesise PPV in a molecular-sized cavity which discriminates as to molecular shape or size. The intercalation of the polymer would not only prevent most of the photo-degradation problems; the tight fit imposed by the inorganic hosts could increase the molecular organisation of the polymer, so that the resulting composites would present improved conducting properties.

The photo-degradation of PPV and PPV composites was semi-quantitatively investigated by observing the decay of emission intensity as a function of time while illuminating thin films of PPV, PPV-intercalated MnPS_3 , PPV-intercalated CdPS_3 and PPV-intercalated $\text{MnPS}_3\text{-SiIn}$ cast on quartz slides with white light from a halogen lamp (50 W, 12-V) under ambient conditions.

7.3.1 PPV Photodegradation

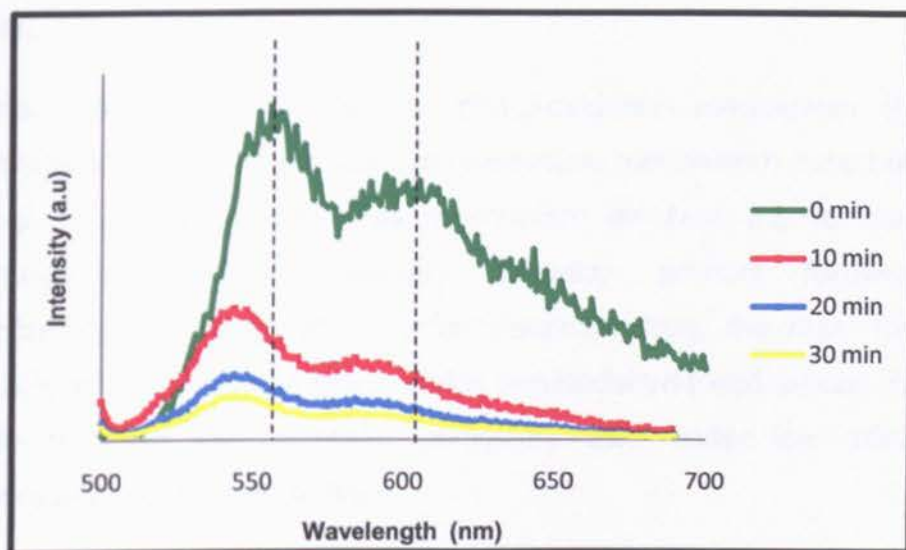


Figure 7.8: Emission spectra caused by 400 nm excitation of PPV films before and after irradiation during several periods of time.

The spectrum shown in Figure 7.8 presented a substantial decrease in the emission peak accompanied by a blue shift caused by photo-degradation. This suggested a reduction of the conjugation length on the polymer most likely due to the scission of the double bonds and the loss of vinylene-type functional groups.⁷⁸⁻⁷⁹ Moreover, it was observed that the most noticeable emission decay occurred after only 10 minutes of irradiation; subsequently, the rate of photodegradation was slower and less significant. This was due to a reduction of the amount of double bonds, which are the most likely species to react with oxygen.⁷⁹

The photo-oxidation of PPV probably begins with the formation of singlet oxygen. When the polymer is photo-excited, some of the singlet excitons formed are converted into the parallel-spin triplet state. This state is long-lived and sufficiently high in energy to form singlet oxygen.⁸¹ This species, which is highly reactive, attacks the double bond in the polymer chain. The double bond in this particular case is prone to react with oxygen

because the extended conjugated length of the polymer increases the electron density around it, in that way making it more reactive to the singlet oxygen.^{79,81}

Several authors have studied the photo-oxidation mechanism of PPV; Chambon *et al* (2011)⁸² proposed a reasonable mechanism based on their findings (see Figure 7.9). This mechanism involved the formation of hydroperoxides as the primary oxidation product followed by photochemical decomposition. After decomposition, the main route of evolution is the β -scission which yields benzaldehyde end-groups that are rapidly oxidised into aromatic carboxylic acid under the effects of temperature and UV-visible light.

The formation of carboxylic acids after irradiation of PPV films was monitored by infrared analysis. The spectra shown in Figure 7.10 were obtained prior to and after 2 hours of irradiation. The most noticeable change was the absorption band in the carbonyl region around 1695 cm^{-1} which had started to form prior to irradiation by simply having the polymer exposed to environmental conditions while all measurements were carried out; the intensity of this peak increased with increasing irradiation time. A less intense but broad band between 3200 and 3400 cm^{-1} was also starting to form due to the OH stretching of carboxylic acids. Furthermore, a substantial reduction in the intensity of the band around 958 cm^{-1} was also observed due to the loss of some the double bonds.

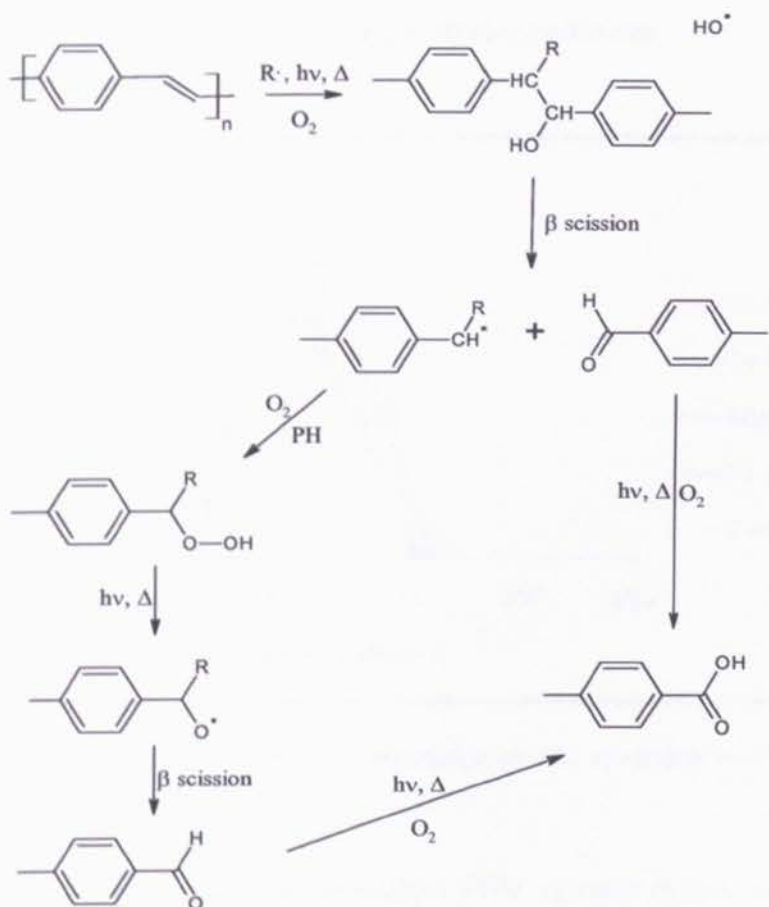
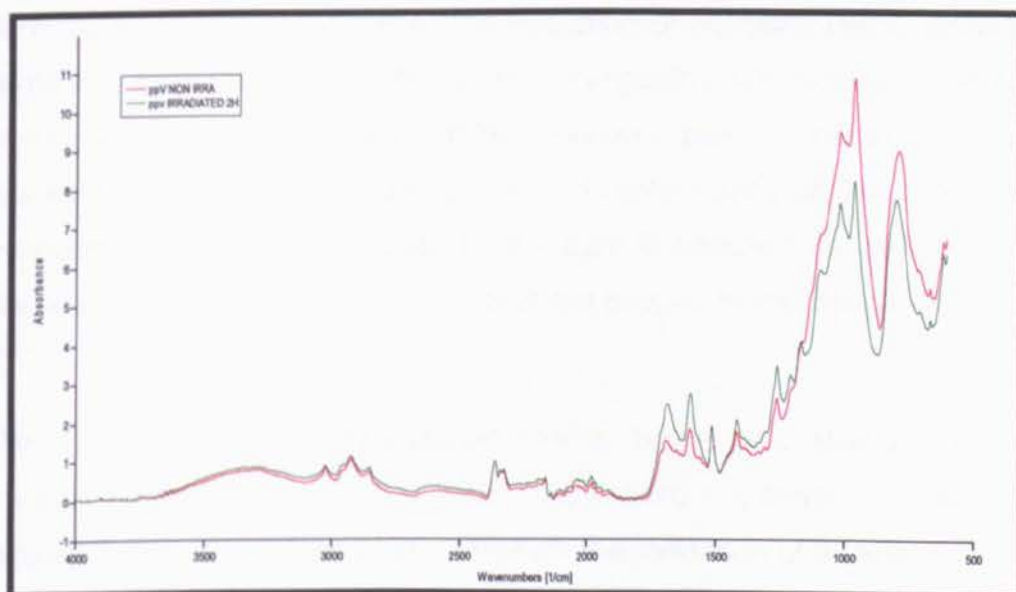

 Figure 7 9: Photodegradation mechanism proposed by Chambon *et al* (2001)⁸²


Figure 7 10: IR spectrum of PPV prior to irradiation (red) and after 2 h of irradiation (green)

7.3.2 PPV intercalated MnPS₃ photodegradation

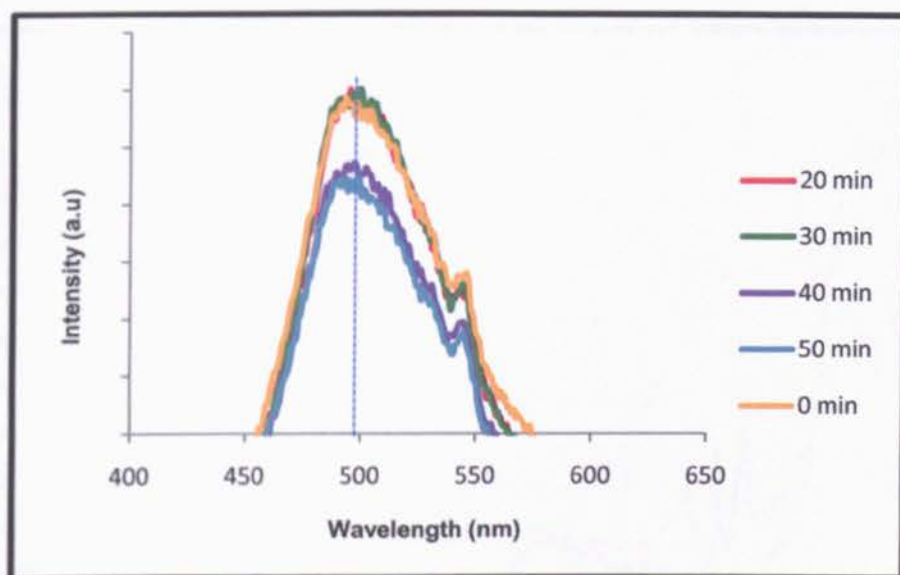


Figure 7.11: Emission Spectra of PPV-intercalated MnPS₃ at various irradiation times.

The emission intensity of un-intercalated PPV is remarkably reduced by about 88 % of the initial intensity after irradiation for 30 minutes. On the other hand, the emission of the intercalated PPV is much less reduced during the same period of time. The reduction of emission decay probably originates from the fact that the layered inorganic hosts can block oxygen penetration into the intercalated PPV. Moreover, even if oxygen and water molecules were simultaneously present in certain parts of the matrix, the geometrical restrictions imposed by the tight fit between the polymer and the host, would hinder any approach of the oxygen to the double bonds.^{79, 83-84}

The IR spectra of PPV-intercalated MnPS₃ before and after 2 hours of irradiation are shown in Figure 7.12. There were not many changes with respect to the original spectrum. Although the formation of a carbonyl band around 1700 cm⁻¹ was not evident, some broadening of the band around 1650 cm⁻¹ was seen. Changes in the region below 1000 cm⁻¹ were very

difficult to monitor due to the low intensity of the bands as a result of the intercalation.

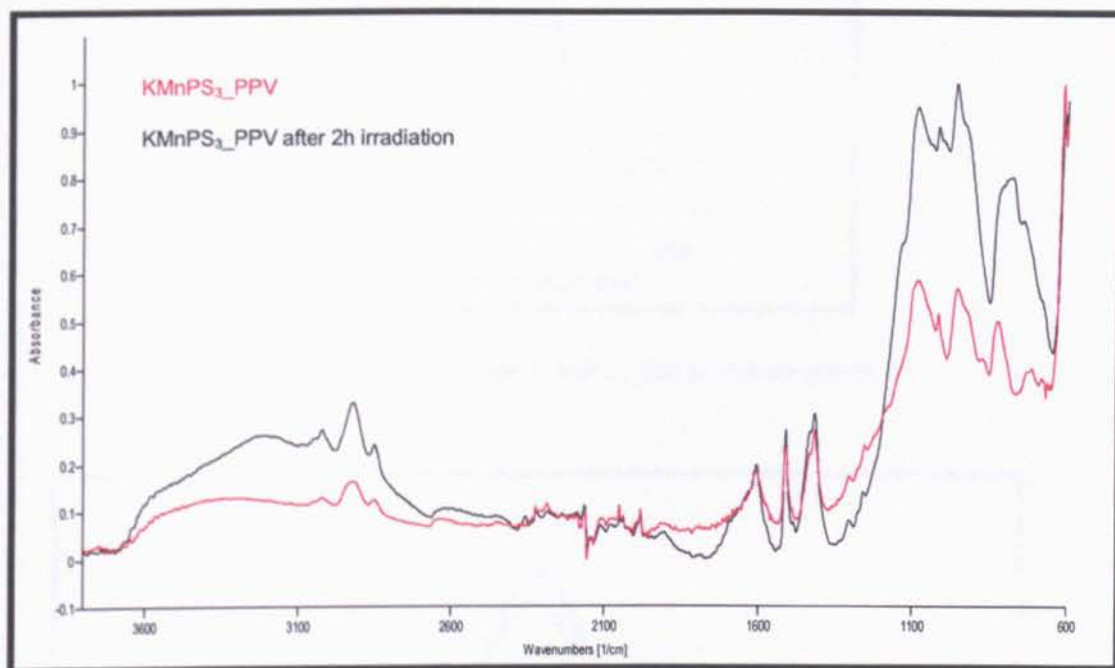


Figure 7 12: IR spectra of PPV-intercalated MnPS_3 before and after 2 hours of irradiation.

3.3.3 PPV intercalated MnPS_3/Sn

In the case of PPV intercalated into MnPS_3/Sn , the emission spectrum showed a main peak at about 505 nm and shoulders at 463 and 541 nm. These were assigned to the 0-1, 0-0 and 0-2 transitions respectively. The main peak was blue shifted in comparison to the emission bands of pure PPV, suggesting that the conjugation length of the polymer was slightly smaller. The peak around 463 nm indicated that there were traces of precursor polymer still present. Additionally, it was observed that after irradiation this peak became less intense while the intensity of the main band increased; this could possibly indicate that the precursor polymer was being photochemically converted into PPV, though further investigation would be required to confirm this assumption.

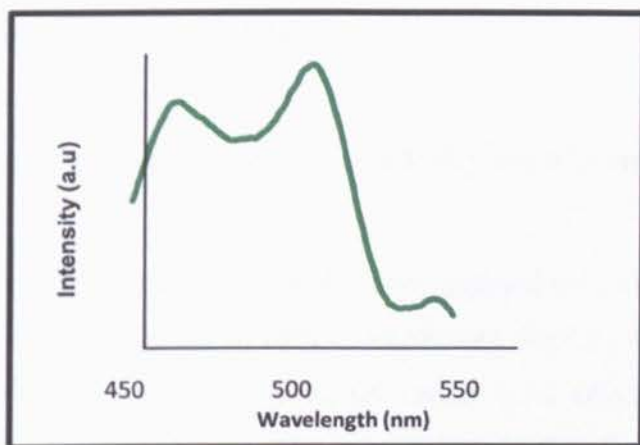


Figure 7 13: PPV intercalated MnPS₃_SIn emission spectrum.

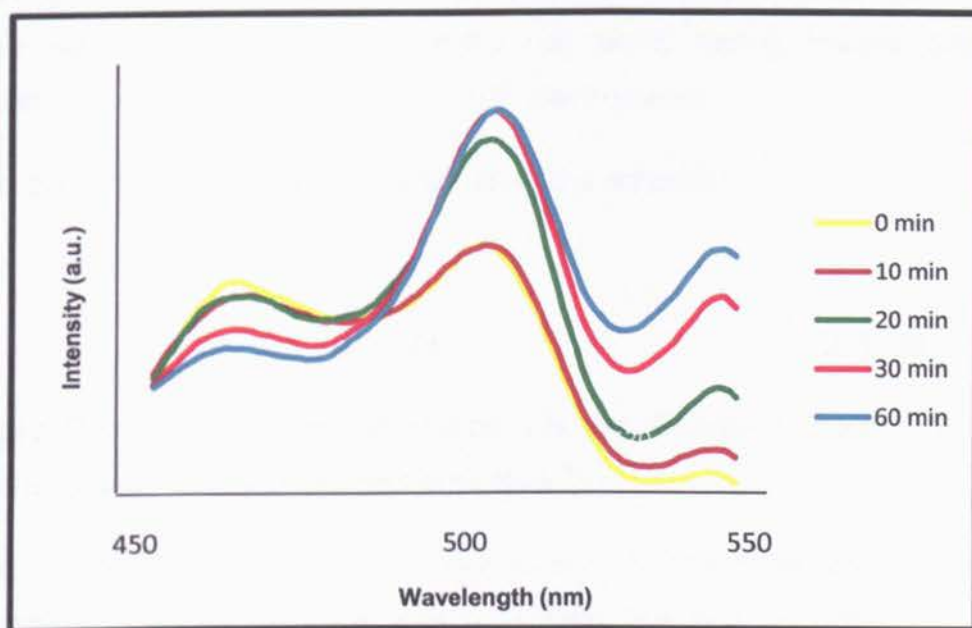


Figure 7 14: Emission Spectra of PPV intercalated MnPS₃_SIn at various irradiation times.

7.4 Electrical Characteristics

7.4.1 Ambient temperature conductivity measurements

Two-probe conductivity measurements were carried out on single crystals of MnPS₃, and single crystals of PPV-intercalated MnPS₃. Sample holders were designed to fit the small crystals using gold electrodes and the conductivity was measured along the sample (parallel to the layers).

In the case of the polycrystalline and amorphous material, the samples were ground and pressed into discs (5 mm diameter). The samples were then placed in a PTFE two-probe cell using spring loaded copper electrodes connected to a Keithley 197 electrometer.

The conductivity was calculated by using the equation:

$$\sigma = (l / R * A) \quad \text{[Equation 7.2]}$$

where R is the measured resistance, l is the distance between the two contacts and A is the cross sectional area.⁸⁵

The I-V curve of MnPS₃ is shown in Figure 7.15. The relationship between current and applied voltage was a straight line and indicated that the sample obeyed Ohm's law:

*"Ohm's law states that the current through a conductor between two points is directly proportional to the potential difference between the two points"*⁸⁵

$$I = V / R \quad \text{[Equation 7.3]}$$

where I is the current through the conductor, V is the potential difference measured across the conductor and R is the resistance of the conductor.⁸

7.4.1.1 Conductivity measurements of single crystals

The resistance of MnPS_3 and PPV intercalated MnPS_3 (both single crystals) were found from the slope ($1/R$) of the I-V plots. The results of conductivity and resistance measurements are summarised in Table 7.3.

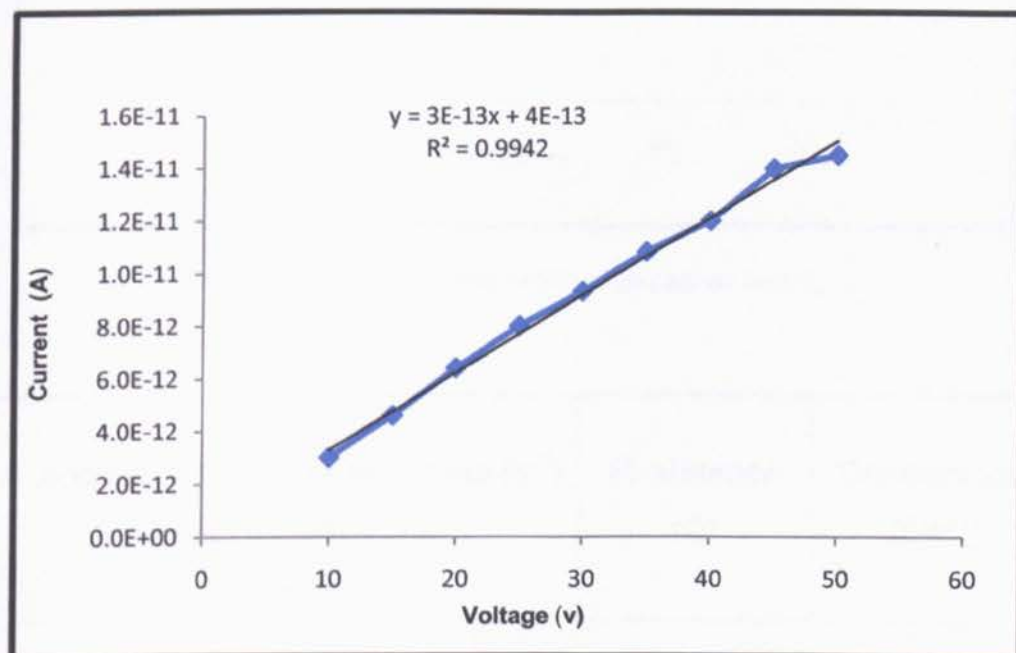
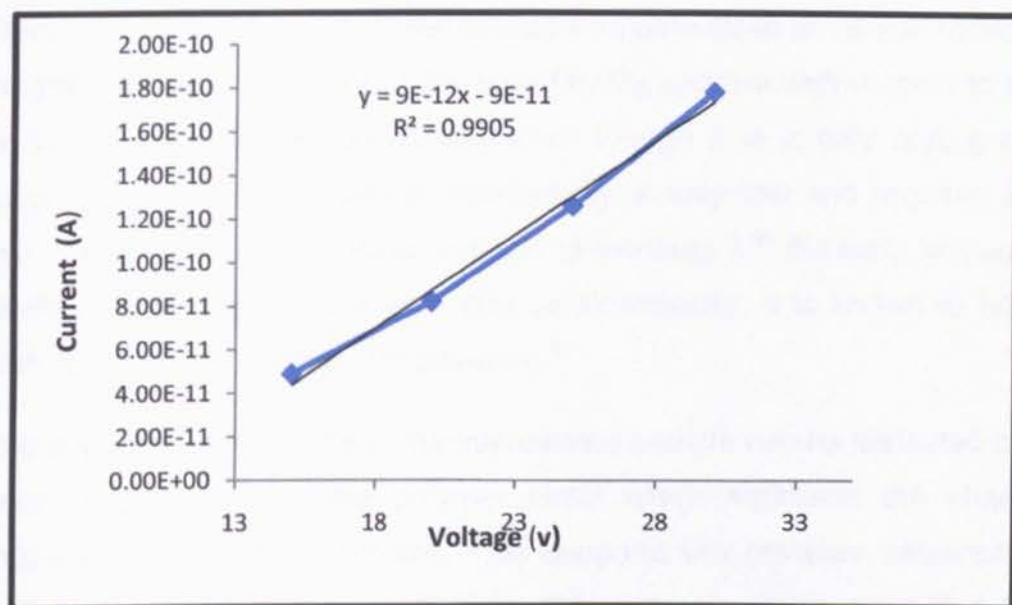


Figure 7 15: I-V curve of a single crystal of MnPS_3

Figure 7.16: I-V curve of PPV intercalated MnPS₃

Sample	Electrodes distance (m)	Area (m ²)	Resistance (Ω)	Conductivity (Sm ⁻¹)
PPV	-	-	-	10 ⁻¹³ (Ref 75 and 88)
MnPS ₃	2.0 x 10 ⁻⁴	3.0 x 10 ⁻⁸	3.3 x 10 ¹²	2.20 x 10 ⁻⁹
PPV_MnPS ₃	1.5 x 10 ⁻⁴	2.5 x 10 ⁻⁸	1.1 x 10 ¹¹	5.45x 10 ⁻⁸

Table 7.3 Conductivity of single crystals of MnPS₃ and PPV intercalated MnPS₃

The conductivity of the PPV intercalates was calculated to be one order of magnitude higher than that of the pure MnPS_3 and five with respect to the un-intercalated polymer for which, even though it is a fully conjugated polymer, the intrinsic electrical conductivity is very low and requires the use of dopants such as iodine, in order to increase it.⁸⁶ Similarly, because MnPS_3 is catalogued as a wide gap semiconductor, it is known to have high resistance at ambient temperature.¹⁴

The improved conductivity of the intercalated sample can be attributed to a better organisation of the polymer chain which facilitates the charge mobility throughout the sample. This supports the previous assumption that the confined spaces created by the inorganic matrix permitted the formation of polymer chains with less conformational disorder and reduced configurational coordinate displacement (ΔQ).

7.4.1.2 Conductivity measurements of pressed samples

The conductivities measured on the pressed samples were a lot lower compared with those of the single crystals (see Table 7.4). Based on these results, it seems likely that the powdered platelets showed preferred alignment parallel to the pressed pellet surfaces. It appears that the conductivity of the intercalated materials is anisotropic, and that the conductivity parallel to the layers is larger than that perpendicular to the layers.

Sample	Disc thickness (m)	Area (m ²)	Resistance (Ω)	Conductivity (Sm ⁻¹)
PPV_MnPS ₃	4.0 x 10 ⁻⁴	1.96 x 10 ⁻⁵	5.3 x 10 ¹¹	3.8 x 10 ⁻¹¹
PPV_Mn ₂ P ₂ S ₆	3.0 x 10 ⁻⁴	1.96 x 10 ⁻⁵	9.6 x 10 ¹⁰	1.6 x 10 ⁻¹⁰
PPV_VOPO ₄	3.0 x 10 ⁻⁴	1.96 x 10 ⁻⁵	3.6 x 10 ⁸	4.2 x 10 ⁻⁸

Table 7.4 Conductivity of pressed pellets of PPV intercalated in different inorganic hosts.

7.4.2 Diode Preparation

Indium tin oxide (ITO) coated glass substrates were cleaned by sonication in methanol first and subsequently with sodium hydroxide and then washed again with methanol to improve wettability for coating. Conducting poly(3,4-ethylenedioxythiophene) poly(styrenesulfonate) (PEDOT:PSS) was dip coated onto the ITO and heated for 30 min at 100 °C. This material was used as an interfacial buffer layer to increase the collection of the generated carriers and decrease the leakage of carriers as described in the literature.²²

In cases where PPV was the active layer, methanolic solutions of the precursor polymer were drop-cast onto the PEDOT:PSS layer and then heated to 220 °C under nitrogen to form PPV.

In cases where the active layer was an intercalated sample (PPV_MnPS₃, PPV_MnPS₃_Sn), methanolic suspensions were prepared ultrasonically and drop cast onto the PEDOT:PSS layer and then heated for 30 min at 100 °C.

Finally aluminium (Al) contacts were vacuum-deposited on the active layer at a pressure of 6×10^{-5} torr.

I-V measurements were carried out on all fabricated diodes using a Keithley 230 programable voltage source and a Keithley 485 picoammeter.

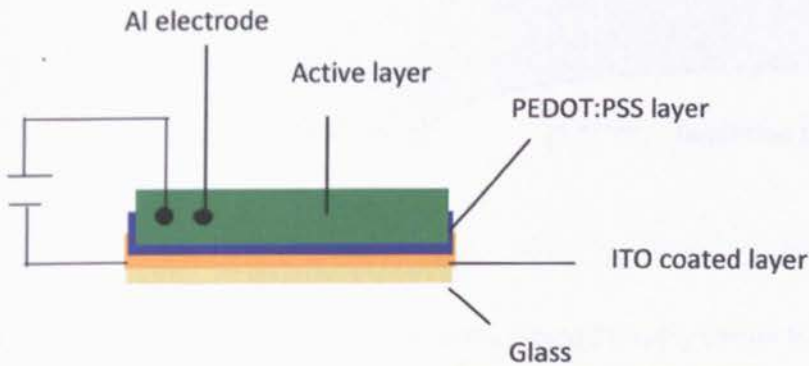
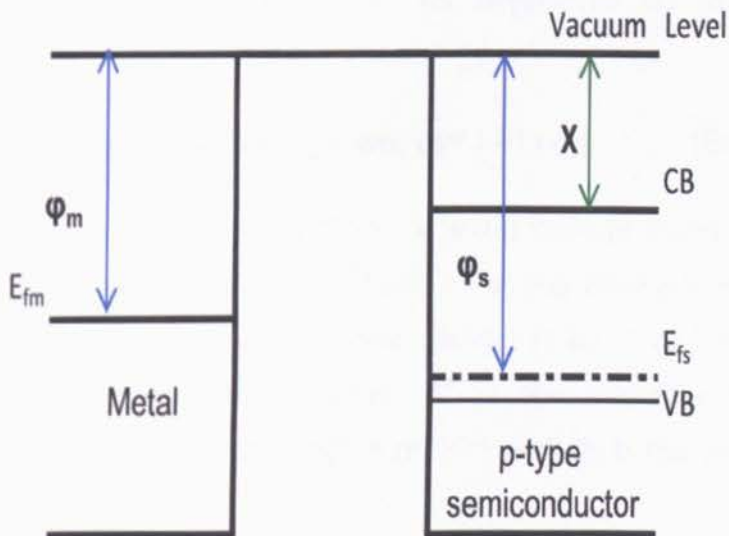


Figure 7 17: Schematic diagram of a Schottky diode.



(a)

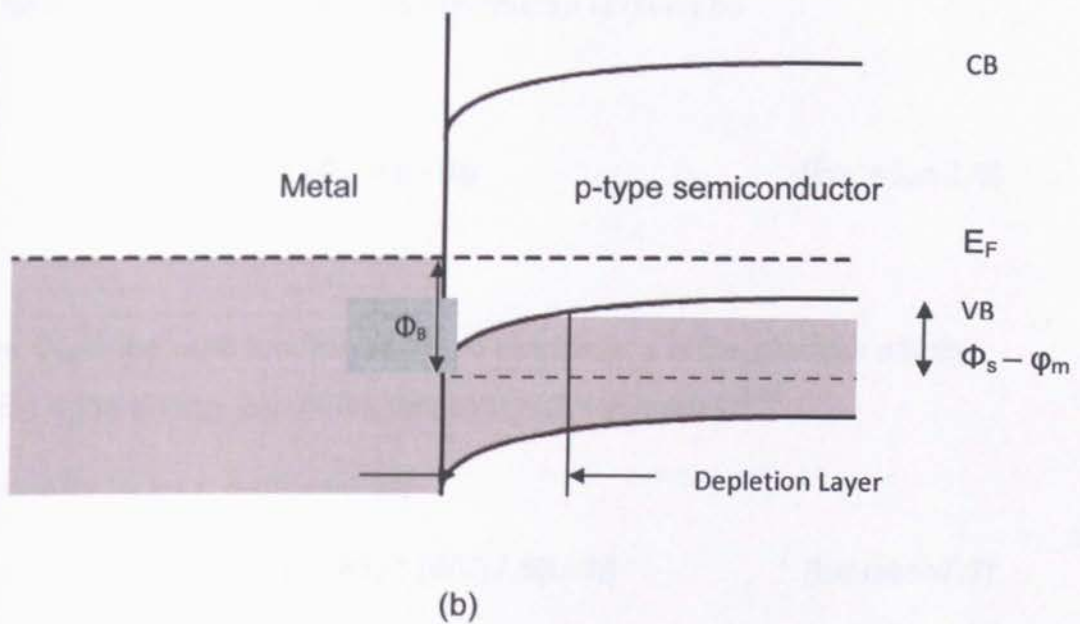


Figure 7 18: Schematic representation of the p-type Schottky barrier formation. (a) The initial positions of the energy levels of the metal and the semiconductor; (b) the barrier height and the depletion layer of the junction under forward bias.⁸⁵

The characteristics of the diode can be expressed by the following relation:^{85,88}

$$I = AA^* T^2 \exp \{-q\Phi_B/nkT\} \{ \exp (qV / kT) -1\} \quad [\text{Equation 7.4}]$$

where I is the current through the diode, V is the voltage across the diode, k is Boltzman's constant ($1.38 \times 10^{-23} \text{ JK}^{-1}$) T is the absolute temperature of the diode (294 K), q is the electronic charge ($1.60 \times 10^{-19} \text{ C}$), n is the ideality factor, A is the contact area, A^* is the effective Richardson constant (theoretical value $1.20 \times 10^6 \text{ A m}^{-2}\text{K}^{-2}$) and Φ_B is the barrier height in eV.^{85,88}

The reverse saturation current I_0 is given by the equation:

$$I_0 = AA^* T^2 \exp (-q\Phi_B / nkT) \quad [\text{Equation 7.5}]$$

The barrier height for a p-type semiconductor is given by

$$\Phi_B = -\Phi_m + \chi - E_g \quad [\text{Equation 7.6}]$$

where Φ_m is the work function of the Al electrode, χ is the electron affinity and E_g is the energy gap of the semiconductor material.^{85,88}

The ideality factor n is defined as:

$$n = (q / kT) * [d(V) / d(\ln I)] \quad [\text{Equation 7.7}]$$

7.4.2.1 ITO / PEDOT:PSS / PPV / Al device

The I-V measurements shown in Figure 7.19 have the characteristic behaviour of a rectifying device, and the rectification ratio (which is the ratio of the forward current to reverse current at a certain voltage) was found to be 2.04 at ± 2 V.

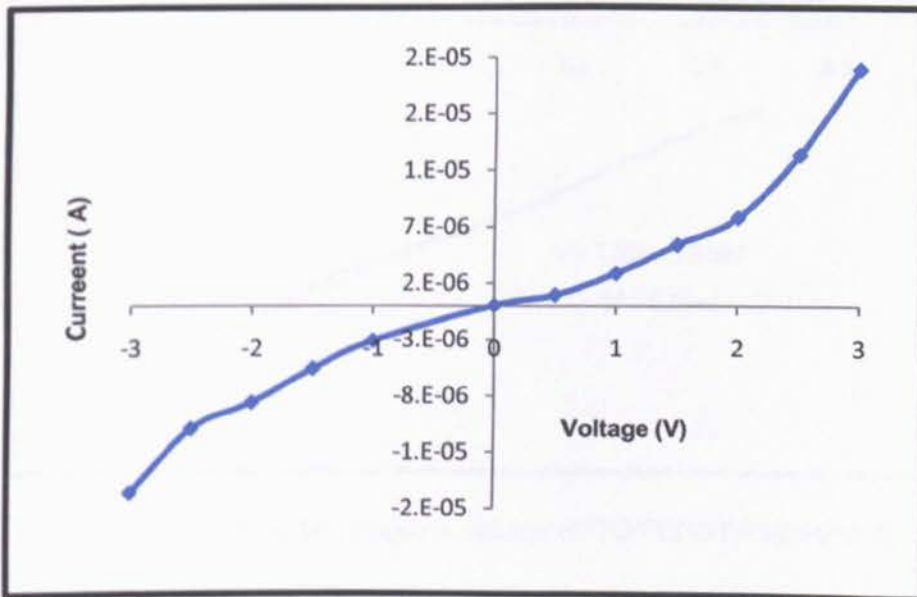


Figure 7.19: I-V curve of ITO/PEDOT:PSS/PPV/Al

The device indicated a non-ideal behaviour due to the series resistance; therefore a plot of $\ln(I)$ against V was drawn in order to remove the effect of the series resistance (Figure 7.20). The barrier height and ideality factor were determined from the y-intercept and the slope of the fitted curve, respectively using equations 7.5 and 7.7.

The calculated value of Φ_B was 0.64 eV and the ideality factor was found to be 39, which is much higher than the values found for inorganic semiconductors such as silicon diodes ($n = 1.02$).²³ In a classical Schottky diode, n should be nearly 1; but in real situations (especially in organic devices), this value is often increased due to factors such as inhomogeneities of the films and film thickness. Additionally, the high resistance of the undoped PPV can also contribute to such high apparent values of n .

The calculated parameters for the ITO/PEDOT:PSS/PPV/Al device are all shown in Table 7.5

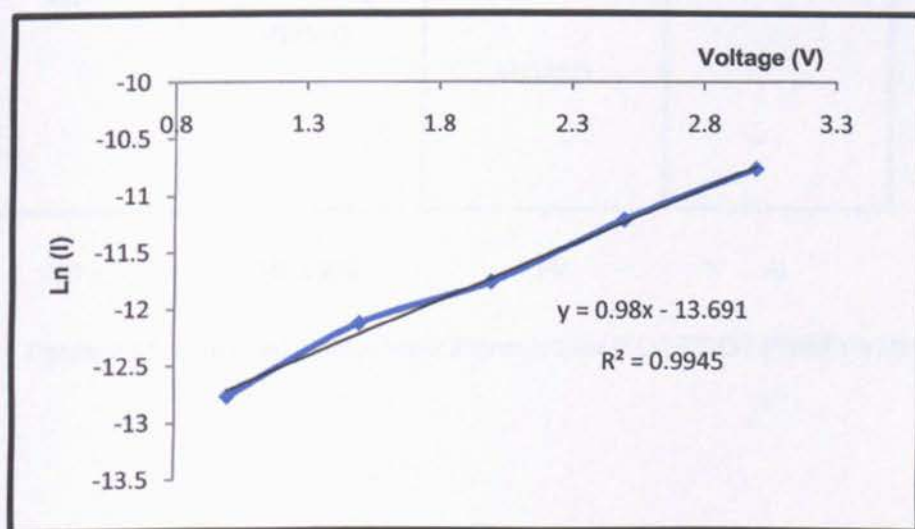


Figure 7.20: Plot of $\ln(I)$ against voltage of ITO/PEDOT:PSS/PPV/Al

Saturation current density (A m^{-2})	Φ_B (eV)	n	x (eV)	Φ_s (eV)
0.99	0.64	39	2.39	4.73

Table 7.5 Calculated parameters of the ITO/PEDOT:PSS/PPV/ Al device

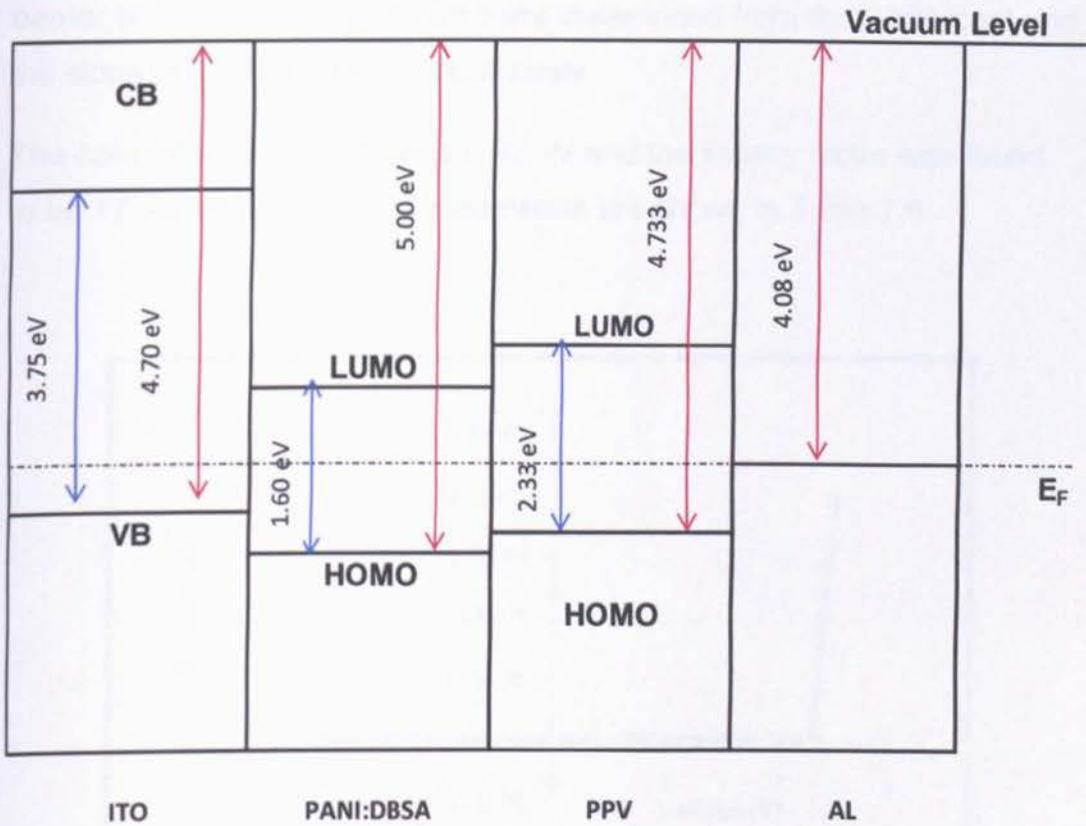


Figure 7 21: Proposed energy level alignment for ITO/PEDOT:PSS/PPV/Al

7.4.2.2 ITO/PEDOT:PSS/PPV intercalated MnPS₃/Al diode

The I-V curve of the device containing PPV intercalated MnPS₃ as the active layer is shown in Figure 7.22. It also showed the characteristic behaviour of a rectifying device and the rectification ratio was found to be 1.49 at ± 4 V.

Similarly to the previous device, a plot of $\ln(I)$ against V was drawn in order to assess the effect of the series resistance (Figure 7.23) and the barrier height and ideality factor were determined from the y-intercept and the slope of the fitted curve, respectively.

The calculated value of Φ_B was 0.92 eV and the ideality factor was found to be 17. All other calculated parameters are shown in Table 7.6

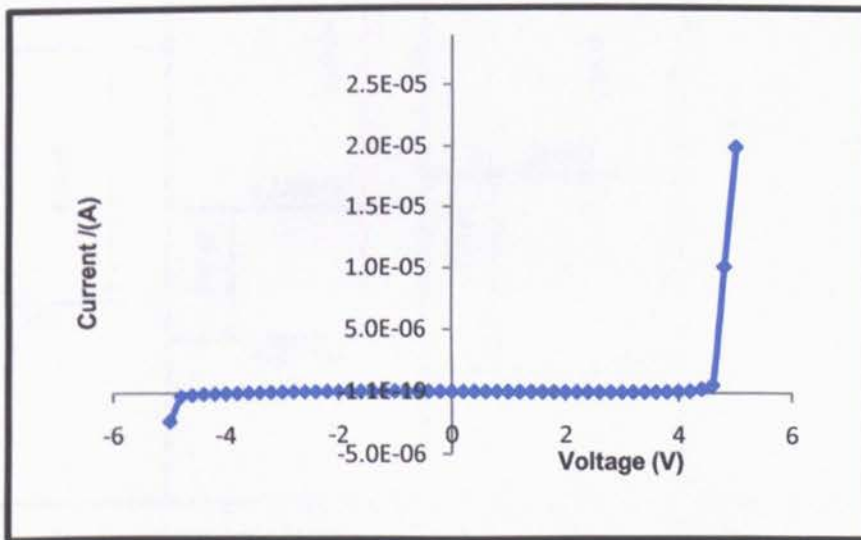


Figure 7 22: I-V curve of ITO/PEDOT:PSS/PPV_MnPS₃/Al

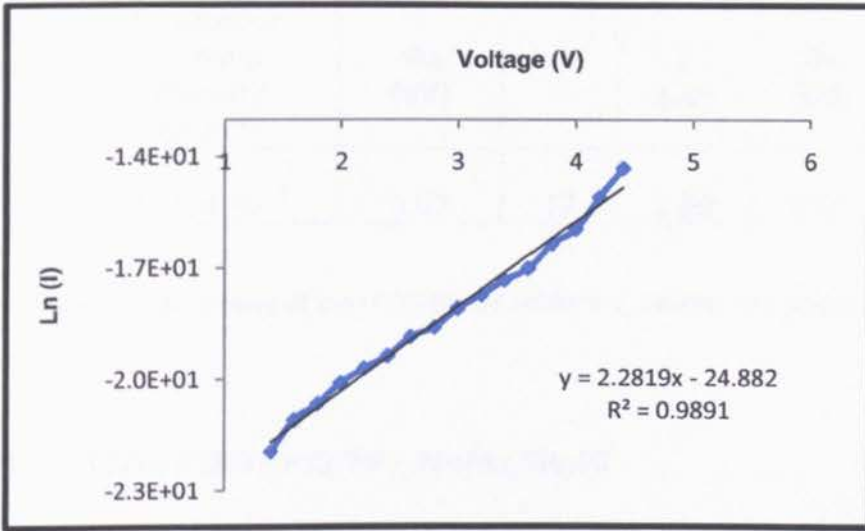


Figure 7 23: Plot of Ln(I) against V for ITO/PEDOT:PSS/PPV_MnPS₃/Al

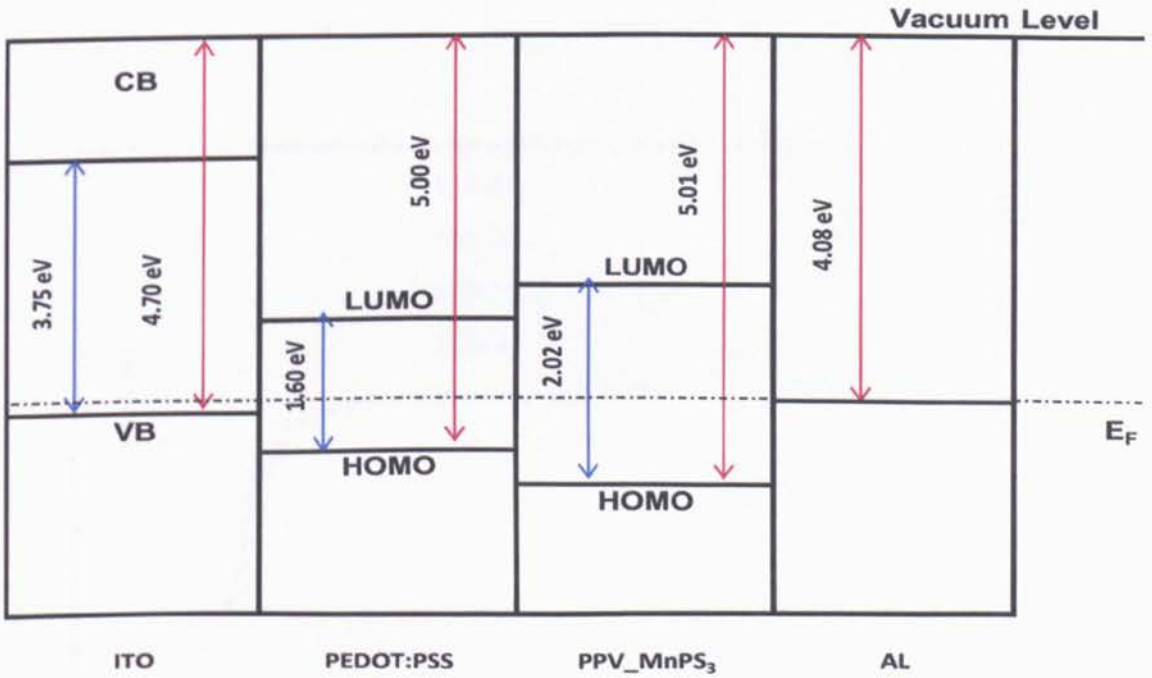


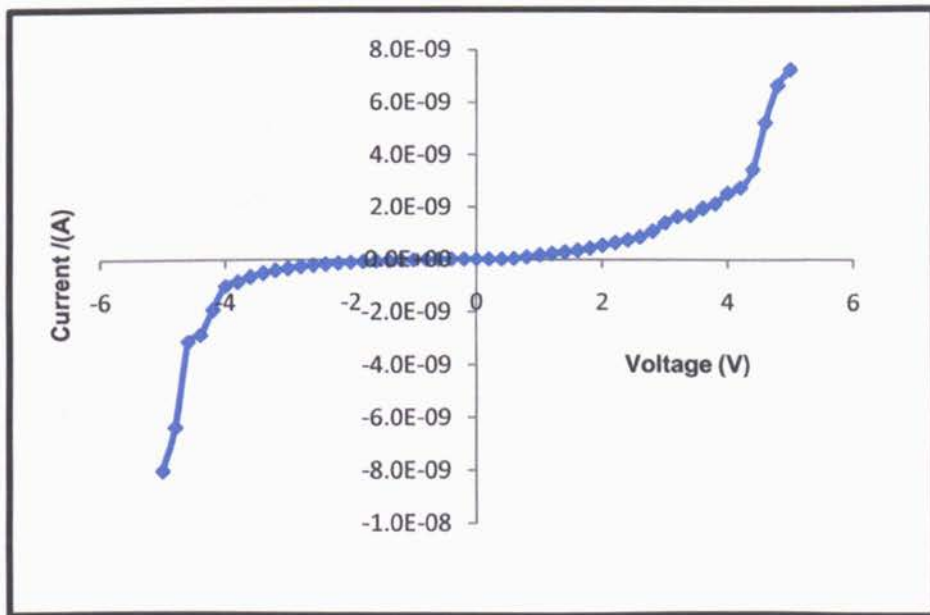
Figure 7 24: Proposed energy level alignment for ITO/PEDOT:PSS/PPV_MnPS₃/Al

Saturation current density (A m^{-2})	Φ_B (eV)	n	χ (eV)	Φ_S (eV)
1.38×10^{-5}	0.93	17	2.99	5.01

Table 7.6 Parameters of the ITO/PEDOT:PSS/PPV_MnPS₃ / Al device

7.4.2.3 ITO/PEDOT:PSS/PPV_MnPS₃_SIn/Al

The I-V curve is presented in Figure 7.25 It shows the characteristic behaviour of a rectifying device and the rectification ratio is 2.5 at ± 4 V.

Figure 7.25: Plot of I against V for ITO/PEDOT:PSS/PPV_MnPS₃_SIn/Al

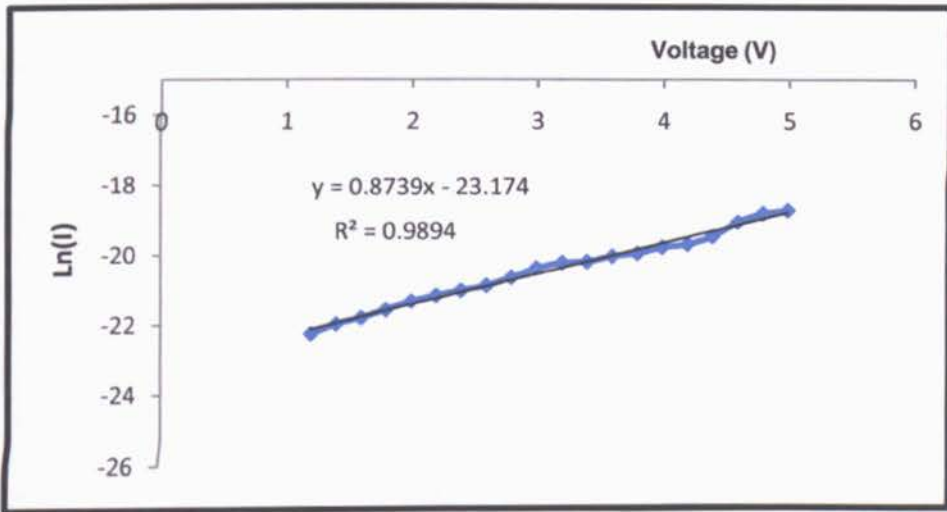


Figure 7.26: Plot of $\ln(I)$ against V for ITO/PEDOT:PSS/PPV_MnPS₃_Sn/Al

The calculated value of Φ_B was 0.88 eV and the ideality factor was found to be 45. All other calculated parameters for the diode are all shown in Table 7.7

Saturation current density ($A m^{-2}$)	Φ_B (eV)	n	χ (eV)	Φ_s (eV)
7.63×10^{-5}	0.88	45	2.94	4.96

Table 7.7 Parameters of the ITO/PEDOT:PSS/PPV_MnPS₃_Sn/Al device

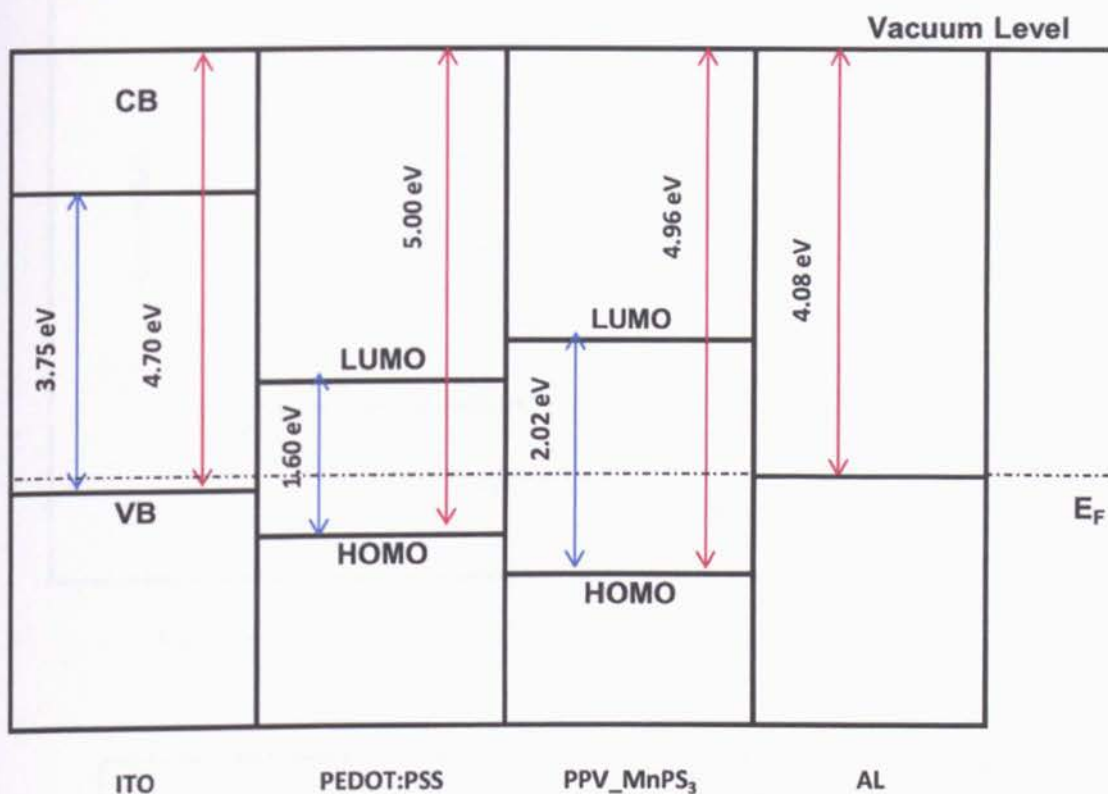
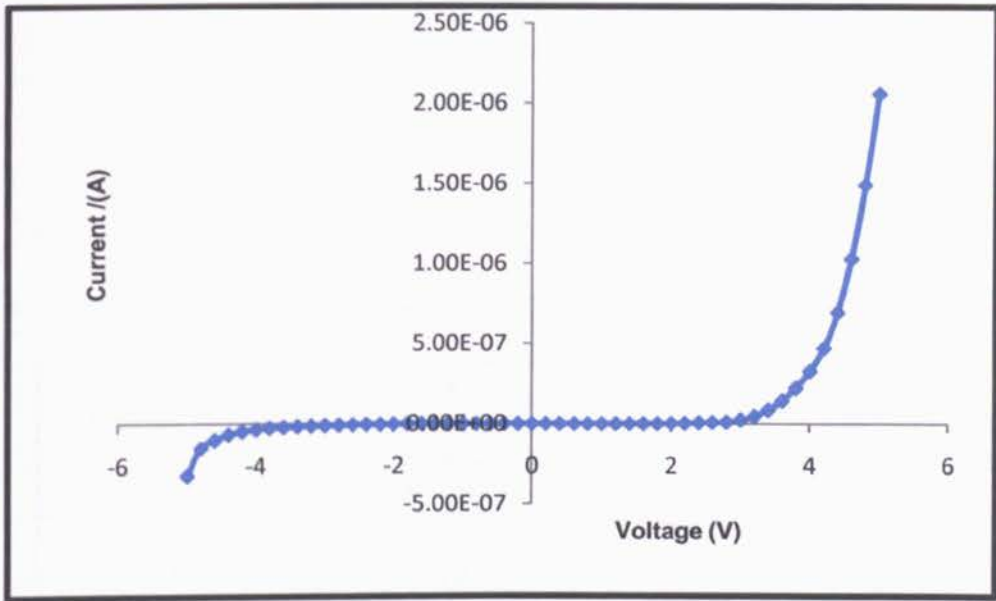
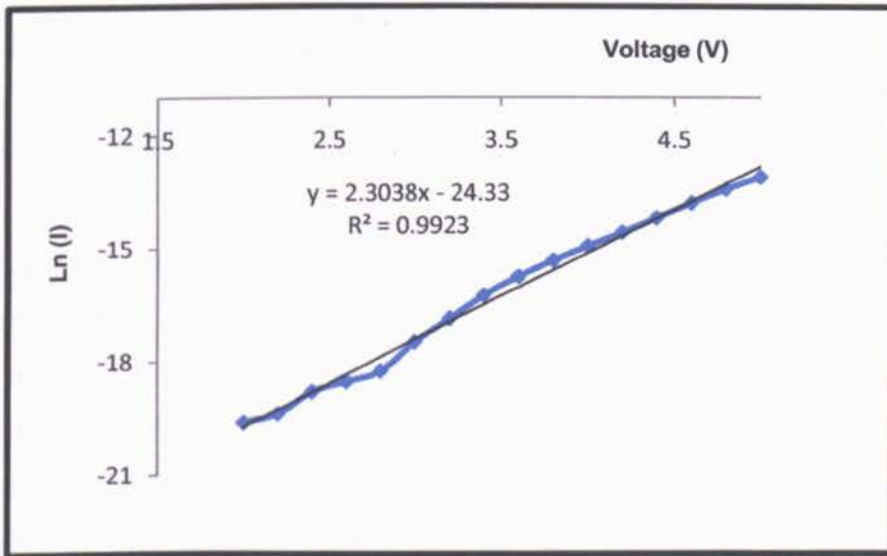


Figure 7.27: Proposed energy level alignment for ITO/PEDOT:PSS/PPV_MnPS₃_SiIn/Al

7.4.2.4 ITO / PEDOT:PSS / PPV_VOPO₄ / Al

The I-V curve is shown in Figure 7.28. It exhibits the characteristic behaviour of a rectifying device and the rectification ratio is 9.65 at ± 4 V.

Figure 7 28: Plot of I against V for ITO/PEDOT:PSS/PPV_VOPO₄/AlFigure 7 29: Plot of Ln (I) against V for ITO/PEDOT:PSS/PPV_VOPO₄/Al

The calculated value of Φ_B was 0.91 eV and the ideality factor was found to be 17. All other calculated parameters for the diode are all shown in Table 7.8

Saturation current density (A m^{-2})	Φ_B (eV)	n	χ (eV)	Φ_s (eV)
2.20×10^{-5}	0.91	17	2.55	4.99

Table 7.8 Parameters of the ITO/PEDOT:PSS/PPV_VOPO₄ / Al device

Active layer	Saturation current density (A m^{-2})	Φ_B (eV)	n	χ (eV)	Φ_s (eV)
PPV	0.99	0.64	39	2.39	4.73
PPV_MnPS ₃	1.38×10^{-5}	0.93	17	2.99	5.01
PPV_MnPS ₃ _Sn	7.63×10^{-5}	0.88	45	2.94	4.96
PPV_VOPO ₄	2.20×10^{-5}	0.91	17	2.55	4.99

Table 7.9 Calculated electrical parameters from the I-V measurements of all fabricated diodes

The Schottky diode is one of the most commonly used devices in electronics, including solar cells. Some of the first photovoltaic devices were made using polyacetylene, polythiophene and poly(p-phenylene vinylene), the last one being the most successful candidate for single layer polymer photovoltaic devices. Moreover, the radiative recombination channels of the injected electrons and holes within PPV lead to the formation of light emitting diodes (LEDs).³² The electronic properties of devices containing PPV sandwiched between various low and high work function materials have been researched in the past, and in many cases the I-V characteristics of the devices showed good rectification behaviour with the formation of Schottky contacts at the PPV/ Metal (Al) interface.³²

The characteristics of the Schottky contact are important to investigate both the material's properties and the characteristics of the interface. The efficiency of the devices is highly dependent on the efficiency of charge injection into the polymer at the electrode. In some cases, chemical interactions between the electrodes and the polymer could lead to the degradation of the polymer, hence reducing the lifetime of the devices.⁹⁰ Some metals are known to dope the polymer with luminescence quenching ions.⁹¹ Calcium, for example, is known to interact with conjugated polymers by doping them with calcium ions, whereas aluminium can form covalent linkages which disrupt the conjugation of the polymer.⁹¹

In this work, the electronic characteristic parameters of the ITO/PEDOT:PSS/PPV intercalated composites/Al interface were studied by means of I-V measurements and the results are all listed in Table 7.9 and compared with those of ITO/PEDOT:PSS/PPV/Al. In all cases the semiconductor/Al contact showed rectifying behaviour. The ideality factor of all devices was very high, including that of un-intercalated PPV devices; this was partly due to the high resistivity of the materials, which were all used in the intrinsic form and therefore the electrical conductivity was quite low. Another factor that could have led to such high values of n is the possibility of some contribution from thermally-activated electron hopping between the PPV and the hosts.

The saturation current density of all the samples was around 10^{-5} A m⁻² except for that of un-intercalated PPV which was 0.99 A m⁻². Since the saturation current density is independent of the applied voltage but dependent on the thermal excitation of the minority charges, it was difficult to make any assumption of the variation of those values. Temperature-dependent I-V measurements are therefore necessary to clarify the conduction mechanism.

Chapter 8:

EXPLORATORY WORK ON PALLADIUM THIOPHOSPHATE

At the start of this research, several layer inorganic materials were studied in order to have a better understanding of the intercalation chemistry and the electronic properties. Amongst those materials was $\text{Pd}_3\text{P}_2\text{S}_8$; it exhibited photophysical properties that were valuable for the development of this work as well as an unusual interleaved structure that might be subject to intercalation processes that so far have not been investigated on this material.

However, attempts to intercalate this sample were unsuccessful and it was therefore abandoned. Nevertheless the results of the studies carried out on this sample are reported in this chapter.

8.1 Palladium Thiophosphate ($\text{Pd}_3(\text{PS}_4)_2$)

This material possesses an unusual interlocked layered structure that consists of isolated anions of thiophosphate (PS_4)³⁻ coordinated to Pd^{2+} cations through the sulphur atom in a square planar arrangement giving rise to a plane of Pd atoms sandwiched between PS_4 layers (see Figure 8.1). The alternating units are held together by weak van der Waals interactions which make it a promising host material for intercalation.⁹² It is also a semiconductor with an optical band gap of 2.2 eV and shows appreciable photosensitivity and due to the presence of palladium (a commonly used catalyst) it may provide surfaces where photocatalytic reactions can take place making it a potential electrode material in photovoltaic cells.⁹³

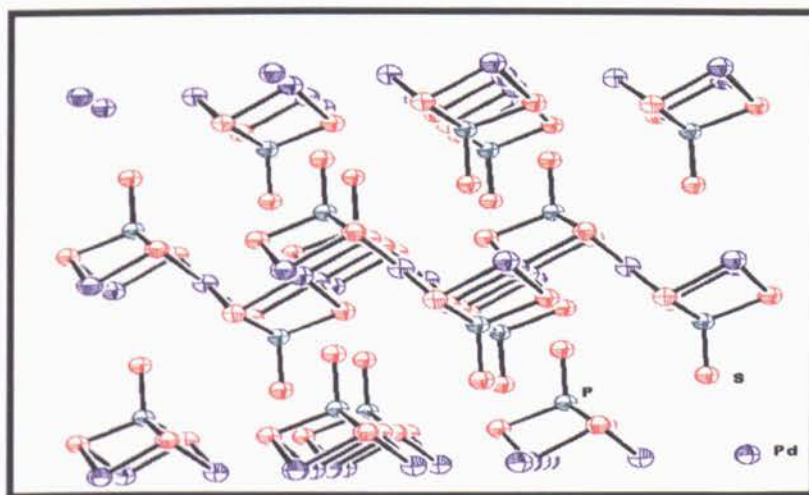


Figure 8 1: $\text{Pd}_3(\text{PS}_4)_2$ Crystal Structure.

8.2 Synthesis of Pd₃P₂S₈ and intercalates

8.2.1 Pd₃P₂S₈

Palladium, red phosphorus and sulphur were used, and general procedure A (chapter 4) was followed. The growth temperature and time were 520 °C (sublimation temperature 450 °C) and 21 days. Red- purple plate-like single crystals were obtained. The average size of the crystals was 3.2 x 1.0 x 0.1 mm³

8.2.2 Intercalation of Na⁺ ions into Pd₃P₂S₈

Sodium dithionite was used as a reducing agent in aqueous solution. A solution of sodium dithionite (10.5g) and water (30cm³) was prepared. Powdered Pd₃P₂S₈ (0.05g) was added to sodium dithionite solution (5 cm³). The solution was stirred for several hours and then left to react for seven days before the product was filtered off. The filtered product was washed firstly with sodium dithionite solution, then with deoxygenated water and finally with deoxygenated acetone. The product was then filtered and dried in the vacuum oven for 30 min at 40°C

8.2.3 Intercalation of 2,2'-bipyridine into Pd₃P₂S₈

Pd₃P₂S₈ (0.07g) was reacted with 2,2'-bipyridine (0.21g) and acetonitrile (0.6 cm³) in a two necked round-bottom flask. The mixture was refluxed under nitrogen for two weeks at 80°C. The product was filtered off and washed with acetone.

8.3 Results and discussion

8.3.1 Elemental analysis

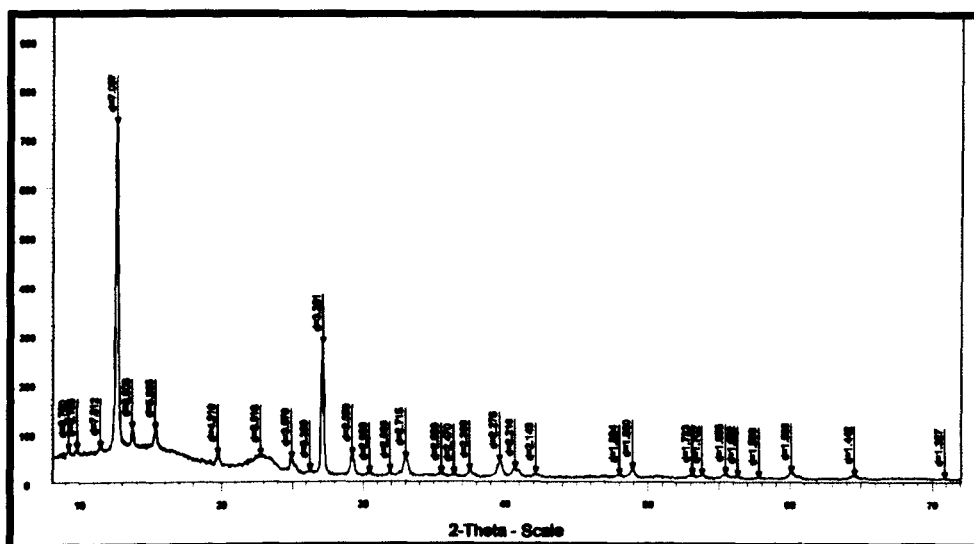
8.3.1.1 $Pd_3P_2S_8$

Silvery-purple plates were obtained. Elemental analysis (EDX) of the sample suggested the formula to be $Pd_{0.23}P_{0.15}S_{0.619}$ (Pd, 50.790%, P, 39.87%, S, 9.63 %)

8.3.2 X-Ray Diffraction

8.3.2.1 $Pd_3P_2S_8$

The first reflection peak (001) was observed at about 12.52° and it represents an interlayer distance of 7.07 Å; this value is close to the literature value of 7.23 Å in Reference 94. Other peaks also present were: 3.57 Å (about 24.94°), 2.39 Å (about 37.54°), 1.86 Å (48.97°); they represent the same interlayer spacing, but they are reflections of 2nd, 3rd, 4th and 5th order respectively (refer to Table 8.1).


 Figure 8 2: X-ray diffractogram of polycrystalline $\text{Pd}_3\text{P}_2\text{S}_8$

θ (2θ) ^o	d / (Å)	Calculated Interlayer Spacing (Å)	(h k l) parameters	d / (Å) literature Brither (1973) ⁹⁴
12.52	7.07	7.07	0 0 1	7.23
15.26	5.80		1 0 0	5.93
24.86	3.58	7.16	0 0 2	3.62
30.41	2.94		2 0 0	2.96
37.54	2.39	7.17	0 0 3	2.41
50.63	1.80	7.20	0 0 4	-----
64.49	1.44	7.20	0 0 5	-----
79.56	1.20	7.20	0 0 6	-----

 Table 8.1 Assignment of XRD data of $\text{Pd}_3\text{P}_2\text{S}_8$

8.3.2.2 Intercalation of Na⁺ into Pd₃P₂S₈

No change of colour or physical appearance was observed upon addition of the sodium dithionite solution to the Pd₃P₂S₈. Intercalation did not seem to have occurred. No changes in the XRD pattern were observed.

8.3.2.3 Intercalation of 2,2'-bipyridine into Pd₃P₂S₈

In the first few days, there was no change in the appearance of the compound; however after the second week, the single crystals were dissolved and a colloidal suspension was observed. The bright red colour of Pd₃P₂S₈ changed to dark brown.

8.3.3 Infrared and Raman Spectral Data

In the case of the Pd₃P₂S₈ strong infrared bands were expected around 512 and 492 cm⁻¹ corresponding to the P-S stretching vibrational modes in the [PS₄]³⁻ ion; however it was only possible to observe peaks at 689, 713 and 735 cm⁻¹ as the spectrometer's lowest wavenumber was 650 cm⁻¹. Nevertheless one of these lower range vibrations was confirmed by Raman spectroscopy where a small peak at about 490 cm⁻¹ was observed. Other peaks also present in the Raman spectra were attributed to the degenerate S-P-S bending at 189 cm⁻¹ and to the symmetric Pd-S stretching mode at 310 cm⁻¹. All these assignments are in good agreement with the reported values in the literature.⁹⁵

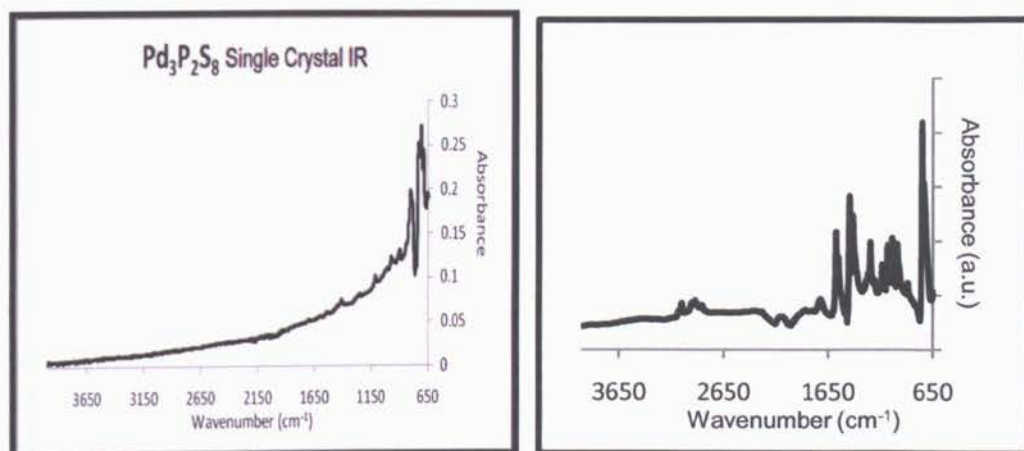


Figure 8 3: $\text{Pd}_3\text{P}_2\text{S}_8$ IR Spectrum (left) and $\text{Pd}_3\text{P}_2\text{S}_8$ _Bipy IR Spectrum (right)

Even though XRD data did not show any signs that intercalation had occurred, evidence of the presence of 2,2'-bipyridine ligand was observed in the infrared spectrum of the samples where the C=N and C=C characteristic peaks occurred from 1600 to 1400 cm^{-1} .⁹⁶ In the lower region of the Raman the P-P band at 380 cm^{-1} did not seem to be affected by the presence of the organic guests. This suggested that the presence of the organic ligand was only superficial.

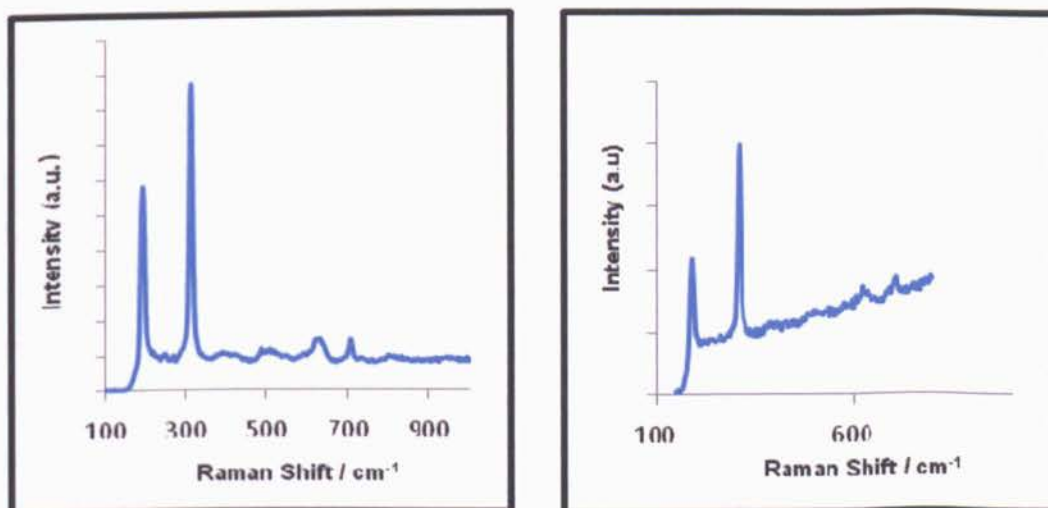


Figure 8 4: $\text{Pd}_3\text{P}_2\text{S}_8$ (left) and $\text{Pd}_3\text{P}_2\text{S}_8$ _Bipy (right) Raman Spectra.

8.3.4 Conductivity and Photoconductivity Measurements

The variation of photo-current as a function of applied voltage was measured while irradiating with monochromated light from a tungsten lamp at a constant wavelength of 690 nm. Dark current was also measured. It was observed that both of them increased linearly with applied voltage.

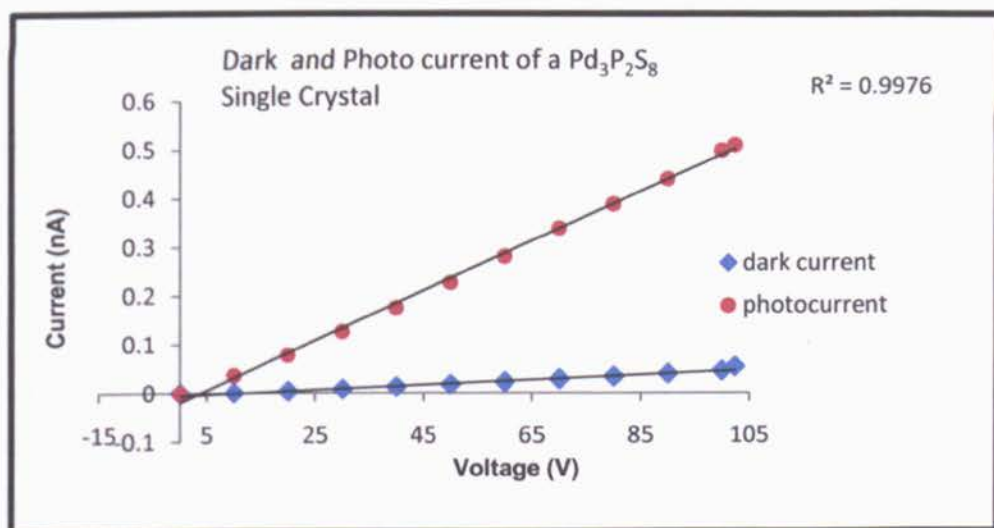


Figure 8 5: Variation of dark current and photocurrent with applied voltage at 690 nm.

Photoconductivity was also measured while varying the wavelength from 350 to 1000 nm in steps of 50 nm. (or 10 nm when it approached the maximum absorption) with a constant applied voltage of 102 V. An increase in the current was observed when the sample was exposed to light; this immediate response was an indication of intrinsic character of the Pd₃P₂S₈ (the radiation is absorbed by a valence band electron and the energy of excitation is sufficient to promote an electron from the valence band to the conduction band). Intrinsic photoconductors usually present maximum photosensitivity at the wavelength corresponding to the minimum energy required to produce a free electron (absorption edge).⁹⁷ In this case, the maximum photosensitivity was found at 690 nm corresponding to a band gap of 1.79 eV.

Chapter 9:

FINAL CONCLUSIONS AND FUTURE WORK

A fundamental point of this work has been the synthesis and study of the physical and chemical properties of the MPS_3 family and other layer-structured inorganic compounds as host materials for the preparation of organic/inorganic nanocomposites. Whereas much previous investigation has been carried out on other MPS_3 intercalates, this work has particularly focused on the investigation of the intercalation of poly(p-phenylene vinylene) (PPV) and their properties relevant to possible uses in electronic devices.

PPV was successfully prepared following a standard thermal conversion route proposed by Wessling and Zimmerman which involved a three-step reaction mechanism where the monomer, p-xylylene-bis(tetrahydrothiophenium chloride), was first prepared and polymerised to form the sulfonium polyelectrolyte precursor polymer, poly(p-xylylene tetrahydrothiophenium chloride). This was finally converted into PPV by thermal elimination above 200 °C.

Single crystals of $MnPS_3$ and polycrystalline $CdPS_3$ have been synthesised by a solid state method at temperatures above 600 °C and were used to prepare composites by intercalation of K^+ and PPV. The intercalation of PPV was achieved by a two-step reaction where K^+ ions were intercalated first and then exchanged with PPV precursor polymer, which was finally converted into PPV by thermal elimination.

The crystallinity and layer spacing of MnPS_3 and CdPS_3 samples have been confirmed by analysis of the XRD data, which was in good agreement with the existing literature. For the intercalated compounds, the XRD patterns showed that the main (0 0 l) peaks shifted towards lower angles indicating the expansion of the interlayer space. Minor defects such as cracks were observed on the surfaces of the samples due to mechanical stress during the intercalation process, but the overall layered structure of the host was kept throughout, as observed in the SEM images.

IR spectroscopy showed the vibrational features characteristic of the MPS_3 compounds at 572 cm^{-1} due to the P-S stretching frequencies of the P_2S_6 unit. This peak was split after intercalation, due to the formation of metal vacancies which broke the degeneracy of the P-S bond vibrations. The characteristic peaks of PPV were also seen in the IR spectra; however, the intensities were reduced due to the polymer being intercalated inside the inorganic hosts.

MnPS_3 was also synthesised as colloidal particles by reacting a solution of the divalent metal cation (Mn^{2+}) with the hexathiophosphate anion (P_2S_6)⁴⁻. Some similarities were observed between the macrocrystalline MnPS_3 (obtained by solid state reaction) and the amorphous material obtained in solution. First of all, the XRD pattern showed the preferred orientation of the platelets, approximately parallel to the substrate, hence making the (0 0 l) lines the most dominant feature. The d-spacing in both materials was close to 6.5 Å.

Similarly to the crystalline material after intercalation, the XRD showed that the interlayer spaces were expanded; moreover, infrared spectroscopy showed similar changes, with the characteristic band split due to the metal vacancies.

Intercalation of PPV resulted in the formation of polymer chains with less configurational disorder aligned inside the layers of the inorganic hosts; this caused a decrease in the band-gap of PPV from 2.33 to 2.02 eV. The

planarization of the backbone was also reflected in the emission spectra of the intercalated sample which showed an increase of the intensity of the 0-0 vibronic transition and a reduction of the intensity of the 0-1 transition due to a reduction of the configurational displacement (ΔQ).

Photoluminescence studies of both un-intercalated and intercalated PPV, showed similar features, with both samples emitting between 500 and 550 nm (green light), although in the case of intercalated PPV, the intensities of the peaks were reduced due to the presence of the inorganic matrices.

The intercalation of PPV not only resulted in the straightening of the polymer chains; it also provided environmental stability as the inorganic hosts could block the oxygen penetration into the intercalated polymer.

Some photodegradation studies were also carried out on PPV-intercalated MnPS_3 _Si but the results obtained were unexpected; the intensity of the main peaks was increased with increased irradiation time. This could mean that the intercalated polymer had not been fully converted into PPV by thermal means prior to irradiation, and therefore prolonged exposure to the tungsten lamp could have resulted in the elimination of any remaining sulfonium groups. Further investigation of this phenomenon would be necessary in order to test this proposal.

Layered $\text{VOPO}_4 \cdot 2\text{H}_2\text{O}$ was also synthesised and characterised by XRD, ATR-IR and Raman spectroscopy. Even though this material has been previously intercalated with small ions such as lithium and potassium, the intercalation of polymers has been limited to polyaniline and polypyrrole only, and its use as a host material for conducting polymers such as PPV has not been attempted.

New compounds were made by intercalation of PPV precursor polymer into VOPO_4 compounds and by subsequent thermal elimination to form PPV. After intercalation, the x-ray pattern showed an increase of 3.89Å in

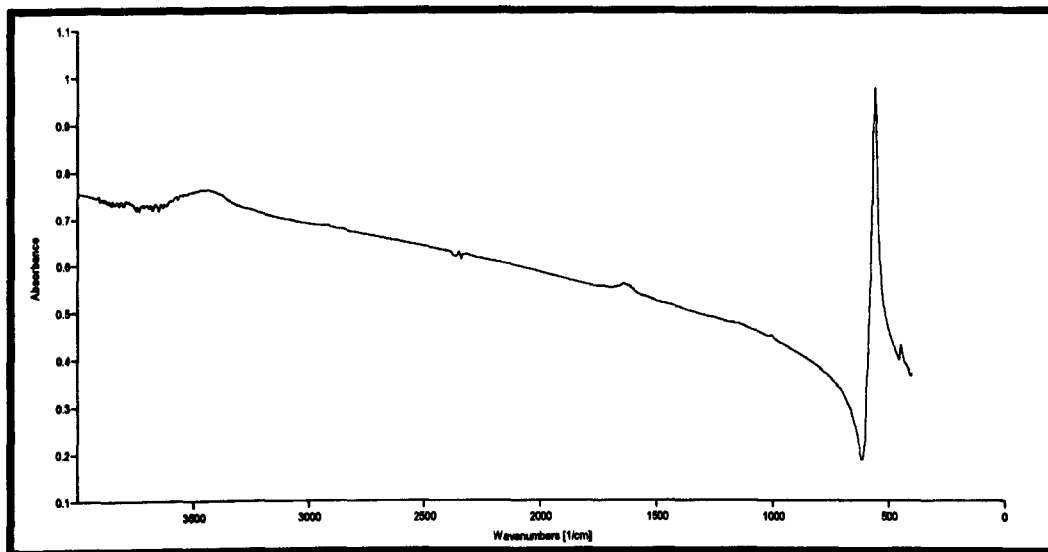
the d-spacing and a slight reduction of the crystallinity due to the stress the samples endured during intercalation.

The emission spectrum of PPV-intercalated VOPO₄ was red-shifted in comparison to that of the un-intercalated PPV, which indicated the formation of longer polymer chains. Although no photodegradation studies were carried out on this compound, the photoemission results (see Appendix D) are promising for possible applications, and further analysis could potentially reveal the enhancement of the environmental stability of PPV, as clearly demonstrated for PPV in MnPS₃.

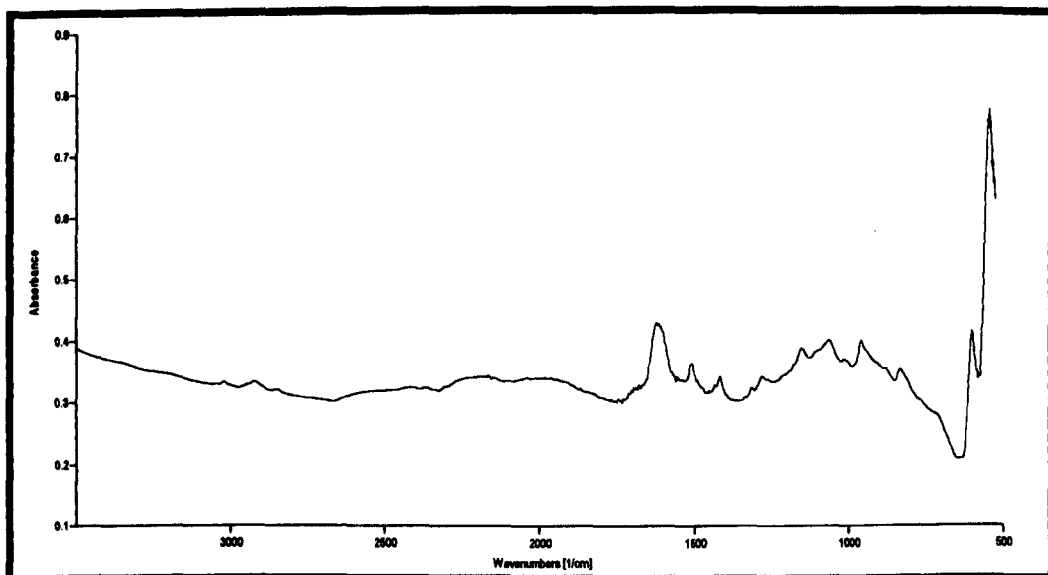
Finally, in order to check the potential applications of the prepared composites in electronic devices, Schottky diodes were fabricated and several parameters such as saturation current, ideality factor and barrier height were calculated. All the prepared diodes were found to have rectifying behaviour. In all cases, the ideality factor was greater than 1 and the values of the barrier height were between 0.85 and 0.95 eV. Since all measurements were made at room temperature, some uncertainty as to the conduction mechanism still remains. I-V measurements at different temperatures would be necessary in order to confirm if the diodes follow the thermionic model for Schottky devices.

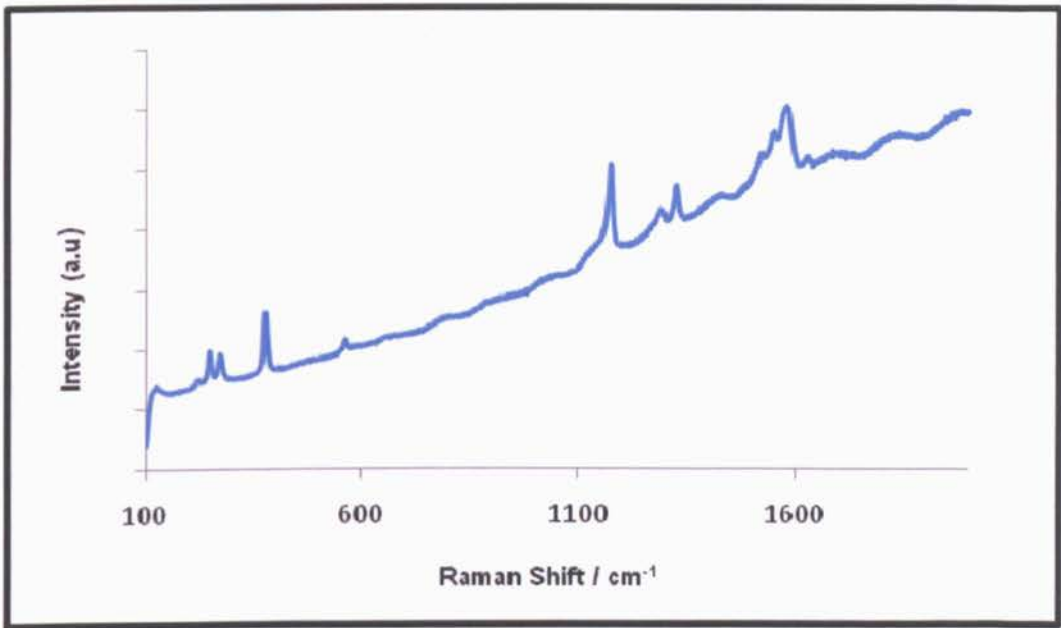
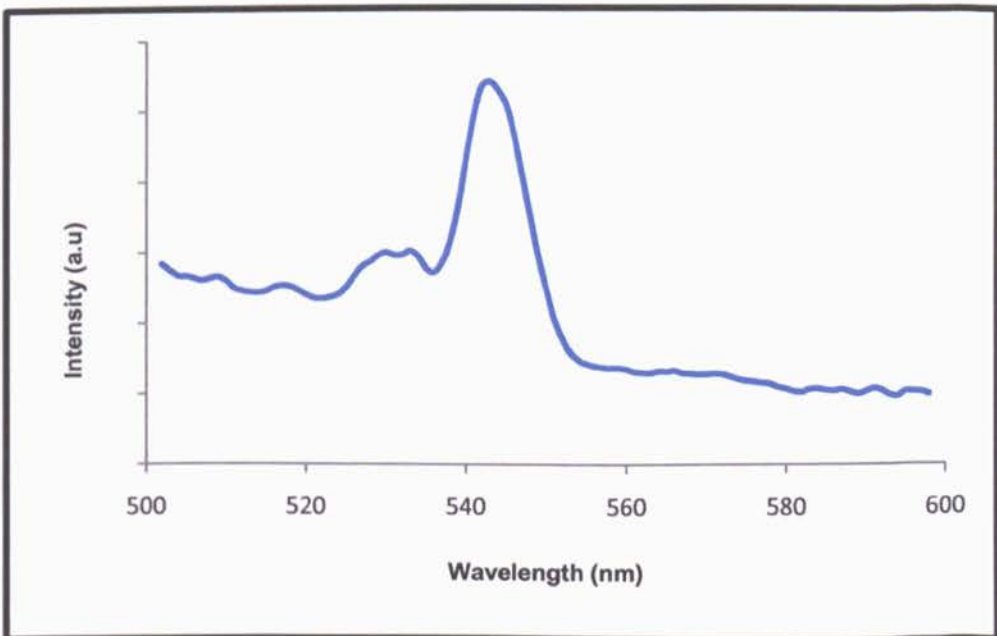
Appendix

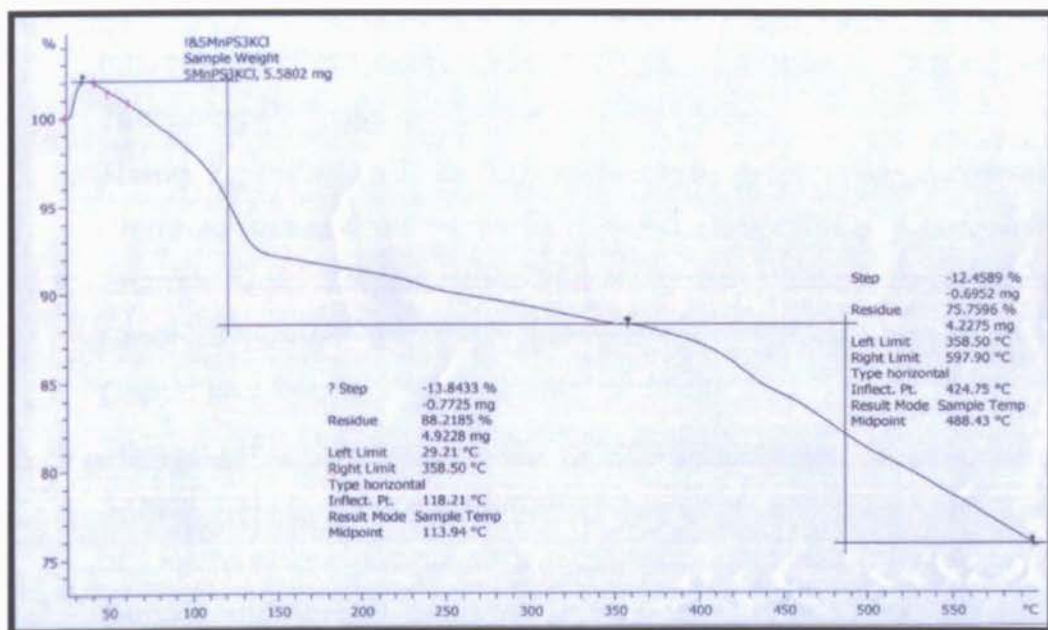
Appendix A : CdPS₃ IR Spectrum



Appendix B: PPV intercalated CdPS₃ IR Spectrum



Appendix C: PPV intercalated CdPS₃ Raman SpectrumAppendix D: PPV Intercalated VOPO₄ Emission Spectrum

Appendix E: TGA of K^+ intercalated $MnPS_3$ 

References

1. Oriakhi, C.O., Lerner, M.M. (2002) Nanocomposites and Intercalation Compounds. *Encyclopedia of Physical Science and Technology*. 3rd edition. USA: Academic Press.
2. Zhang, L., Webster, T. (2009) Nanotechnology and Nanomaterials: Promises for improved tissue regeneration. *Nanotoday*. 4. p. 66-80
3. Sharma, V.K., Yngard, R.A., Lin, Y. (2009) Silver Nanoparticles: Green Synthesis and their Antimicrobial Activities. *Advances in Colloid and Interface Science*. 145. p. 83-96
4. Silva, I.P.F., Santos, J.C.O., Conceicao, M.M., Nunes, L.M., Santos, I.M.G., Souza, A.G. (2005) Synthesis and Characterization of Intercalation Compounds between Lamellar Molybdenum Trioxide and Amines. *Materials Letters*. 59. P. 2510-2514
5. Duncan, W.B., O'Hare, D. (1997) *Inorganic Materials*. 2nd edition. UK: John Wiley & Sons Ltd
6. Cheetham, A.K., Day P. (1992) *Solid State Chemistry Compounds*. UK: Oxford University Press
7. Intercalation compounds, University of Pardubice, Faculty of chemical technology,
<http://www.upce.cz/en/fcht/slchpl/vyzkum/interkalacni.html>
Accessed 3rd November 2013
8. Sukpirom, N., Oriakhi, C.O., Lerner, M.M. (2000) Preparation of layered nanocomposites of PEO with MnPS₃, CdPS₃, and MoO₃ by melt intercalation. *Materials Research Bulletin*. 35. p. 325-331
9. Clement, R. (1980) A Novel Route to Intercalation into Layered MnPS₃. *Journal of the Chemical Society, Chemical Communications*. p. 647-648

10. Zima, V., Benes, L., Melanova, K., Vlack, M. (2002) Ion-exchange Properties of Alkali-metal Redox-Intercalated Vanadyl Phosphate. *Journal of Solid State Chemistry*. 163. p. 281-285
11. Manriquez, V., Barahona, P., Pena, O., Mouallem-Bahout, M., Avila, R.E. (2001) Physical Properties of layer-type MPS_3 Coomounds: $M_{0.5}In_{0.33}PS_3$ (M= Cd, Fe, Mn). *Journal of Alloys and Compounds*. 329. p. 92-96
12. Yi, T., Tancrez, N., Clement, R. Ledoux-Rak, I., Zyss, J. (2004) Organic- MPS_3 nanocomposites with Large Second Order Non-linear Optical Response. *Journal of Luminescence*. 110. p. 389-395
13. Jeevanandam, P., Vasudevan, S. (1997) Preparation and Characterisation of $Cd_{0.75}PS_3A_{0.5}(H_2O)_y$ [A= Na, K, and Cs]. *Solid State Ionics*. 104. p. 45-55
14. Grasso, V., Neri, F., Santangelo, S., Silipigni, L., Piacentini, M. (1989) Electronic Conduction in the Layered Semiconductor $MnPS_3$. *Journal of Physics: Condensed Matter*. 1. p. 3337-3347
15. Zima, V., Benes, L., Melaova, K., Svoboda, J. (2004) Preparation of Ammonium Intercalated Vanadyl Phosphate by Redox Intercalation. *Journal of Solid State Chemistry*. 177. p. 1173-1178
16. Sukanta, D. (2007) Electrical transport and optical properties of vanadyl phosphate-polyaniline nanocomposites. *Journal of Physics and Chemistry of Solids*. 68. p. 66-72
17. Eftekhari, A. (2010) *Nanostructured Conductive Polymers*. UK: John Wiley & Sons Ltd
18. Foot, J.S.J., Kaiser, A.B. (2004) Conducting Polymers in *Kirk-Othmer Encyclopedia of Chemical Technology*. USA: J Wiley and Sons Inc.
19. Shriver, D.F., Atkins, P.W. (1999) *Inorganic Chemistry*. 3rd edition. UK: Oxford University Press

-
20. Pratt, C. Conducting Polymers,
<http://homepage.ntlworld.com/colin.pratt/cpoly.pdf> Accessed 3rd
November 2013
21. Laidler, K.J., Meiser, J.H., Sanctuary, B.C. (2003) *Physical Chemistry*. 4th edition. USA: Houghton Mifflin.
22. Wessling, R.A., Zimmerman, R.G. (1968) *Polyelectrolytes from Bis Sulfonium Salts*, US Patent 3401152
23. Partridge, R.H. (1983) Electroluminescence from Polyvinylcarbazole Films: 1 Carbazole Cations. *Polymer*. 4. p. 733-738
24. Burroughes, J.H., Bradley, D.D.C., Brown, A.R., Marks, R.N., Mackay, K., Friend, R.H., Burns, P.L. (1990) Light-emitting Diodes Based on Conjugated Polymers, *Nature*. 347. p. 6293, 539-541
25. Service, R.F. (1996) Organic Light Emitters Gain Longevity. *Science*. 273 (5277) p. 878-880
26. Valeur, B. (2001) *Molecular Fluorescence Principles and Applications*. UK: Wiley-VCH.
27. Leni, A. (2003) Electroluminescent Polymers. *Progress in Polymer Science*. 28. p. 875-962
28. Greenham, N.C., Moratti, S.C., Bradley D.D.C., Friend, R.H., Holmes, A.B. (1993) Efficient Light Emitting Diodes Based on Polymers with High Electron Affinities. *Nature*. 365 (6447). p. 628-630
29. Grindsale, A.C., Chan, K.L., Rainer, E.M., Jokisz, P.G., Holmes, A.B. (2009) Synthesis of Light Emitting Conjugated Polymers for Applications in Electroluminescent Devices. *Chemical Reviews*. 109. p. 897-1091
30. Skotheim, T.A., Elsenbaumer, R.L., Reynolds, J.R. (1998) *Handbook of conducting polymers*. 2nd edition. USA: Marcel Dekker, INC.

-
31. Wessling, R.A. (1985) The Polymerisation of Xylylene Bisdialkyl Sulfonium Salts. *Journal of Polymer Science: Polymer Symposium*. 72. p. 55-66
32. Lahti, P.M., Modarelli, D.A., (1988) Polymerisation of α,α' -Bis(dialkylsulfonio)-p-xylylene Dihalides via p-Xylylene Intermediates: Evidence for a non-radical Mechanism. *Journal of the American Chemical Society*. 110. p. 7258-7259
33. Halliday, D.A., Burn, P.L., Friend, R.H., Holmes, A.B. (1992) A Study of the Elimination Reaction of Sulfonium Polyelectrolyte Precursor Polymers to Poly(p-phenylene vinylene). *Journal of the Chemical Society, Chemical Communications*. 22. p. 1685-1687
34. Kesters, E., Kok, M.M., Carleer, R.A.A., Czech, J.H.P.B. (2002) The Thermal Conversion Reaction of Sulphonyl Substituted Poly(p-xylylene): Evidence for the Formation of PPV structures. *Polymer*. 43. p. 5749-5755
35. Skotheim, T.A., Reynolds, J.R. (2007) *Handbook of Conducting Polymers: Conjugated Polymers Processing and Applications*. 3rd edition. USA: CRC Press.
36. Aarab, H., Baitoul, M., Wery, J., Almairac, R., Lefrant, S., Faulques, E., Duvail, J.L., Hamedoun, M. (2005) Electrical and Optical properties of PPV and single-walled Nanotubes Composites Films. *Synthetic Metals*. 1. p. 63-67
37. Wise, D.L., Wnek, G.E., Trantolo, D.J., Cooper, T.M., Gresser, J.D. (1998) *Photonic Polymer Systems: Fundamentals, methods and Applications*. USA: Marcel Dekker Inc.
38. Hadziioannou, G., Hutten, P.F. (2000) *Semiconducting Polymers, Chemistry Physics and Engineering*. Germany: WILEY-VCH.
39. Pichler, K., Halliday, D.A., Bradley, D.D.C., Burn, P.L., Friend R.H., Holmes, A.B. (1993) Optical Spectroscopy of Highly Ordered Poly(p-phenylene vinylene). *Journal of Physics: Condensed Matter*. 5. p. 7155-717

40. Bradley, D.D.C., Evans, G.P., Friend, R.H. (1987) Characterisation of Poly(phenylene vinylene) by Infrared and Optical Absorption, *Synthetic Metals*, 17. p. 651-656.
41. Burn, P.L. Bradley, D.D.C., Friend, R.H., Halliday, D.A. (1992) Precursor Route Chemistry and Electronic Properties of Poly(p-phenylene vinylene), Poly[(2,5-dimethyl-p-phenylene)vinylene] and Poly[(2,5-dimethoxy-p-phenylene)vinylene]. *Journal of the Chemical Society, Perkin Transactions 1*. p. 3225-3231
42. Cowie, J.M.G., Arrighi, V. (2008) *Polymers: Chemistry and Physics of modern materials*. 3rd edition. USA: CRC Press.
43. Coradin. T., Clement, R. (1998) From Intercalation to Aggregation: Non Linear Optical Properties of Stilbazolium Chromophores-MnPS₃ Layered Hybrid Materials. *Chemistry of Materials*. 8. p. 2153-2158
44. Yang, D., Frindt, R.F. (2000) Structure of Polymer Intercalated MnPS₃ and CdPS₃
45. Legadic, I., Lacroix, P.G., Clement, R. (1997) Layered MPS₃ (M=Mn, Cd) Thin Films as Host Matrixes for Nonlinear Optical Material Processing. *Chemistry of Materials*. 9. (9). p. 2004-2012
46. Zhang, D., Qin, J., Yakushi, K., Nakazawa, Y. (2000) Preparation of New Nanocomposites of Conducting Polyaniline into layered MnPS₃. *Materials Science and Engineering A*. 286. p. 183-187
47. Pattayil, A.J., Vasudevan, S. (1992) The intercalation Reaction of Pyridine with Manganese Thiophosphate, MnPS₃. *Journal of the American Chemical Society*. 114. p. 7792-7801
48. Hangyo, M., Nakashima, S., Mitsuishi, A. (1988) Raman Spectra of MnPS₃ Intercalated with Pyridine. *Solid State communications*. 65 (5). p. 419-423
49. Mathey, Y., Clement, R., Sourisseau, C., Lucazeau, G. (1980) Vibrational Study of Layered MPX₃ Compounds and Some Intercalates with Co(□⁵-C₅H₅)₂⁺ or C(□⁶-C₆H₆)₂⁺. *Inorganic Chemistry*. 19. p. 2773-2779

50. Hangyo, M., Nakashima, S., Mitsuishi, A. (1988) Raman Spectra of MnPS₃ Intercalated with Pyridine. *Solid State Communications*. 65 (5). p. 419-423
51. Tran, V.H., Massardier, V. (1996) Spectroscopy Studies of the Conversion of Poly(p-phenylene-vinylene) Precursor. *Polymer*. 37 (11). p. 2061-2065
52. Nazar, L.F., Zhang, Z., Zinkweg, D. (1992) Insertion of Poly(p-phenylene-vinylene) in layered MoO₃. *Journal of the American Chemical Society*. 114. p. 6239-6240
53. Kobryanskii, V.M., Kaplanova, T.G., Vitukhnovsky, A.G. (1997) Effect of Storage of Precursor Polymer Solution on the Electronic and Physical Structure of Poly(p-phenylene vinylene). *Synthetic Metals*. 84. p. 257-258
54. Grasso, V., Santangelo, S. (1986) M_{2,3} Absorption Spectra of Transition Metal Ion in MnPS₃, FePS₃, and NiPS₃. *Solid state communications*. 60 (4). p. 3381-1986
55. Foot, P.J.S., Nevett, B.R. (1986) *Cathode Material for Alkali-Metal Rechargeable Cell*, United states Patent Office., Patent N^o 4579724,
56. Falius, H. (1968) Hexathiohypophosphate, Salze einer neuen Saure des Phosphors. *Zeitschrift fur anorganische und allgemeine chemie*. 356. p.189-193
57. Glatzel, E. (905) Uber das Kristallwasserhaltige normale Natriumsulfophosphat, {Na₃PS₄ + 8H₂O}. *Zeitschrift fur anorganische und allgemeine chemie*. 4. p. 186-226
58. Li, C., Wang, X., Peng, Q., Li, Y. (2005) Synthesis and Characterisation of Mn₂P₂S₆ Single-Crystal Nanorods and Nanotubes. *Inorganic chemistry*. 44 (19). p. 6641-6645
59. Zhong-Le, H., Jing-Tai, Z., Jin-Xiao, M., Shao-Yu, M., Lan-Sum, Z. (1999) Room Temperature Solid State Synthesis and

- Characterisation of a New Chromium Thiophosphate $\text{Cr}_4(\text{P}_2\text{S}_6)_3$. *Journal of Solid State Chemistry*. 144. p. 388-391
60. Li, C., Wang, X., Peng, Q., Li, Y. (2005) Synthesis and Characterisation of $\text{Mn}_2\text{P}_2\text{S}_6$ Single-Crystal Nanorods and Nanotubes. *Inorganic chemistry*. 44 (19). p. 6641-6645
61. Fincher, T., LeBret, G., Cleary, D.A. (1998) Single-Crystal Structure Determination of $\text{Na}_4\text{P}_2\text{S}_6 \cdot 6\text{H}_2\text{O}$. *Journal of Solid State chemistry*. 141. p. 274-281
62. Prouzet, E., Fukatani, M., Barj, M., Janvier, P. (1999) Oxygen Substitution of the Hexathiodiphosphate (IV) Ion in Aqueous Solution. *Journal of the Chemical Society, Dalton Transactions*. 4. p. 635-637
63. Yi, T., Clement, R., Haut, C., Catala, L., Gacoin, T., Tancrez, N., Ledoux, I., Zyss, J. (2005) J-Aggregated Dye- MnPS_3 Hybrid Nanoparticles with Giant Quadratic Optical Nonlinearity. *Advance Materials*. 17 (3). p. 335-338
64. De Farias, R.F., Airoidi, C. (2003) Synthesis and Characterisation of a VOPO_4 -polyaniline Lamellar Hybrid Compound. *Solid State Sciences*. 5. p. 611-613
65. Chauvel, A., De Roy, M.E., Besse, J.P., Benarbia, A., Legrouri, A., Barroug, A. (1995) Redox Intercalation of Alkali Metals into Vanadyl Phosphate Dihydrate. *Materials Chemistry and Physics*. 40. p. 207-211
66. Vitezlav, Z., Melanova, K., Benes, L., Trchova, M., Dybal, J. (2005) Intercalation of Cyclic Ketones into Vanadyl Phosphate. *Journal of Solid State Chemistry*. 178 (1). p. 314-320
67. Griesel, L., Bartley, J.K., Wells, R.P.K., Hutchings, G.J. (2004) Preparation of Vanadium Phosphate Catalyst from $\text{VOPO}_4 \cdot 2\text{H}_2\text{O}$:

- Effect of $\text{VOPO}_4 \cdot 2\text{H}_2\text{O}$ Preparation on Catalyst Performance. *Journal of Molecular Catalysis A: Chemical*. 220. p. 113-119
68. Benes, L., Melanova, K., Zima, V., Trchova, M., Capkova, P., Koudelka, B. (2006) Vanadyl Phosphate Intercalated with Dimethyl Sulfoxide. *Journal of Physics and Chemistry of Solids*. 67. p. 956-960
69. Spodine, E., Valenci-Galvez, P., Manzur, J., Paredes-Garcia, V., Pizarro, N., Bernot, K., Venegas-Yazigi, D. (2012) Optical Properties of Composites Formed by Transition Metal Macrocyclic Complexes Intercalated in Thiophosphate Layered Phases. *Polyhedron*. 44. p. 187-193.
70. Yang, D., Westreich, P., Frindt, R.F. (2002) Exfoliated CdPS_3 Single Layers and Restacked Films. *Journal of Solid State Chemistry*. 166. p. 421-425
71. Zhukov, V., Boucher, F., Alemany, P., Evains, M., Alvarez, S. (1995) Electronic Structure, Chemical Bonding, and Jahn-Teller Distortions in CdPS_3 . *Inorganic Chemistry*. 34. p. 1159-1163
72. Sukanta, D., Dey, A., De, S. K. (2006) Electrical Transport and Optical Properties of Vanadyl Phosphate-polypyrrole Nanocomposites. *Journal of Physics D: Applied Physics*. 39. p. 500-505
73. Yoon, K.H., Park, S.B., Yang, B.D. (2004) Size Effect of Nanoparticles on the Conjugated Polymer in PPV/SiO_2 Nanocomposites. *Materials Chemistry and Physics*. 87. p. 39-43
74. Zhang, J., Wang, B., Ju, X., Liu, T., Hu, T. (2001) New Observations on the Optical Properties of PPV/TiO_2 Nanocomposites. *Polymer*. 42. p. 3697-3702

75. Skotheim, T.A., Elsenbaumer, R.L., Reynolds, J.R. (1998) *Handbook of conducting polymers*. 2nd edition. USA: Marcel Dekker, INC.
76. Bakueva, L., Matheson, D., Musikhin, S., Sargent, E.H. (2002) Luminescence of Pure and Iodine Doped PPV: Internal Energetic Structure Revealed through Spectral Signatures. *Synthetic metals*. 126. p. 207-211
77. Yang, B.D., Yoon, K.H., Chung, K.W. (2004) Dispersion Effect of Nanoparticles on Conjugated Polymer-inorganic Nanocomposites. *Materials Chemistry and Physics*. 83. p. 334-339
78. Holzer, W., Penzkofer, A., Pichlmaier, M., Bradley, D.D.C., Blau, W.J. (1999) Photodegradation in Some Luminescent Polymers. *Chemical Physics*. 248. p. 273-284
79. Lee, H., Lee, T., Lim, Y.T., Park, O.O. (2002) Improved Environmental Stability in Poly(p-phenylene vinylene) Layered Silicate Nanocomposite. *Applied Clay Science*. 21. p. 287-293
80. Low, H.Y. (2002) Photo and Photo-oxidative Degradations of Poly(phenylene vinylene) Derivatives. *Thin Solid Films*. 413. p. 160-166
81. Hale, D.G., Oldenburg, S.J., Halas, N.J. (1997) Effects of Photo-oxidation on Conjugated Polymers Films. *Applied Physics Letters*. 71 (11). p. 1483-1485
82. Hale, D.G., Oldenburg, S.J., Halas, N.J. (1997) Effects of Photo-oxidation on Conjugated Polymers Films. *Applied Physics Letters*. 71 (11). p. 1483-1485
83. Chambon, S., Rivaton, A., Gardette, J., Firon, M. (2011) Photo and Thermo-oxydation of Poly(p-phenylene vinylene) and Phenylene-

- vinylene Oligomer. *Polymer Degradation and Stability*. 96. p. 1149-1158
84. Alvaro, M., Corma, A., Ferrer, B., Galletero, M.S., Garcia, H., Peris, E. (2004) Increasing the Stability of Electroluminescent Phenylenevinylene Polymers by Encapsulation in Nanoporous Inorganic Materials. *Chemistry of Materials*. 16. p. 2142-2147
85. Cucinotta, F., Carniato, F., Paul, G., Bracco, S., Bisio, C., Calderelli, S., Marchese, L. (2011) Incorporation of a Semiconductive Polymer into mesoporous SBA-15 Platelets: Toward New Luminescent Hybrid Materials. *Chemistry of Materials*. 23. p. 2803-2809
86. Mishra, U.K., Singh, J. (2008) *Semiconductor Device Physics and Design*. Netherlands: Springer.
87. Gagnon, D.R., Capistran, J.D., Karasz, F.E., Lenz, R.W., Antouni, S. Synthesis, Doping and Electrical Conductivity of high molecular weight Poly(p-phenylene vinylene)
88. Ryu, M.S., Jang, J. (2011) Enhanced Efficiency of Organic Photovoltaic Cells Using Solution-processed Metal Oxide as an Anode Buffer. *Solar Energy Materials & Solar Cells*. 95. p. 3015-3020
89. Edwards-Shea, L. (1996) *The Essence of Solid State Electronics*. Harlow: Prentice Hall.
90. Marks, R.N., Halls, J.J.M., Bradley, D.D.C., Friend, R.H., Holmes, A.B. (1994) The Photovoltaic Respose in Poly(p-phenylene vinylene) thin-film device. *Journal of Physics: Condensed Matter*. 6. p. 1379-1387
91. Antoniadis, H., Hsieh, B.R., Abkowitz, M.A., Jenekhe, S.A., Stolka, M. (1994) Photovoltaic and Photoconductive Properties of Aluminium/Poly(p-phenylene vinylene) Interfaces. *Synthetic Metals*. 62. p. 265-271

-
92. Grimsdale, A.C., Chan, L.C., Martin, R.E., Jokisz, P.G., Holmes, A.B. (2009) Synthesis of Light Emitting Conjugated Polymers for Applications in Electroluminescent Devices. *Chemical Reviews*. 109. p. 897-1091
93. Grasso, V. (1999) Vibrational and low-energy optical spectra of the square planar $\text{Pd}_3(\text{PS}_4)_2$ thiophosphate, *The American Physical Society*. 60. p. 2333-2339
94. Grasso, V., Silipigni, L. (2003) X-ray Photoemission Spectra and X-ray Excited Auger Spectrum Investigation of the Electronic Structure of $\text{Pd}_3(\text{PS}_4)_2$. *The Journal of Vacuum Science and Technology A*. 21. p. 860-865
95. Bither, T.A. E.I. Du Pont de Nemours and Co., Wilmington, Del. (1973) Palladium Phosphide Chalcogenides. United States Patents, Patent 3.761.572
96. Calareso, C., Grasso, V., Silipigni, S. (1999) Vibrational and Low Energy Optical Spectra of the Square Planar $(\text{Pd}_3(\text{PS}_4)_2)$ Thiophosphate. *Physical Review B*. 60. p. 2333-2339
97. Zhang, X. *et al* (2004) The intercalation reaction of 2,2'-bipyridine with layered compound MnPS_3 , *Journal of Solid State Chemistry*. 177. p. 2014-2022
98. Bube, R .H. (1960) *Photoconductivity of Solids*. UK: J Wiley & Sons Inc